UNIVERSIDAD DE CHILE

FACULTAD DE CIENCIAS FÍSICAS Y MATEMÁTICAS

DEPARTAMENTO DE GEOLOGÍA

THE CONTROL OF MAGMATIC SYSTEM PROPERTIES ON VOLCANO DIMENSIONS AND BUILDING: THE CASES OF LASCAR, LONQUIMAY AND LLAIMA VOLCANOES, ANDES OF CHILE

TESIS PARA OPTAR AL GRADO DE MAGISTER EN CIENCIAS MENCIÓN GEOLOGÍA

MARÍA ANGÉLICA CONTRERAS VARGAS

PROFESOR GUÍA

ÁNGELO CASTRUCCIO ÁLVAREZ

MIEMBROS DE LA COMISIÓN

CLAUDIA CANNATELLI

JORGE CLAVERO RIBES

SANTIAGO DE CHILE

2017

RESUMEN DE LA MEMORIA PARA OPTAR AL TÍTULO
DE: Grado de Magister en Ciencias Mención Geología
POR: María Angélica Contreras Vargas
FECHA: diciembre de 2017
PROFESOR GUÍA: Ángelo Castruccio Álvarez

THE CONTROL OF MAGMATIC SYSTEM PROPERTIES ON VOLCANO DIMENSIONS AND BUILDING: THE CASES OF LASCAR, LONQUIMAY AND LLAIMA VOLCANOES, ANDES OF CHILE.

Los estratovolcanes son la manifestación en superficie de complejos sistemas magmáticos profundos. En el presente trabajo, se ha desarrollado un modelo cuyo objetivo es contribuir a la comprensión de la influencia de las propiedades del sistema magmático de un estratovolcán, en el perfil topográfico y dimensiones del mismo.

Se asume un volcán construido por la acumulación de flujos de lava emitidos desde un centro de emisión único, excluyendo otros procesos que pueden afectar el crecimiento tales como erosión, avalanchas, volcanismo adventicio, acumulación de piroclastos, entre otros. Se considera que cada erupción es gatillada por la inyección de nuevo magma en el reservorio, y que la resultante sobrepresión asociada provoca la removilización de una parte del magma almacenado que es posteriormente extruido.

El modelo se probó en 3 estratovolcanes de los Andes de Chile, con diferencias morfológicas y composicionales: el volcán Lascar ubicado en la Zona Volcánica Central, y los volcanes Lonquimay y Llaima localizados en la Zona Volcánica Sur. Los resultados obtenidos tras aplicar el modelo fueron validados con otros métodos independientes: termobarometría en muestras seleccionadas de estos volcanes y estudios geofísicos previos.

Los resultados obtenidos revelan una fuerte influencia de las propiedades del sistema magmático en la morfología de los volcanes en superficie. Volcanes que superan los 2000 m de altura desde su base y poseen un radio basal de más de 10 km, estarían asociados a cámaras profundas, ubicadas a más de 10 km bajo la superficie. En volcanes de altura menor a 1500 m y radio basal menor a 10 km, el reservorio alimentador de las erupciones se ubicaría a menos de 6 km de profundidad. Si además se considera la densidad de la corteza y del magma, esto es más complejo pues a mayor flotabilidad se espera un estratovolcán más alto. Por otra parte, mientras mayor es el tamaño del reservorio, los flujos de lava emitidos también lo serán y, en consecuencia, se espera un radio basal mayor y un volcán de mayor volumen.

Nuestro análisis sugiere que los volcanes Lonquimay y Llaima están cerca de alcanzar su altura máxima, por lo tanto, erupciones efusivas de volumen considerable ocurrirían probablemente en sus flancos, mientras que erupciones más bien moderadas son esperables que ocurran desde su cima. Al contrario, el volcán Lascar no habría alcanzado su altura máxima, en consecuencia, flujos de lava de volumen considerable podrían ser emitidos desde la cima.

Agradecimientos

En primer lugar, quisiera agradecer el financiamiento otorgado por el proyecto FONDECYT 11121298, con el cual fue posible realizar el trabajo de terreno y análisis necesarios para elaborar este trabajo. En la misma línea, agradezco al Centro de Excelencia en Geotermia de los Andes (CEGA) que me entregó el apoyo necesario para realizar mis estudios de postgrado, y brindó soporte para mi participación en diversos congresos y cursos internacionales. Finalmente, no puedo dejar de agradecer al Departamento de Postgrado y Postítulo de la Universidad de Chile que, a través de su programa de ayuda para estadías cortas de investigación, me permitió realizar una pasantía en la Universidad de Bristol. Inglaterra.

También agradezco a los profesores miembros de la comisión evaluadora por su valiosa contribución a este trabajo. Agradezco a mi profesor guía Ángelo Castruccio por darme la oportunidad de realizar esta investigación. Por involucrarse durante todo el proceso, compartiendo sus conocimientos e impulsando mi pensamiento analítico. A la profesora Claudia Cannatelli por su preocupación y apoyo, y particularmente por su tremenda ayuda en este desafío de escribir esta tesis en inglés. Y finalmente a Jorge Clavero, quien desde su experiencia me entregó valiosos comentarios que sin duda ayudaron a construir un mejor trabajo.

No puedo dejar de mencionar a todas las personas que aportaron de distintas formas a la elaboración de este trabajo. Alison Rust y Stuart Kearns por su apoyo durante mi estadía en la Universidad de Bristol. A Edmundo Polanco, Dawn Sweeney Ruth y Matthieu Kervin quienes me entregaron apoyo en alguno de los tópicos que toca esta tesis.

Agradezco además a todas esas mentes inquietas que en algún momento y en las más variadas circunstancias, compartieron conmigo sus valiosos conocimientos sobre el apasionante mundo de la volcanología: Javier Reyes, Christian Pizarro, Cami Leal, Cami Pineda, Raimundo Brahm, Pancho Cáceres, Claudio Contreras, Eduardo Morgado, Diego

Aravena, Cami Pineda, Marce Pizarro, Cami Vera, Gabi Pedreros, Daniele. Y con especial cariño agradezco el apoyo de Caro Geoffroy y Rayen Gho, compañeras y amigas durante todo este proceso, riendo y sufriendo juntas.

En último lugar, y no menos importante, agradezco a todas esas personas que de algún modo y muchas veces sin notarlo, me ayudaron a tolerar la frustración recurrente propia de un trabajo de tesis, y convirtieron mi paso por el postgrado de geología en una etapa maravillosa. Muchas gracias chiquillos de la “salita de postgrado” por las oncesitas y cafecitos y a mi querido equipo BdR F.C. que me ha dado tantas alegrías.

Finalmente, doy gracias infinitas a mi más grande soporte: mi familia. Gracias por el apoyo, la comprensión y la paciencia infinita. Y sobre todo, por permitirme ser una soñadora en esta vida.

Table of contents

List of figures

List of tables

List of Appendix

1. INTRODUCTION

Stratovolcanoes are the expression on the surface of complex and enigmatic magmatic plumbing systems. Over the past few decades, geophysical and petrologic techniques have been enormously useful to increase the knowledge about magma storage. A considerable number of tomographic studies have provided insights into magma distribution beneath a volcano (e.g. Agostinetti and Chiarabba, 2008; Waite and Moran, 2009; Paulatto et al., 2012), as well as inferring the temporal evolution of reservoirs (Koulakov et al., 2013). Concerning magma distribution on surface and accumulation of erupted material, morphological studies of stratovolcanoes have been focused mainly on a quantitative characterization of the size and shape of volcanic edifices (e.g. Grosse et al., 2009; Karátson et al., 2010; Grosse et al., 2012). Differences on volcano form have been attributed to the number of growth stages, composition, eruptive rate, vent position and migration, degree of erosion, lava/tephra ratio, deformation, and ultimately underlying factors such as magma flux and tectonic setting (Grosse et al., 2009). The variability of topographic profiles on composite volcanoes has been also addressed. Davison and De Silva (2000) suggested that straight line profiles are associated to primary volcanoes, whereas concave-upward profiles are linked to a “maturity state”. Karátson et al. (2010) on the other hand, defined C-type volcanoes and P-type volcanoes, both with a logarithmic topography profile on lower flanks, but different upper flanks. C-types volcanoes have a constant and steep upper flank and they should grow, in addition to short lava flows, by a high frequency of mild explosive eruptions. The upper slope construction mechanism includes deposition of fallout and ballistic tephra, occasional welding and slope creep. Conversely, P-type volcanoes with curved slopes are associated to a more effusive activity and scarcer mild explosive eruptions (strombolian) forming the upper cone. Thereby, the upper flanks are more strongly shaped by lava flows than by pyroclastic deposits. The logarithmic shape of stratovolcanoes has also been explained by Francis (1993) providing the formula $r=B*e^{Mh}$, where r=basal radius, h=volcano height and B and M are constants.

Despite it is reasonable to conceive the eruptive products as a reflection of the deep magmatic system characteristics, joint analysis of magma plumbing system and morphometric properties of the stratovolcanoes are scarce. Few authors have made efforts to understand the influence of the magmatic system properties on the observed volcanic edifice shapes or the emitted products forming it. Magma density and viscosity, volatile content, magma chamber overpressure and depth, crustal structure, magma supply rate to the chamber and eruption frequency, have been recognized as factors influencing the resulting erupted material (Ben-Avraham and Nur, 1980; Wilson et al., 1992; Stasiuk and Jaupart, 1997; Vergniolle and Mangan, 2000; Huppert and Woods, 2002).

It has been suggested that some factors control the maximum height that a volcano can attain, such as: the nature of the volcanic products, the duration of magma supply, differentiation of the magmas, and the crustal density profile (Davison and De Silva, 2000). Above certain height (observational evidence suggests the limit is around 3000 m height) it would be physically unlikely that lava flows can be emitted from the summit (Davison and De Silva, 2000). As volcano grows, a load is exerted at the crust's surface modifying the stress field at depth and controlling the volcanic activity (Pinel and Jaupart, 2000; Pinel et al., 2010). Morphological observations at stratovolcanoes have been linked to this control. First, early lavas erupted from the summit tend to be more voluminous and extensive than later lavas (e.g. Licancabur volcano; Davison and De Silva, 2000). Second, it has been recognized an evident increase of eruption rate after a major episode of edifice destruction (e.g. Parinacota volcano; Clavero et al., 2002). And third, it has been proved the dependence of vent distribution to volcano edifice with analogue experiments (Kervyn et al., 2009).

The available evidence has not been put together to propose a theoretical model that links the magmatic system properties and the surface volcano morphology. The similar height and volume of volcanoes associated to a certain tectonic regime suggests there are few processes that control their sizes (Wood, 1982). However, the current knowledge is not enough to quantify the control of the reservoir properties on volcano morphology.

In this work, we applied a model based on volcano topographic profile, with the aim of providing insights into the link between magmatic system properties and the resulting volcano morphology. Our simple model considers a volcano built only by pilling of lava flows erupted from a single summit and not affected by degradational processes (caldera formation, avalanche, long-term erosion), changes in vent location, pyroclastic accumulation or adventitious volcanism. An eruption which generates every lava flow is triggered by the influx of new magma in the reservoir with fixed depth and size. First, we seek to evaluate the magma storage location influence on volcano profile. Next, we assess the effect exerted by the reservoir depth and size, magma density and viscosity, overpressure on the reservoir and crustal density, on lava flow volumes erupted, and finally on volcano dimension and the number of eruptions required to build it. Field data and morphological observations of composite volcanoes (topographic profile, lava flow volume estimates) are needed to infer the value of magma chamber depth and size, as well as the estimated overpressure regarded to trigger an eruption.

The model was tested on three stratovolcanoes of the Central and Southern Volcanic Zones of the Andes of Chile with noticeable morphological differences: Lascar, Lonquimay and Llaima (Fig. 1). Llaima volcano is one of the most bulky volcanoes of the Andes, has almost 400 km^3 in volume and 2430 m height above its base (Naranjo and Moreno, 2005). Lonquimay and Lascar volcanoes do not more than 1500 m height and exhibit a moderate volume of 59 km^3 (Polanco, 2010) and 15 km^3 (Gardeweg et al., 2011) respectively. Topographic profiles are also different. As Llaima volcano has a concave upward topographic profile, Lonquimay volcano presents a straight line topographic profile. Vent migration in Lascar volcano leds to a notorious asymmetry in flanks.

The erupted magmas in Lascar, Lonquimay and Llaima are significantly different. Lascar volcano products range from dacite to andesite, with changes linked to vent migrations (Gardeweg et al., 2011). Llaima volcano effusive activity, is characterized by mainly basaltic andesitic compositions. However, along its time of activity, this volcano has shown stages characterized by basaltic lava flows (current activity) and dacitic pyroclastic flows (~13 ka and ~7 ka; Naranjo and Moreno, 2005). Lonquimay volcano eruptive products are

predominantly basaltic-andesitic, although along its entire timespan, there was the occurrence of basaltic and andesitic lavas. Despite every volcanic system has undergone magma compositional variations, we believe that the range of magma composition is limited, as well as the viscosity, considering the effusive activity during the timelife. Viscosity estimates in this study are obtained by using samples collected from different stages of the growth of these volcanoes (See Appendix 5). We believe that Lascar, Lonquimay and Llaima are appropriate volcanoes to test our model as they show contrasting morphology and magma composition, as well as similar compositions along the time of effusive activity, allowing us to use an average magma composition value.

We first present the volcano morphology-magmatic system properties linking model and a briefly methodology used in this work. Next, we applied the proposed model on the above-mentioned Chilean stratovolcanoes obtaining estimates of magma chamber depth and size, volcanic edifice volume, among others. Additionally, we used classic methods to constrain values of reservoir location and volcanic edifice volume at Lascar, Lonquimay and Llaima volcanoes. We applied petrological methods and collected available geophysical data to estimate magma chamber depth, and DEMs to obtain volcano volume estimates. Finally, we compare our model results and values obtained by using other methodologies, and validate (or not) the proposed physical model as well as discus about its implications on the field of volcano morphology.

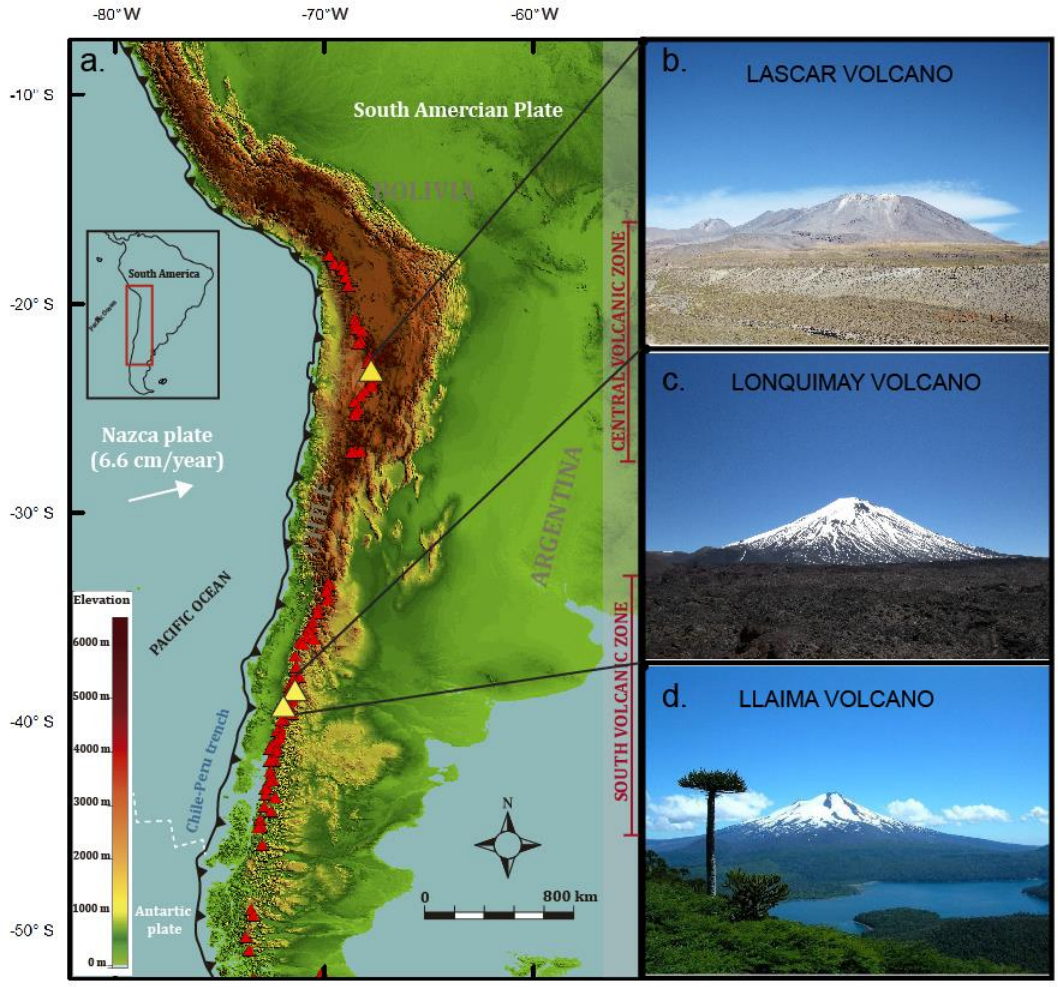

Fig. 1. (a) Map of the western part of South America with major tectonic features. The Andean volcanic arc is represented for the set of volcanoes (red triangles) and Lascar, Lonquimay and Llaima are highlighted as yellow triangles. (b) NW-SE panoramic view of Lascar volcano. (c) SE-NW view of Lonquimay volcano and Navidad cone. (d) SE-NW view from Llaima volcano

2. METHODS AND APROACHES

We first carried out a morphological characterization of Lascar, Lonquimay and Llaima volcanic edifices with the aim of estimating the height, average slope, the volume and basal area of the main edifice, as well as to analyze its topographic profile. We used a Geographical Information System and Digital Elevation Models (DEMs) based on the Shuttle Radar Topography Mission (SRTM) with a special resolution of 1 arc-second for global coverage. We complement this information with geological maps of these volcanoes elaborated by the Survey of Geology and Mining of Chile (SERNAGEOMIN), Google Earth software images and field observations. Due to the fact that our analysis is focused on the main volcanic edifice only, some criteria to define the basal extent must be defined. The surrounding rough basement, dense vegetation, adventitious volcanism and emplacement of lava flows in valleys far away from the volcanic edifice, make difficult to delineate the base of the volcano. Our approach consist in identifying the significant change in the slope gradient between the volcanic edifice and surrounding terrain and then trace manually the baseline, considering observation from DEMs parameters (curvature and slope maps), geological maps, satellite and field observations.

We performed field work at Lascar, Lonquimay and Llaima volcanoes, with the aim of sampling and morphologically characterizing some lava flows from different volcano units that build up the main edifice. We studied 3 lava flows from Lascar, 5 from Lonquimay and 4 from Llaima volcanoes (Table 1 and Fig. 2). We measure lava flow thickness (using a laser distance meter, an inclinometer and geometric considerations), and we complemented with aerial images to finally estimate the lava flow volumes. We sampled lava flows based on age, from the oldest to the youngest ones, ensuring that the selected samples are representative of the overall volcano growth process (Table 3 and Fig. 2). We carried out a petrographical study of the samples with the aim of selecting the appropriate crystals for thermobarometric models (available in the literature) to estimate the reservoir(s) location associated to the above-mentioned volcanoes. Mineral chemical composition measurements were obtained by Electron Microprobe Analyzer (EMPA).

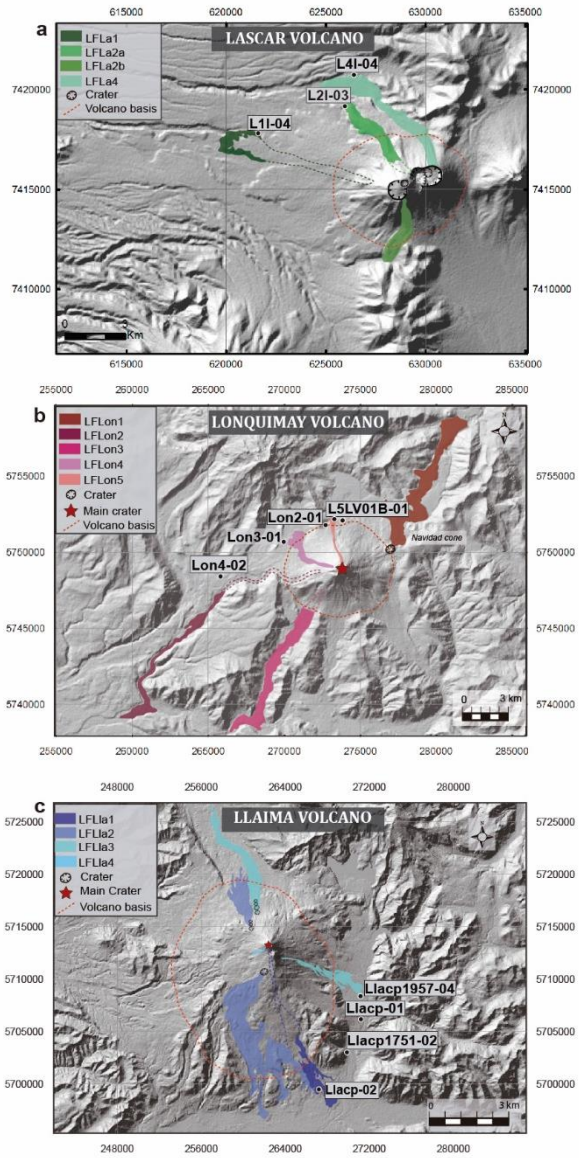

Fig. 2. DEMs from (a) Lascar, (b) Lonquimay and (c) Llaima volcanoes based on the Shuttle Radar Topography Mission (SRTM). Highlight in colors the lava flow units whose volumes have been estimated in this study and have been listed in Table 1. The baseline shown in the maps was defined according to approaches explained above and has been used to estimate the volcanic edifice volume. Outcrops locations logged for this study are shown in these maps.

3. MODEL FORMULATION

3.1. General framework

We developed a simple model of magma ascent with the aim of evaluating the influence of some of the magmatic system properties in the construction period of the volcano. For simplicity, the volcano will be considered as a cone made up only by lava flows. A diagram illustrating the geometry of the model is shown in Fig. 3.

We consider a deep source, which provides magma to a shallower magma chamber of constant volume V_C and located at depth H, which in turn is connected to the volcanic edifice at surface through a cylindrical conduit. We suppose that every eruption occurs due to the input of new magma (ΔV) into the magma chamber, driving an increase in its pressure until its walls fail, which occurs at a critical overpressure ΔP_C. For simplicity, in this model the replenishment rate of magma to the reservoir is constant during the growth of the volcano and it is calibrated according to the chronology data of each volcanic system.

Effusive eruptions contain small quantities of gas. In subaerial eruptions the volatile fraction volume is significant only within tens of meters of surface (Stasiuk and Jaupart, 1997 and references therein). Considering these observations, we assume magma ascent as a laminar and volatile free. The volumetric flow rate of the ascending magma in a dike following Munson et al. (1990) is given by:

$$Q = \frac{w^3 l}{12\mu}\left(\Delta\rho g + \frac{\Delta P_c}{H}\right) \quad (1)$$

Where w and l are the dike width and length ($w << l$) respectively and μ is the magma viscosity. If we consider the ascent conduit as a cylindrical conduit instead of a dike, the

term out of parenthesis is replaced by $\frac{\pi r^3}{8\mu}$ where r is the radius of the conduit. The terms in parenthesis are the gradient generated by the overpressure in the magma chamber over lithostatic pressure and the buoyancy, being $\Delta\rho$ the difference between mean crust density ρ_c and mean magma density ρ_m . Previously, similar expressions were suggested by Wadge (1981) but without considering the buoyancy and by Stasiuk and Jaupart (1997) considering an extra term associated to the effect of the thickness of a lava flow emplaced on surface.

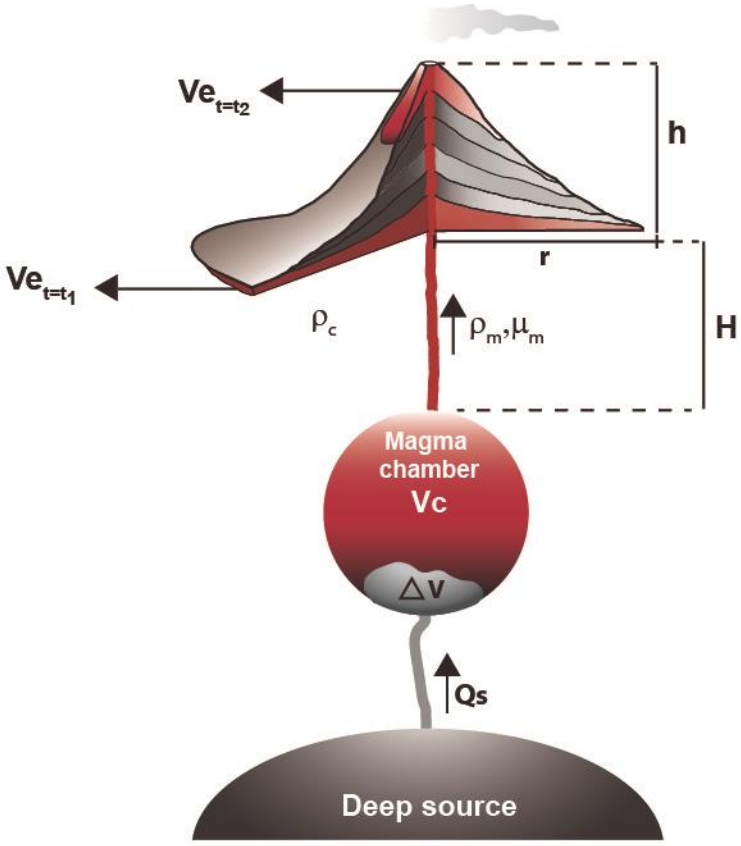

Fig. 3. Model geometry of the magmatic system.

3.2. Model assumptions and parameters determination

We assume that an eruption will end when the pressure gradient driving the eruption becomes negligible, i.e. $\Delta\rho g + \frac{\Delta P_c}{H} = 0$. While the eruption is in progress, ΔV varies through time due to the evacuation of magma from the chamber as follows:

$$\Delta V(t) = \Delta V_i - V_e(t) \tag{2}$$

Where ΔV_i is the initial injected volume of magma in the chamber that generates an overpressure ΔP_{ci} and $V_e(t)$ is the erupted volume at time t. According to Blake (1981) the relationship between ΔP_{ci} and ΔV_i is:

$$\Delta V_i = \frac{\Delta P_{Ci} \cdot V_c}{k} \tag{3}$$

Where k is the effective bulk modulus of the magma that incorporates the effect of the bulk modulus of the surrounding wall rock (Huppert and Woods, 2002). Combining Eqs. (1) and (3) we obtain an expression that relates the erupted volume with the magmatic system properties:

$$Q(t) = \frac{\partial V_e(t)}{\partial t} = \frac{w^3 l}{12\mu}\left(\Delta\rho g + \frac{k}{V_c H}\left(\Delta V_i - V_e(t)\right)\right) \tag{4}$$

$$\frac{\partial V_e(t)}{\partial t} = \frac{w^3 l}{12\mu}\Delta\rho g + \frac{w^3 l k \Delta V_i}{12\mu H V_c} - \frac{w^3 l k V_e(t)}{12\mu V_c H} \tag{5}$$

The development of the analytical solution of Eq. (5) is explained in more detail in Appendix 1. Here we assume that the conduit dimension remains unchanged through time as well as the magma viscosity. Otherwise Eq. (4) is more complex and can be solved

numerically. The total erupted volume of magma evacuated during an eruption is given by:

$$V_e(t \to \infty) = \frac{V_c}{k}(\Delta P_{ci} + \Delta\rho g H) \quad (6)$$

This expression can be modified if the effect of the volcano edifice height is considered. Pinel and Jaupart (2000) suggested that the lithostatic pressure at the chamber level is not affected by the volcanic edifice if this is deep enough. At a depth around 2 r_{basal} (basal radius) the normal stress due to the volcanic edifice is negligible. If we consider the effect of height of a volcano edifice, Eq. (1) must be modified considering the hydrostatic pressure exerted by the magma in the conduit of length $H + h$ instead of H at the base of the system obtaining:

$$Q = \frac{w^3 l}{12\mu}\left(\frac{\Delta\rho g H + \Delta P_c - \rho_m g h}{H + h}\right) \quad (7)$$

And the expression (6) changes to:

$$V_e = \Delta V_i - \frac{V_c}{k}(\rho_m g h - \Delta\rho g H) \quad (8)$$

We can evaluate the effect of the volcanic edifice height on the ascent of magma observing 2 lava flows emitted at different stages (t_1 and t_2) during the construction of the volcano. We first addressing the simplest case: we will consider the first lava flow emitted being $t_1 = 0$ and $h_1 = 0$, and a second one erupted through the current summit h_2 at t_2. From Eq. (8) the ratio between the emitted volumes will be:

$$\frac{V_{e(t=t_2)}}{V_{e(t=t_1)}} = 1 - \left(\frac{\rho_m g h}{\Delta\rho g H + \Delta P_c}\right) \quad (9)$$

From field data and morphometric analyses, we can estimate the volumes of lava flows emitted at different heights, obtaining a value for the ratio $\frac{V_{e(t_2)}}{V_{e(t_1)}}$. The magma chamber depth can be estimated from several approaches, such as geophysics methods, thermobarometry and, as we will show in Section 3.4, using the volcano topography. The above-mentioned parameters will allow us to extrapolate the value of ΔP_c which satisfies Eq. (9).

From Eq. (8) we can derive an expression for V_c. The volume of the chamber of course is not constant. The magma that enters in the chamber during an eruptive episode is not equal to the magma that leaves it. However, with the aim of modeling the growth of a volcano depending on their magma system properties, we will consider a fixed dimension and depth of the magma chamber.

3.3. Volcano edifice construction

We model the growth of a volcanic edifice depending on the overmentioned parameters of the deep systems. After each eruption, the edifice size increases due to the addition of a new volume of lava given by Eq. (8). The growth mechanism depends on the following assumptions:

1. The total volume erupted in each eruption will add material to the stratocone; accordingly, we do not consider loss of material through erosion, as erosional processes did not modify the regular shape. Some authors suggest that in fresh cones erosion only operates through the development of gully systems called parasol ribbing (Karátson et al., 2010). This implies:

$$\sum_{t=0}^{t=t_f} V_e(t) = V_v \tag{10}$$

Where V_v correspond to the total volcano edifice volume.

2. The lava flows length can be approximated by the relationship proposed by Kilburn and Lopes (1991):

$$L_{\max} = CV_e^{0.5} \tag{11}$$

Where $L_{\max}$ is the maximum extension of a lava flow. C is a constant whose values fluctuate between 1-2 for basaltic flows and around 0.5 for more differentiated compositions. The basal radius of a volcano will be equal to the length of the first lavas emitted as these are the longest ones.

3. The required overpressure ΔP_C to trigger an eruption will be considered constant through volcano growth time as well as ΔV_i. Nevertheless, the volume injected in the magma chamber, responsible to lead the critical overpressure and hence an eruption, is not constant. After every effusive event, some of material remains in the reservoir. Here we impose that the input of volume triggering an eruption is equal to the volume erupted during the previous eruption:

$$\Delta V_i(t = t') = V_e(t = t'-1) \tag{12}$$

4. Eruptive activity will stop due to the growth of the volcanic edifice without taking into account other possible mechanisms. An eruption only can be triggered if exist a positive pressure gradient ($\Delta P_c + \Delta\rho gH - \rho_m gh > 0$). The growth of the volcano will decrease the pressure gradient, driving the eruption to zero, i.e. preventing the ascent of magma to the surface. The volcano will extrude lava flows until it reaches its maximum height $h_{\max}$

$$h_{\max} = \frac{\Delta P_c}{\rho_m g} + \frac{\Delta \rho H}{\rho_m} \quad (13)$$

5. The replenishment rate of magma from a deep source to the magma chamber Q_s, for simplicity considered constant through time, is equal to:

$$Q_s = \frac{\Delta V_i}{\Delta t} \quad (14)$$

With Δt the time between two consecutive eruptions and replenishment time of the magma chamber. We assume $\sum_{n=0}^{n=n_f} \Delta t_n$ correspond to the time of eruptive activity of each volcano. As Lascar, Lonquimay and Llaima volcanoes have chronology data, we know how old these volcanoes are.

3.4. Constraining the magma chamber depth (H) by assessing the volcanic edifice profile

We will use a set of equations developed by Castruccio et al. (2017) which are explained on Appendix 2. This model relates the shape profile of a volcano with the location of the magma chamber where the injection of new magma triggers the eruptions. Using geometrical considerations, the topographic profile of a volcanic edifice of height $h_{\max}$ and basal radius r_{basal} which has been built by a pile of lavas distributed radially from a central vent, is represented by Eqs. (15) and (16). For distances close enough to the vent, the slope will be greater than the repose angle ϕ_{crit}. We imposed that for distances $r < r_{crit}$ (with r_{crit} the distance point where the slope angle attains ϕ_{crit}), a constant slope equal ϕ_{crit} will be used. The average slope of the whole upper profile of composite volcanoes is approximately 30° (Karátson et al., 2010), very similar to the angle of repose of scoria cones ranging 30-31° (Wood, 1980).

$$h(r) = \alpha\left(\frac{1}{r} - \frac{1}{r_{basal}}\right) \quad r > r_{crit} \tag{15}$$

$$h(r) = (r_{crit} - r)\tan\phi_{crit} + \alpha\left(\frac{1}{r_{crit}} - \frac{1}{r_{basal}}\right) \quad r < r_{crit} \tag{16}$$

$$r_{crit} = r_{basal}\left(1 - \sqrt{1 - \frac{h_{\max}}{r_{basal}\tan(\phi_{crit})}}\right)\tan(\phi_{crit}) \tag{17}$$

$$\alpha = r_{basal}{}^{2}\left(1 - \sqrt{1 - \frac{h_{\max}}{r_{basal}\tan(\phi_{crit})}}\right)^{2}\tan(\phi_{crit}) \tag{18}$$

$$V_v = \pi\alpha(r_{basal} - r_{crit}) + \frac{\pi r^{3}{}_{crit}\tan(\phi_{crit})}{3} \tag{19}$$

With Eqs. (15), (16), (17), (18), (19) and (13) and assuming the volcano is close to its maximum height, we can constrain the value of H which allow us to obtain the best adjustment between the model and the real profile of the volcano. We therefore link the depth of the magma chamber with the shape of the volcano on surface, obtaining an alternative method to estimate the magma storage location.

4. APLICATIONS

4.1. Principle and data analysis

Here we apply the physical model described in Section 3 at Lascar, Lonquimay and Llaima volcanoes (Fig. 4 and 5). With Eqs. (13), (15) and (16) we fitted the model predicted profile with the volcano topography and estimated the depth of the magma chamber for these volcanoes. We selected the most regular profile for each volcano (black full lines in Fig.7, 9 and 11), task especially difficult for volcanoes like Lascar and Llaima, as they show notorious asymmetries in their profiles. The parameters used are displayed in Table 2 and the results are shown in Fig. 7, 9 and 11. In the following section, we will assess our model application results comparing with data obtained by geobarometry and geophysics studies available in the literature.

We also modelled the growth of these volcanic edifices by piling of lavas with volume defined by using Eq. (8), and calculated the topographic profiles according to Eqs. (15) and (16). We aimed to simulate the growth of the current edifices, so we imposed that the model execution stops when a volcano attains its current height. This model allowed us to approximate the number and frequency of effusive eruptions required to build these volcanic edifices. For each volcano, we used estimates of magma chamber depth and size, magma and crustal average densities, overpressures and rates of replenishment of magma to the chamber from a deep source (Table 2). Some morphological estimations as basal radius, height and slope are also required to run the model. We used values of H obtained applying the topographic model, while the procedure and assumptions to acquire the value of the other parameters will be explained in the paragraphs below. We adjusted the replenishment rate to obtain a lifetime similar to the oldest age according to the chronology data available. Results are shown in figure 12 and 13.

We estimated the magma density value including the density of the melt and the solid phase represented by crystals. We defined the density of the crystals considering the

fraction of phenocrysts (we assume that crystals were formed before ascent) and an average density of plagioclase of 2680 kg/m^3 as it is the predominant mineral phase in all samples. We constrain the melt density considering bulk rock compositions, magma temperature and variations of pressure from chamber to surface, averaging the density. The average crustal densities for each volcano were taken from Lucassen et al. (2001) and Tašárová (2007).

The overpressure required to trigger an eruption was constrained applying Eq. (9) presented in Section 3, using volumes of lava flows erupted at different time (and altitude) during the edifice construction (Table 1 and Fig. 3). At Lascar and Lonquimay we selected lava flow volumes erupted from the base and the summit: LFLa1 and LFla4 (Lascar) and LFLon1 and LFLon5 (Lonquimay). At Llaima volcano the volumes of lava used were LFLla_a and LFLla3, erupted from the base and ~1700 m above the base approximately. Volume estimation of the mentioned lava flows are shown in Table 1.

Table 1**:** Volume of lava flows from Lascar, Lonquimay and Llaima volcanoes. Mostly estimated using morphometric observation. LFLla_a and LFLla_1957 lava flow volumes were obtained using Eq. (11).

Lava flow	Volcano/ unit	Age (ka)	Age reference	Volume (km^3)	Volume reference
LFLa1	Lascar/ Unit 1	230±40	Gardeweg et al. (2011)	0.29000	This report
LFLa2a	Lascar/ Unit 2	22±9	Gardeweg et al. (2011)	0.19000	This report
LFLa2b	Lascar/ Unit 2	63±13	Gardeweg et al. (2011)	0.10000	This report
LFLa4	Lascar/ Unit 4	7.17±1.25	Gardeweg et al. (2011)	0.14000	This report
LFLon1	Navidad cone	*1988-1990		0.19000	Castruccio and Contreras (2016)
LFLon2	Lonquimay/ Unit 2	70±40	Edmundo Polanco, personal comunication (2015).	0.03000	Gho (2013)
LFLon3	Lonquimay/ Unit 3	-		0.15000	Gho (2013)
LFLon4	Lonquimay/ Unit 4	-		0.03800	Gho (2013)
LFLon5	Lonquimay/ Unit 5	-		0.02800	Gho (2013)
LFLla_a	Llaima/ Unit Llaima Ancestral	185 ka		0,48400	This report
LFLla1	Llaima/ Unit Llcp	< 3		0.15488	This report
LFLla2	Llaima/ Unit Llcp	*1640		0.16460	This report
LFLla3	Llaima/ Unit Llcp	*1957		0,23725	This report
LFLla4	Llaima/ Unit Llcp	*1994		0.00048	This report

*A.C years.

For deep magma chambers like the one constrained for Llaima volcano, the magma is undersaturated and hence less compressible and with a larger bulk modulus of ~10^{10} Pa. For shallower magmas, we consider volatile saturation and the presence of the gas phase

leads to a more compressible magma, with a bulk modulus smaller in a range of 10^8 and 10^9 Pa (Huppert and Woods, 2002). For our calculations, we used a value of $5*10^9$ Pa for both Lascar and Lonquimay volcanoes.

We used Eq. (10) to estimate the volume of the magma chambers associated to Lascar, Lonquimay and Llaima volcanoes. For each on one, we tested the model by using different erupted volume measurements and their respective vent elevations, which gave us similar values for V_c. Finally, we used an average value.

Table 2: Summary of constrained parameters used to apply our model on Lascar, Lonquimay and Llaima volcanoes.

	Lascar	Lonquimay	Llaima
Height H (m)	1050	1286	2430
Basal radius r_{basal} (m)	6.38	4.5	15
Critical angle ϕ_{crit} (°)	25	30	22
Bulk modulus k (Pa)	$5*10^9$	$5*10^9$	10^{10}
Magma density ρ_m (Kg/m^3)	2543	2603	2653
Crustal density ρ_c (Kg/m^3)	2680	2750	2820
Magma chamber volume V_c (km^3)	40	30	50
Overpressure ΔP_C (Pa s)	30	26	40
Replenishment rate Q_s (km^3/ky)	0.053	0.13	0.95
Magma chamber depth H (km)	12	6	18

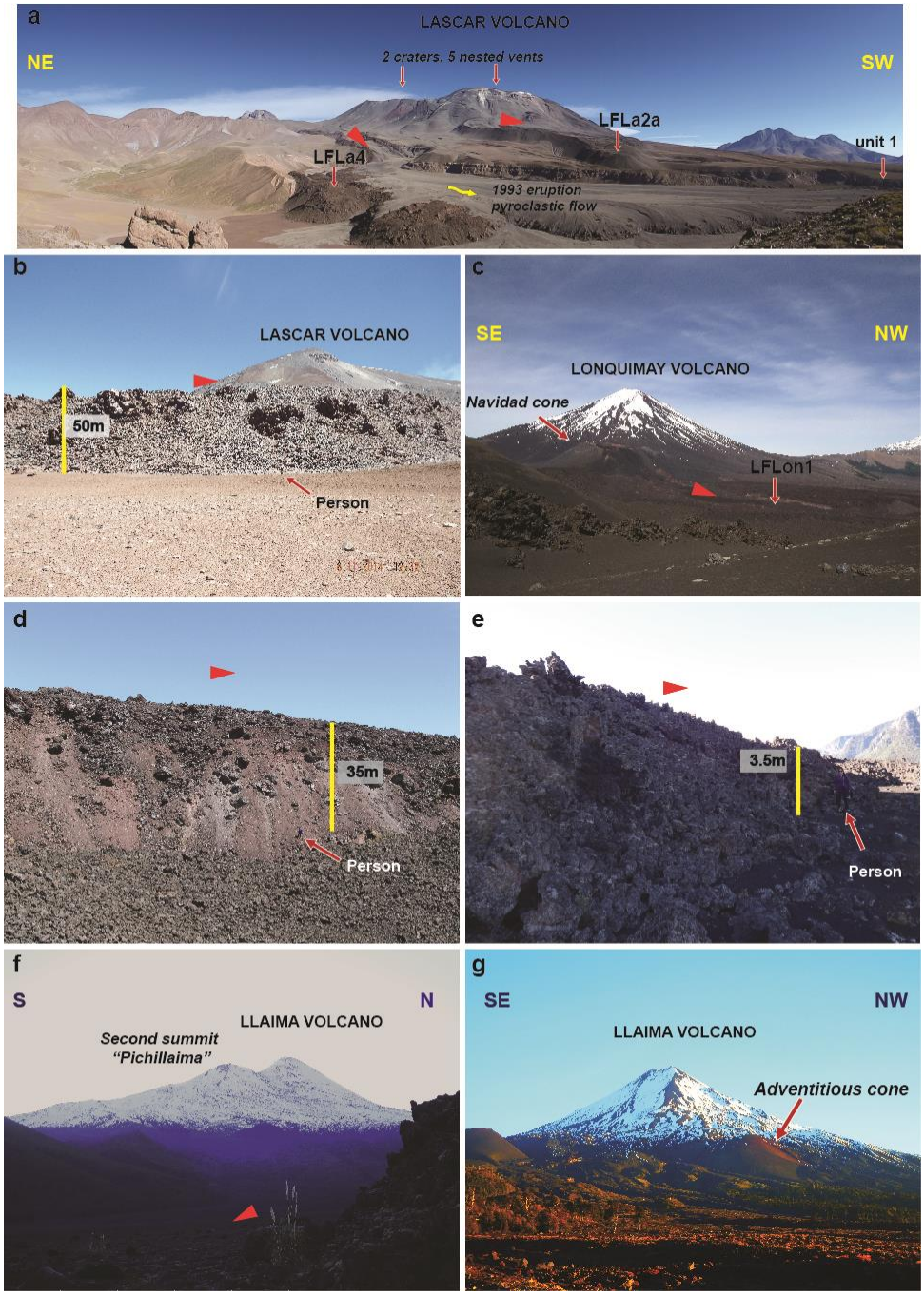

Fig. 4. Photos from Lascar, Lonquimay and Llaima volcanoes. (a) NE-SW view from Lascar volcano, highlighting the overlap of lava flows units and a pyroclastic flow associated to 1993 eruption resting in the central channel of one of these. (b) Middle part of blocky LFLa4 lava flow (around 6 km from the emission center). (c) SE-NW view from Lonquimay volcano. On its NW flank is located the Navidad cone and the lava flow emitted during the eruption on 1998-1990. (d) 1988-1990 'a'ā -blocky transitional Navidad lava flow unit. LFLon-1 in this work. (e) Eastward 'a'ā lava flow unit from 1957 eruption. (f) S-N view from Llaima volcano. Here can be distinguished the second summit called "Pichillaima". (g) SE-NW view from Llaima, with the before mentioned second summit is hidden and a regular upper part of the main edifice can be recognized.

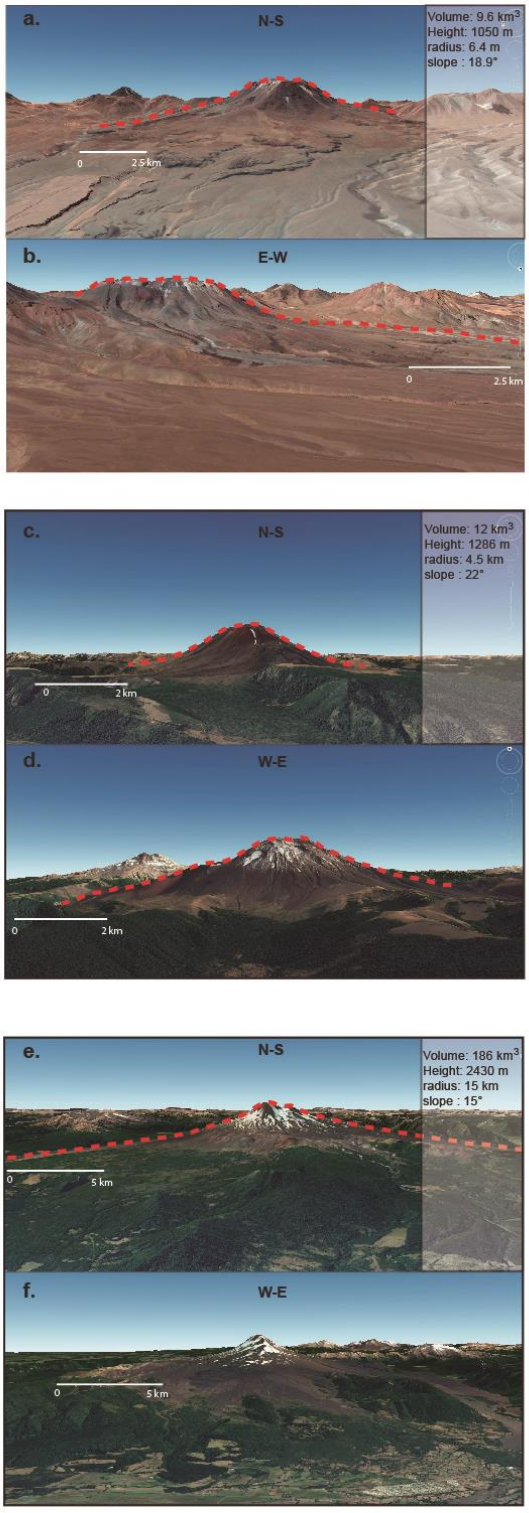

Fig. 5. Topographic profiles of (a and b) Lascar, (c and d) Lonquimay and (e and f) Llaima volcanoes. Notice the concave upwards topographic profile of Llaima and the more straight line slopes of Lascar and Lonquimay.

4.2. Lascar volcano

4.2.1. Eruptive history and geological setting

Lascar volcano (23,3ºS; 67,7ºW) is located in the Central Volcanic Zone (CVZ) (16°-28°S). Here the crust is >70 km thick and the volcanic front is located 240-300 km east of the trench, reaching a maximum distance of 400 km from the Perú-Chile trench at around 23°S (Díaz et al., 2012). Lascar is an asymmetrical composite stratovolcano. It is considered the most active volcano in Northern Chile during historical times, having produced about 30 explosive eruptions since the XIX century, mostly vulcanian with some exception like the 1993 sub-plinian eruption. Emission of lava flows during the recent time have been not reported (Matthews et al., 1997). Along its entire life, Lascar volcano showed effusive and explosive style, involving the extrusion of thick lava flows and domes. Major explosive events with medium to small volume pyroclastic flows are also recorded although no calderas have been formed (Gardeweg et al., 1998; Gardeweg et al., 2011). The eruptive activity in Lascar always occurs at the summit with no evidence of flank activity. The emitted products are predominantly two-pyroxene andesites and dacites, with subordinated hornblende dacites and andesites (Matthews et al., 1994). The volcanic history of this volcano began in the middle Pleistocene (ca. 240 ka) (Gardeweg et al., 2011) with the construction of an eastern andesitic cone. Then, the active vent migrated westward accompanied by a shift to a more silicic composition and the formation of the mainly dacitic coalescent western cone (Gardeweg et al., 2011). The current activity is concentrated at the central and deepest crater (Gardeweg et al., 1998).

4.2.2. Morphological characterization

Lascar volcano is an irregular composite volcano elongated on the NE-SW direction, with evidences of continuous changes in vent location (Fig. 4a and 6). Two truncated cones are recognized with five nested craters, aligned in E-W direction, being the central and deepest crater the active one (Gardeweg et al., 2011). These cones are aligned along

with Aguas Calientes volcano to the east. This trend lies astride a major N-S crustal lineament; The Miscanti Line which controls the location of some stratovolcanoes like Lascar and Lejías (Matthews et al., 1994; Gardeweg et al., 2011). The average flank slope is 18.9°, with lower values (~5°) in distal zones. Toward the summit, slopes reach a maximum angle of 36.5° (Fig. 5a and b). Lascar volcano shows numerous well-preserved lava flows with mainly blocky morphology. Oldest units show evidence of erosion and oxidation, while several flows belonging to units 2 and 4 display marked levées and central channels. Pyroclastic material accumulated in central channels and distal zones (including ash fall, lahars and pyroclastic flows) is observed in several of them (Fig. 4a). The Miscanti fault activity, the presence of the oldest *Aguas Calientes* volcano located just at the eastern flank and the tilted basement to the west, have probably prevented the homogenous distribution of Lascar lavas, stacking them mainly to the west side. This process has caused major differences in the height at the volcano which ranges from 777 to 1329 m from east to west. The length of lava flows which moved to the west, reaches maximum extensions at around 16 km. Contrasting, northern and southern flank lava flows do not exceed 4 km length. We estimated some lava flow volumes from different evolutionary stages of the volcano using field observations and image analysis (Table 1). Results revealed values ranging from 0.27 to 0.1 km^3, showing a general decrease with time of dimensions and length. Thickness increases from proximal to distal zones, going from 15 to 60 m in average, reaching 100 m in the front of some lava flows like LFLa2a. The blocks in the lava flows have sizes between 1-4 m and show flat surfaces and sometimes banding and striation (Fig. 4b). Using methodology described in Section 2, we constrained a basal area for Lascar volcano around 29 km^2 and a volume of 9.6 km^3 (Fig. 6).

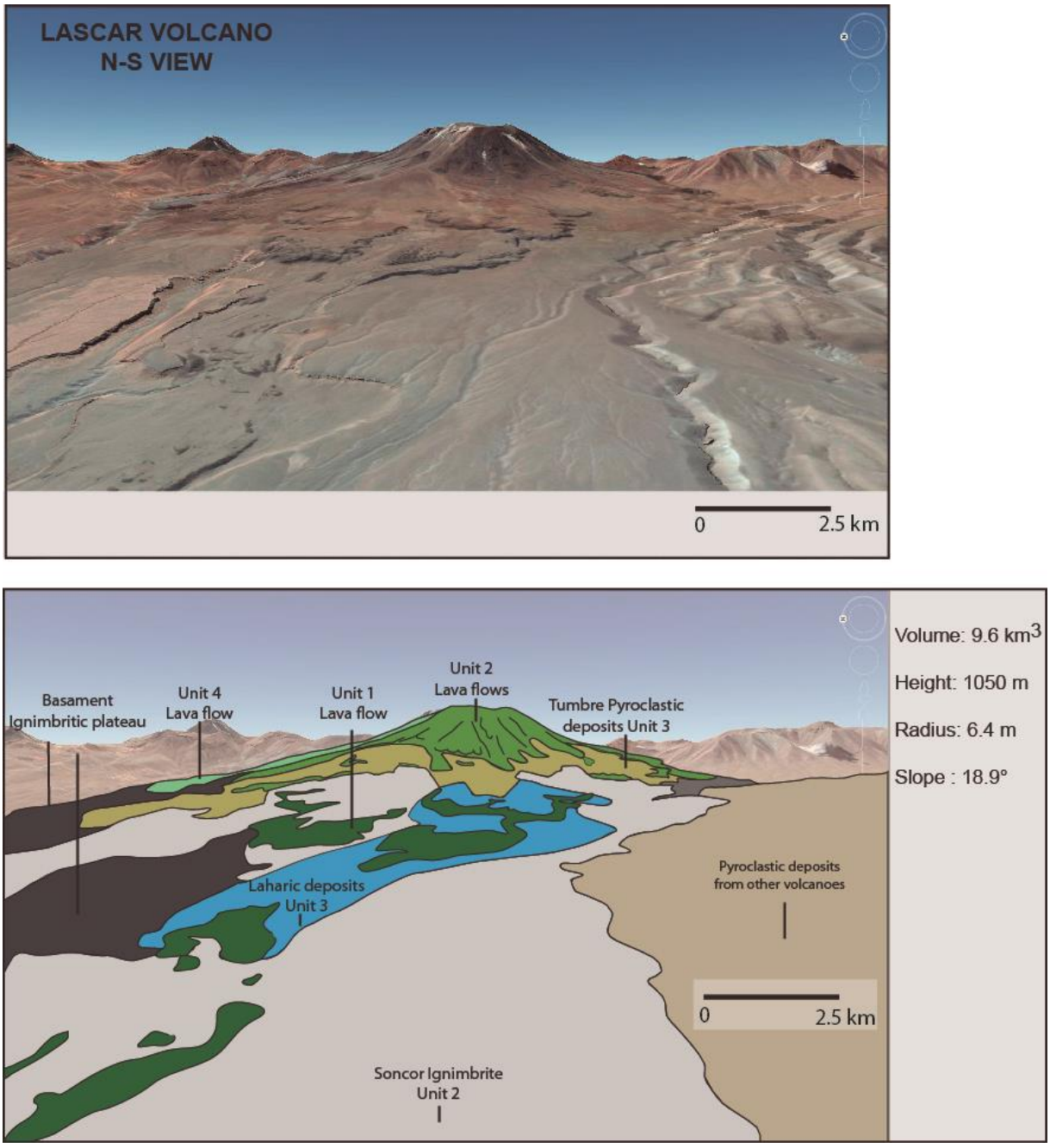

Fig. 6. N-S view of Lascar volcano. Mapped of eruptive deposits of Lascar volcano are drawn in the bottom panel. Deposits are named according to unit names defined on geological map (Gardeweg et al., 2011).

4.2.3. Volcano edifice topography and magma chamber location (H)

In order to implement the model on Lascar volcano, we estimated an average basal radius of 6.38 km and a critical angle of 28° (Table 2). The sustained shift of the Lascar volcano's vent location, introduces an extra complexity for an appropriate testing. Indeed, the model assumes a volcano growing from a single vent, contrasting with the Lascar volcano building process. Comparing the model profile and the topography of Lascar volcano, noticeable differences are shown but they are associated to the lateral growth, direct consequence of the vent displacement. However, we believe that a good strategy to address this problem, is to apply the model, fitting the theoretical profile to only one flank. Hence, we prevent the lateral growth influence on the results. In this case, we fitted the model predicted profile to the northern flank of the NW-SE profile because we focused our morphological and petrological analyses on lava flows emitted from the NW crater.

In the other side, the model works for volcanoes which are close to reach their maximum height. Opposing, the Holocene activity of Lascar volcano encompasses extrusion of a sizable lava flow (LFla4), small domes within the crater, quiescent degassing and explosive events. Despite the evidence suggests that Lascar volcano is far from attaining its maximum height, we applied the model without major difficulties associated to its prevailing activity. Our results reveal a good fit of the model profile and the Lascar volcano topography, especially in the upper flank. The best fitting was obtained using a value for the magma chamber depth of 12 km depth. (Fig. 7c).

4.2.4. Volcano building: eruption quantity and frequency

For Lascar volcano, we considered a 40 km^3 magma chamber volume located at 12 km depth, subjected to an overpressure of 30 MPa and a reservoir magma replenishment rate of 0.053 km^3/ky. Results show that in order to attain its current average altitude (1050 m), 50 effusive eruptions are required, with lava flow volumes in the range of 0.3 to 0.1 km^3 in a period of 204 ka (Fig. 12 and 13). The volcanic edifice generated by the pile of lavas attains 11 km^3 and the average eruption recurrence is around 4 ky. Using Eq. (13),

depending on the depth of its magma chamber, the maximum height that Lascar volcano could reach is 1850 m.

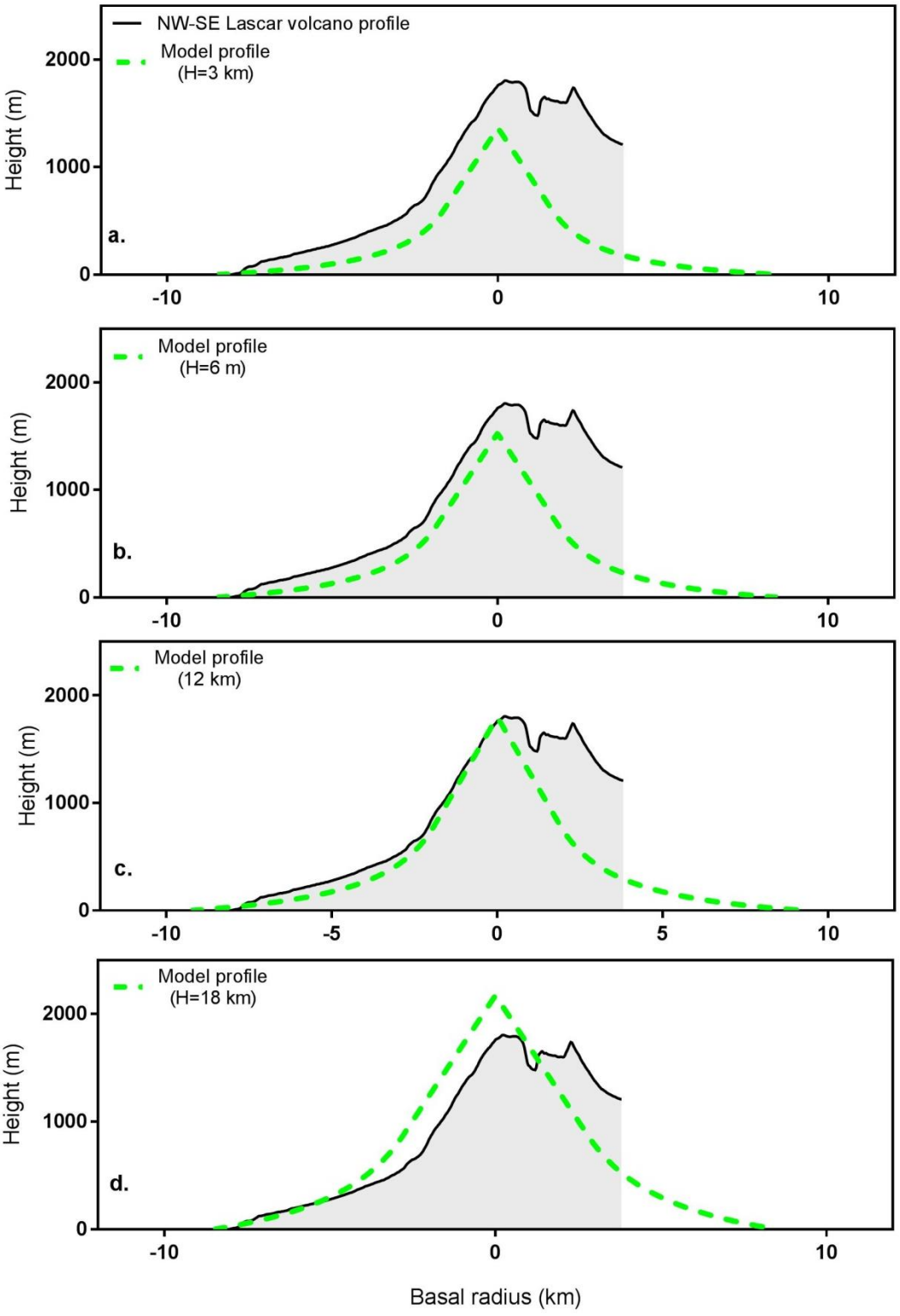

Fig. 7. Topographic profile of Lascar volcano (black line) and predicted obtained applying the model presented in Section 3 (colored dashed lines). From (a) to (d) Lascar volcano fit tests. The best result obtained is shown in (c).

4.3. Lonquimay volcano

4.3.1. Eruptive history and geological setting

Llaima (38,6°S-71,7°W) and Lonquimay (38,3°S-71,5°W) volcanoes are located on the Southern Volcanic Zone (SVZ) (33°N-46°S) of the Chilean Andes. Here an increase of the subduction slope from ~20° at the northern end of the SVZ to 25° further south, causes a narrowing of the volcanic arc-trench distance, from more than 290 km in the north to less than 270 km in the south (Stern, 2004). The crustal thickness decreases southwards from ~50 km to 35 km below the southern end. One of the main first-order factors for the along-strike variations in the nature and composition of volcanism, is the N-S trending arc-parallel Liquiñe-Ofqui Fault Zone. This active transpressional dextral strike-slip structure dominates the region between 38° and 47° (Cembrano et al., 1996; Cembrano et al., 2000; Cembrano and Lara, 2009).

The Lonquimay Volcanic Complex is formed by a very regular stratocone and several adjacent aligned NNE minor eruptive centers, evidencing a strong control of the regional tectonic on its evolution (Moreno and Gardeweg, 1989; Polanco, 2010; Gilbert et al., 2012). This volcano presents explosive and effusive activity. The associated products correspond mainly to lava flows of andesitic to basaltic andesitic composition, characterized by a typical mineral association: plagioclase (labradorite and andesine) +olivine (Fo_{44-71}) + clinopyroxene (pigeonite, augite and clinoenstatite) and Fe-Ti oxides, similar to compositions of material associated to the minor eruptive centers (Polanco, 2010). There are few data to constrain the age of units at Lonquimay volcano. An age of 70±40 ka BP was constrained through $^{40}Ar/^{39}Ar$ dating technics on a lava flow from Lonquimay 2 unit (Edmundo Polanco, personal communication 2015), however, the absence of a glacially eroded surface and the excellent state of preservation of the main edifice suggest mainly a Holocene age.

4.3.2. Morphological characterization

Lonquimay volcano is a conical and slightly elongated on a NE-SW direction stratovolcano, with numerous emission centers in its flanks arranged on NE-SW lineaments (Fig. 4c). Its slope has an average value of 22° and a maximum of 45.3°, increasing systematically towards the summit (Fig. 5c and d). The estimated volume and basal area of the main edifice are 12 km^3 and 34 km^2, respectively (Fig. 8). The maximum height above the base is 1273 m and the basal radius is almost constant around 4500 m. The volcanic edifice is formed mainly by lava flows which show ‘a‘ā, blocky and mainly transitional ‘a‘ā-blocky morphology. The flows show massive large blocks of around 2 – 3 m with irregular and rugged faces and massive cores, within a matrix of smaller blocks (few centimeters). Some blocks have vesicles elongated towards the flow direction and evidence of shear. These lava flows have in most cases very marked central channels and lateral levées, as well as transversal rifts and an increase in thickness towards the front, which reaches up to 50 m in some cases (Fig. 4d). A decreasing trend in lava length and volume with time is recognized in Lonquimay volcano. The longest flow measures up 19 km from the summit, while the shortest does not exceed 1 km. The longer flows are strongly controlled by topography, as they are confined into deep valleys far away from the main edifice. The lava flow volumes observed range between $2.8*10^{-3}$ and 0.19 km^3 (Table 1) ($2.8*10^{-3}$ km^3 correspond to the lava flow volume associated to the Navidad cone eruption occurred on 1988-1990. Its vent is located in the low flank of Lonquimay volcano). For the purpose of this study and considering that we are unable to estimate the volume of the firsts lava flows which are overlapped by the subsequent eruptions, we will treat this lava flow as representative, in volumetric terms, of the first lava flow emitted from the stratocone. We assume both were unaffected by the edifice height due to they were extruded from the base, i.e. altitude close to zero.

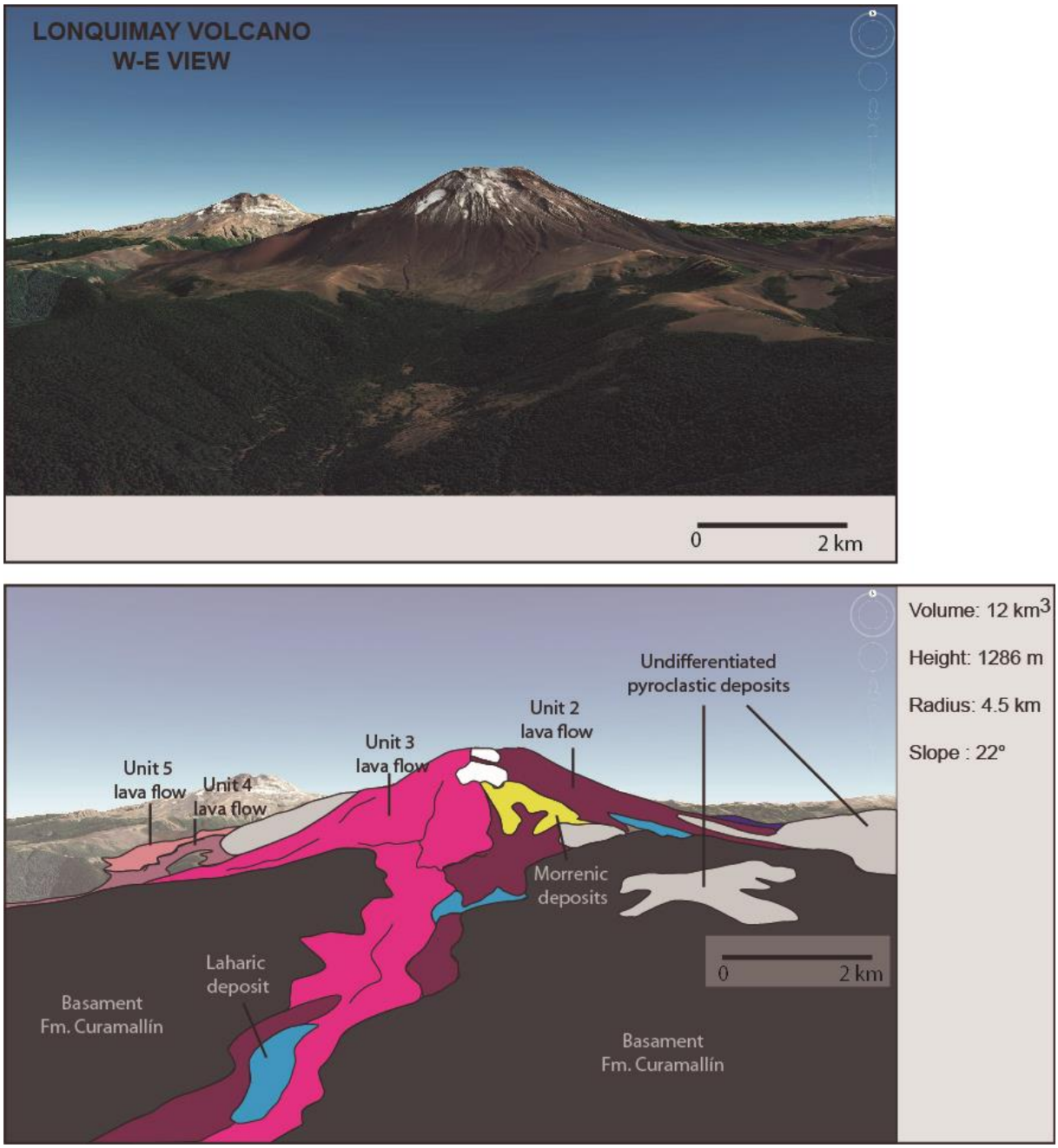

Fig. 8. W-E view of Lonquimay volcano. Mapped of eruptive deposits of Lonquimay volcano are drawn in the bottom panel. Deposits are named according to unit names defined on geological map (Edmundo Polanco, personal communication 2015).

4.3.3. Volcano edifice topography and magma chamber location (H)

With the aim of applying the proposed model on Lonquimay volcano, we first estimated a basal average radius of 4.5 km and a critical angle of 30° (Table 2). Lonquimay volcano's edifice is an almost symmetrical simple cone. Therefore, we did not deal with difficulties associated to a vent shift. In this case, we believe that the edifice is close to its maximum height. We noticed that in Lonquimay volcano the youngest lavas are much smaller than the older ones and all the recent activity has been concentrated in the Cordón Fisural Oriental fissure system. Indeed, there is no evidence of historical activity in the main crater. We think this eruptive behavior suggests that Lonquimay volcano will not follow growing through its summit. Thus, we applied our model fitting the theoretical profile with the SE-NW topographic profile of Lonquimay volcano (There are not substantial differences in topographic profiles oriented in different directions). Results revealed that the most favorable fitting is achieved considering a magma chamber located at 6 km depth (Fig. 9b).

4.3.4. Volcano building: eruption quantity and frequency

For Lonquimay we considered a reservoir volume of 30 km^3 located at 6 km depth. The applied overpressure is 26 MPa and the replenishment rate of magma to the reservoir is 0.13 km^3/ky. By implementing our model, we estimated that 224 effusive eruptions are necessary to build the current volcano, with single volumes between 0.2 and 0.0013 km^3. The resulted volcanic edifice has a volume of 10.9 km^3 in a period of 87.7 ka, with an average eruption recurrence of 390 years (Fig. 12 and 13). Using Eq. (13), we estimated that the maximum altitude that Lonquimay volcano could attain is 1313 m.

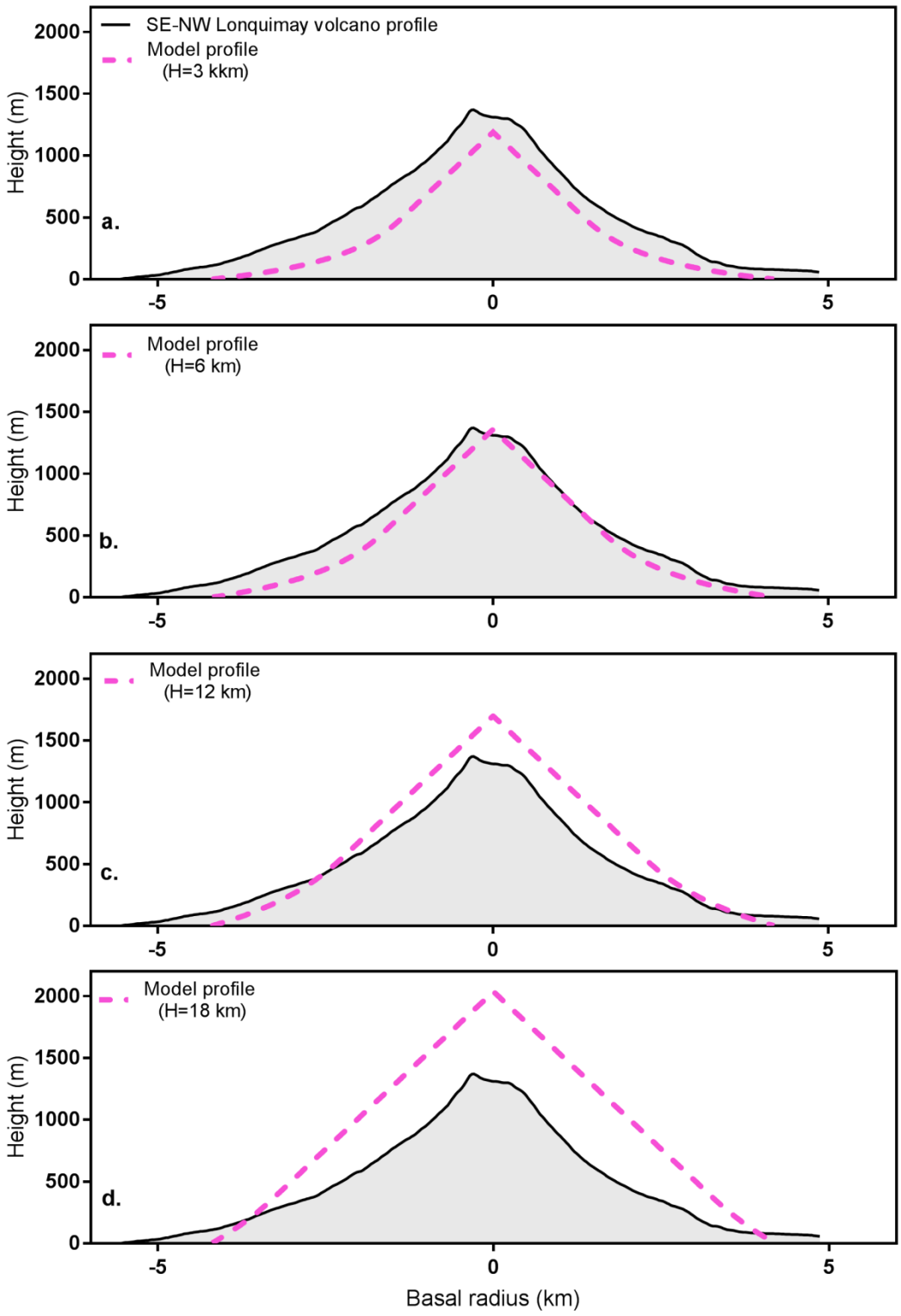

Fig. 9. Topographic profile of Lonquimay volcano (black line) and theoretical profile obtained applying the model presented in Section 3 (Colored dashed lines). From (a) to (d) Lonquimay volcano fit tests. The best result obtained is shown in (b).

4.4. Llaima volcano

4.4.1. Eruptive history and geological setting

Llaima volcano is considered one of the most active and voluminous volcanoes in the Andes and it is formed by the main edifice and almost 40 adventitious eruptive centers. These are mainly distributed on its western and northeastern slopes and are aligned along a 25 km long SW-NE arc structure. A marked feature of Llaima volcano is the two summits of the main edifice, being the northernmost the highest with about ~2.400 m above the volcano base and separated each other for 750 m. The volcanic activity of Llaima displays a variety of eruptive behaviors. According to Naranjo and Moreno. (2005) its eruptive history can be divided into three stages. The first dominantly effusive (185 ka), correspond to the period of construction of a pre-Holocene shield volcano formed by basaltic-andesitic to dacitic lava flows that built an edifice of similar altitude to the current one and collapsed during a great explosive eruption (~ 15 ka). At this time started a shift on the behavior to a more explosive period ending sometime after 9.5 ka and characterized by magma compositions ranging from andesites to dacites, including a large mafic ignimbrite. Finally a less explosive period started, with emission of numerous basaltic to basaltic-andesitic lava flows, with a very high eruptive frequency which allowed to build the Holocene cone in a period of ≤3-5 ka (Bouvet de Maisonneuve et al., 2012).

4.4.2. Morphological characterization

Llaima volcano is a NNW- SSE elongated conical and voluminous stratovolcano, with numerous fissure and adjacent cones in its flanks. The volcano has two summits, with the active and highest located in the north. (Fig. 4f and 4g). The topographic profile is concave-upwards, with an average slope of 15° and a maximum slope of 40.6° in the crater zone (Fig. 5e and f). Our results show a basal area for the main edifice of 222 km^2 and an estimated volume of 153 km^3, with a maximum elevation above its base of 2430 m and maximum and minimum radius of 15 km and 5 km respectively (Fig. 10).

The morphologies of the lava flow units were studied mainly for the youngest units (<3ka), due to the poorly preserved morphology of the oldest ones. They are characterized by an ‘a‘ā morphology, although in isolated sectors, particularly in proximal zones, pahoehoe morphologies are also recognized. The classic arrange of lateral levées and a central channel is only identified in proximal zones, being almost totally absent in the distal areas. Many lava flows have multiple source vents, such as lavas from 1640 (LFLla2) and 1957 (LFLla3) eruptions (Fig. 10). Some reached up to 20 km, with thickness up to 8 m (5 m mean) without noticeable longitudinal trends (Fig. 4e). Several lava units do not have an exposed vent and consequently the volume estimation has to be considered a minimum. Furthermore, the first effusive period which gave rise to the ancestral Llaima shield volcano, was strongly eroded during the Llanquihue glaciation, between 29.4 and 14.6 ka (Denton et al., 1999; Charles Stern, 2004) and now is not widely exposed. However, youngest volumes of lavas from Llaima volcano were calculated, obtaining values in the range of $4.8*10^{-4}$ and $8.9*10^{-2}$ km^3 (Table 1).

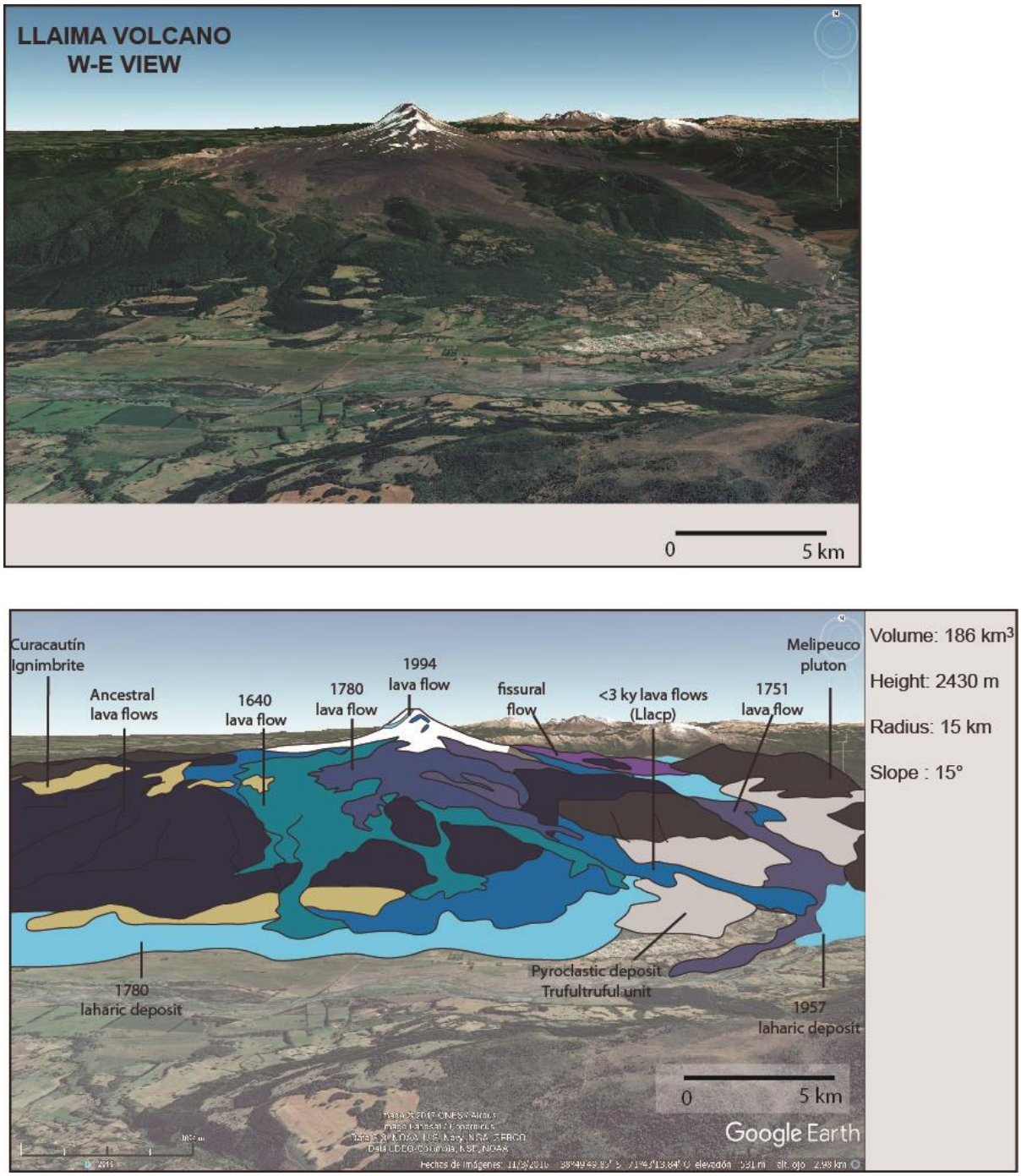

Fig. 10. E-W view of Llaima volcano. Mapped of eruptive deposits of Llaima volcano are drawn in the bottom panel. Deposits are named according to unit names defined on geological map (Naranjo and Moreno, 2005).

4.4.3. Volcano edifice topography and magma chamber location (H)

Likewise Lonquimay, we believe that also Llaima volcano is close to its maximum height. Its recent activity is focused on its flanks and only moderated volumes of lava have been emitted from the summit (1994 eruption/ LFLla4 in table 1). Llaima volcano shows noticeable differences between profiles in different orientation due to pre-existing topography and its vent shift. However, differencing from Lascar volcano, the Llaima volcano second vent is significantly smaller and it is located very close to the main vent (around 700 m). Considering these morphologic evidences, we believe that the effect of the vent displacement in this case is negligible. For this reason, we selected the NW-SE profile to test the model, due to it is one of the most symmetrical profiles and it avoids the second summit. We considered an average radius of 15 km and a critical angle of 22° (Table 2). Our results show that the most favorable fit between the model profile and Llaima volcano's topography is obtained considering a magma chamber located at 18 km depth.

4.4.4. Volcano building: eruption quantity and frequency

For Llaima volcano we considered a magma chamber located at 18 km depth, with a volume of 50 km^3. The overpressure required to trigger an eruption according our estimations is around 40 MPa and the magma is injected in the reservoir at a rate of 0.95 km^3/ky from a deep source. Our results show that 1963 eruptions are required to build the current volcano, with volumes ranging between 0.34 and 0.03 km^3. The volume of lava expected to reach the present altitude is 186 km^3, attained in a period of 196 ky (Fig. 12 and 13). Eruptions should then occur with an average frequency of 100 years. According Eq. (13) and considering that Llaima volcano's magma chamber is located at 18 km of depth, the maximum altitude that Llaima volcano could attain is 2556 m.

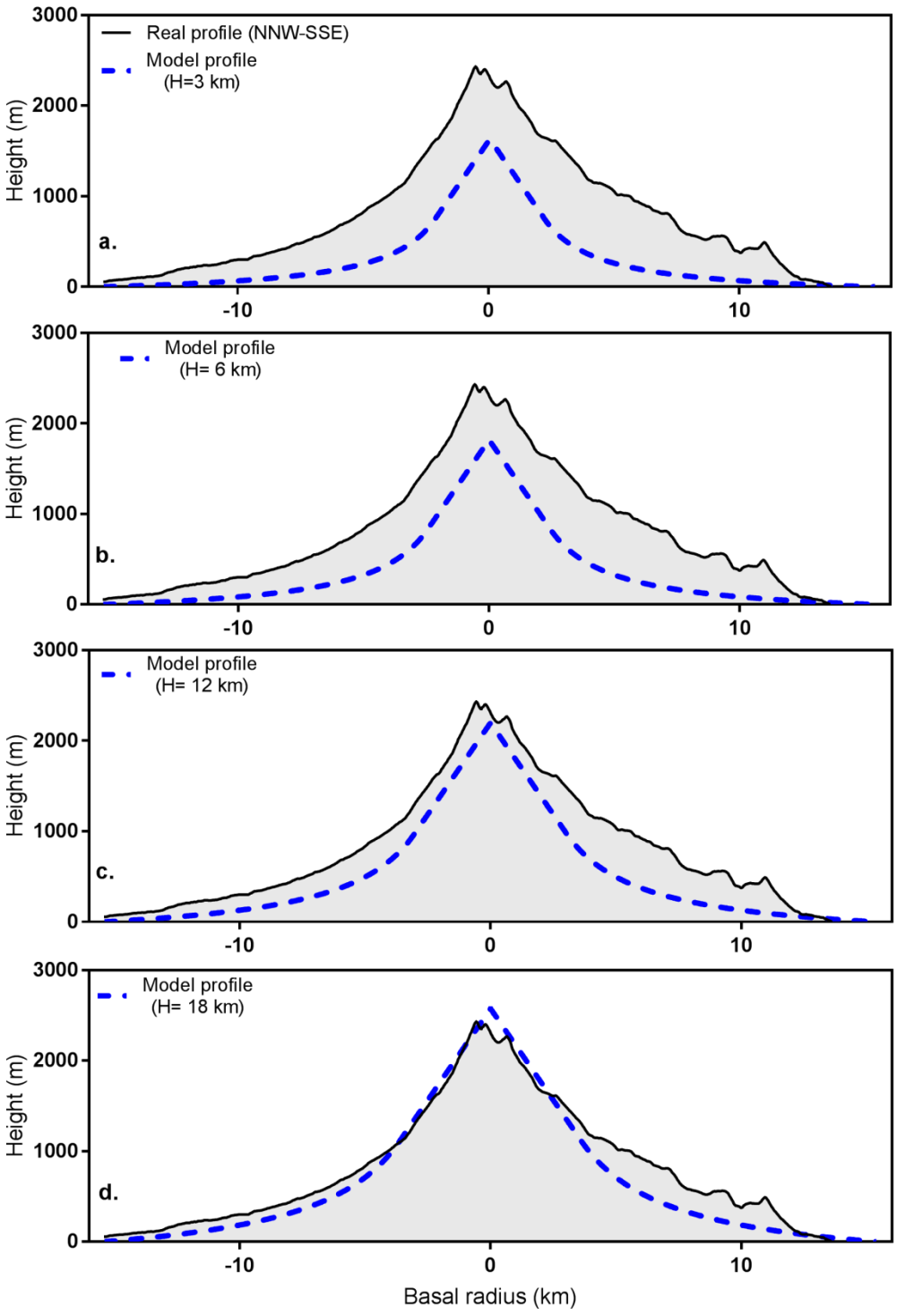

Fig. 11. Topographic profile of Llaima volcano (black line) and theoretical profile obtained applying the model presented in Section 3 (colored dashed lines). From (a) to (d) Llaima volcano fit tests. The best result obtained is shown in (d).

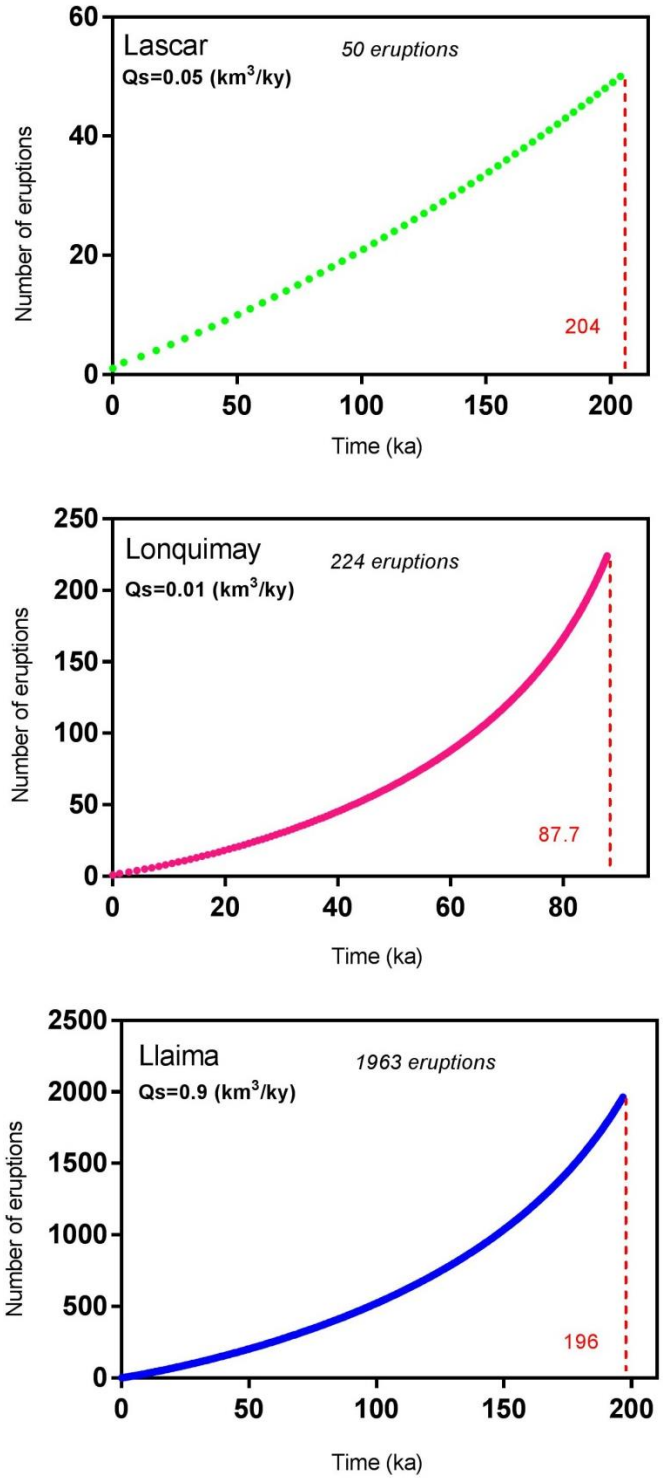

Fig. 12. Number of eruptions required to attain the current height of volcanoes Lascar, Lonquimay and Llaima using the proposed model. Notice the gradual increase on eruptive frequency as volcanoes grow using a fixed replenishment rate.

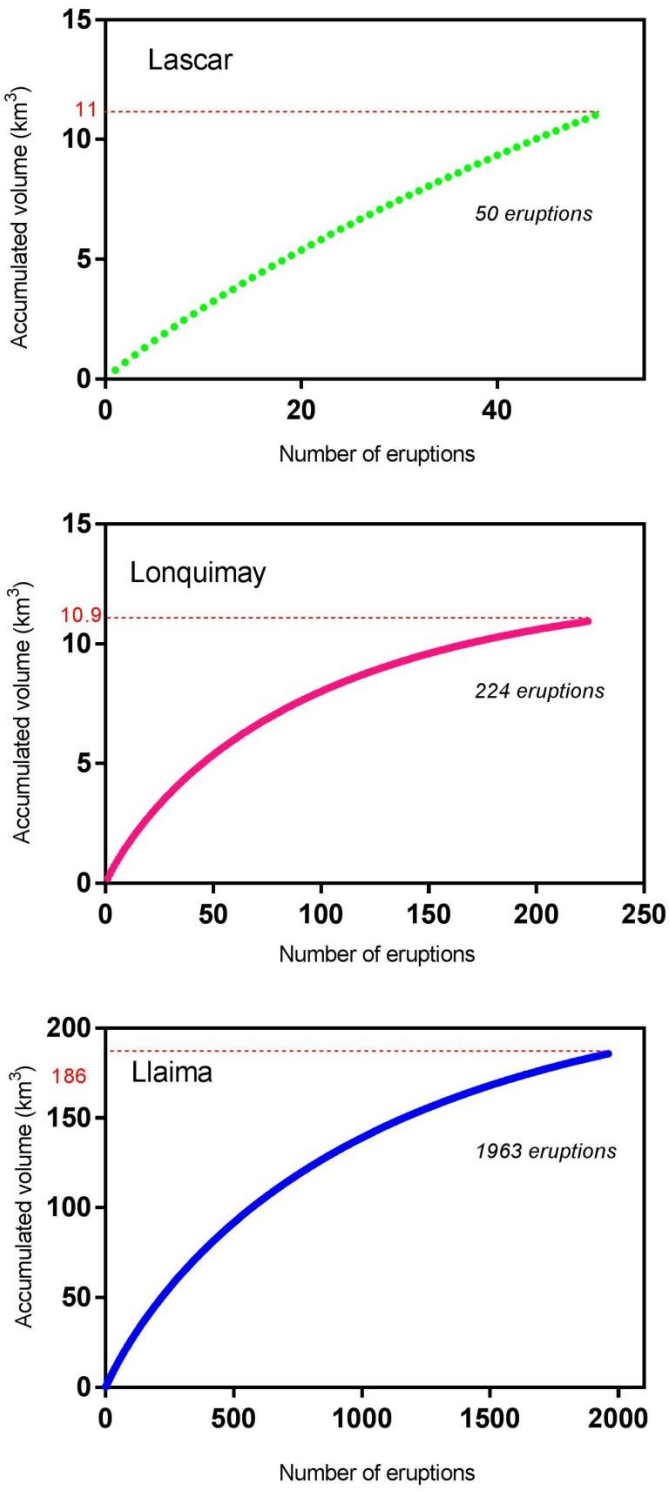

Fig. 13. Number of eruptions required to attain the current height of volcanoes Lascar, Lonquimay and Llaima using the proposed model and the volume predicted by the generated pile of lava flows. Notice the gradual decrease on the rate of accumulated volume as volcanoes grow.

5. MAGMA CHAMBER LOCATION INFERRED FROM PETROLOGICAL TOOLS

In order to provide estimations for the magma chamber location by employing a different methodology than our model, we performed thermobarometric analyses in Lascar, Lonquimay and Llaima volcanoes. We estimated P-T conditions of crystallization interpreting the data as levels of magma storage. Thus, we could compare results and assess the applicability of the model on the selected volcanoes. Through the application of facing this petrologic tool, we are able to identify several storage levels (if two or more constitute the plumbing system of a volcano). This information can be compared to the results on magma chambers obtained using our topographic model. In the following paragraphs, we will first petrologically characterize lava flows collected from these volcanoes, and then we will apply geothermometers and geobarometers available in literature according to the prevailing mineralogy for every case.

5.1. Analytical techniques

In order to characterize the mineralogy of the eruptive products of the volcanoes under study and select the appropriate crystals to perform pressure-temperature estimates, we first used the FEI Quanta-250 Scanning Electron Microscope (SEM) at the Department of Geology of the University of Chile. Then, the mineral chemical composition of Lascar and Lonquimay eruptive products (major and minor elements) was obtained by the CAMECA SX100 Electron Microprobe Analyzer (EMPA) at the University of Bristol. The same analyses on Llaima volcano's samples were carried out using the Jeol JXA-853F Field emission microprobe at the Earth Observatory of Singapore. The following setup was applied on Lascar and Lonquimay mineral measures: 20 kV accelerating voltage, electron beam current of 10 nA and 1 µm diameter beam. In Llaima the used was: 15 kV accelerating voltage, electron beam current of 10 nA and 5 µm diameter beam. Samples analyzed are summarized in Table 3 and outcrops displayed in Fig. 2. Bulk rock

compositions were obtained from Gardeweg et al. (2011), Polanco (2010) and Naranjo and Moreno (2005) (Table 4). We used measurements performed on the same lava flow samples that we have selected for mineral analyses.

Table 3**:** Summary of samples studied in this work and the name of the unit associated according to the geological map of Lascar (Matthews et al., 1994), Lonquimay (Edmundo Polanco, personal comunication 2015) and Llaima volcano ((Naranjo and Moreno, 2005).

Sample	Volcano	Unit
L1l-04	Lascar	Lascar 1: Colada de lava Negrillares
L2l-03	Lascar	Lascar 2: Coladas de lava del cono occidental
L4l-03	Lascar	Lascar 4: Colada de lava andesítica Tumbre-Talabre
Lon2-01	Lonquimay	Lonquimay 2
Lon3-01	Lonquimay	Lonquimay 3
Lon4-02	Lonquimay	Lonquimay 4
L5LV01B	Lonquimay	Lonquimay 5
Llacp-01	Llaima	Llaima cono principal
Llacp-02	Llaima	Llaima cono principal
Llacp1751-02	Llaima	Llaima cono principal
Llacp1957-04	Llaima	Llaima cono principal

Table 4: Bulk rock composition from previous works on Lascar, Lonquimay and Llaima volcanoes (Gardeweg et al. (2011), Polanco (2010) and Naranjo and Moreno (2005)). We selected samples collected from the same lava flows we used to determine the thermobarometry. Column 1 (Sample no) and column 2 (Sample Eq.) show the name used on the publication and the equivalent sample in this work respectively. The following columns show the composition in % wt.

Sample no	Sample Eq.	SiO_2	TiO_2	Al_2O_3	FeO	MnO	MgO	CaO	Na_2O	K_2O	P_2O_5
LA-135	L1l-04	60,63	0,72	17,86	5,15	0,10	2,44	5,79	4,00	1,94	0,25
LA-140	Ll2l-03	63,41	0,61	15,81	4,68	0,09	2,79	4,82	3,68	2,38	0,18
Gla-195	L4l-03	52,49	1,01	19,28	5,67	0,04	1,87	4,38	3,29	1,26	0,32
LOP35	-	57,90	1,41	15,98	9,71	0,22	2,30	5,52	5,07	0,99	0,39
LOP46	Lon2-01	58,92	1,17	16,37	8,61	0,21	2,03	5,26	5,18	1,05	0,36
LOP48	Lon3-01	51,13	1,08	19,51	9,85	0,16	3,82	10,10	3,23	0,50	0,17
BB115	Lon4-02	57,38	1,49	15,84	10,97	0,23	2,36	5,84	4,75	1,03	0,40
LOP45	L5LV01B	54,00	1,45	16,47	11,32	0,21	3,23	7,14	4,16	0,80	0,30
cp-030381-2	Llacp-01	51,79	1,03	17,74	9,85	0,15	5,94	9,69	3,04	0,57	0,19
cp-260483-4	Llacp-02	51,99	0,96	18,11	9,72	0,18	5,52	9,54	3,24	0,56	0,18
030381-3	Llacp1751-02	51,78	1,02	17,82	9,80	0,16	5,92	9,68	3,03	0,58	0,21
111276-1	Llacp1957-04	52,14	1,05	17,70	9,38	0,18	5,54	9,52	3,57	0,68	0,24

5.2. Petrography

5.2.1. Lascar volcano

Lascar volcano lava flow samples (Fig. 14.a and Fig. 14d) show a very high crystallinity, ranging between 56 and 64 vol.%, considering phenocrysts (>1 mm) and microphenocrysts (0.1-1 mm) (Fig. 14g). The groundmass almost does not have residual glass and it is composed mainly by plagioclase microlites. The mineralogy assemblage in all the units is plagioclase + hornblende + clinopyroxene + orthopyroxene + oxides. Plagioclase sizes range from microlites (< 0.01 mm) to crystals with maximum lengths of 2.3 mm, with An_{52-64} in the rims and oscillatory-zoning. The second dominant mineral is hornblende ranging from subhedral to anhedral with a great variety of sizes (generally <2 mm long) and variable degree of aspect ratios. The hornblende is classified according to its chemical composition as magnesiohastingsite and tschermaquite. Pyroxenes are enstatite- pigeonite and augite, with composition ranging between En_{62-70}, $Wo_{0.6-3}$, Fs_{28-37} for orthopyroxene and En_{40-47}, Wo_{42-43}, Fs_{9-17} for clinopyroxene, both with sizes < 1 mm and observed in all the studied units. One isolated olivine crystal (Fo_{84}) was identified in a sample of the unit Lascar 1 being probably a xenocrysts. The common textures observed are porphyritic, oscillatory zoning, patching and sieve in plagioclase, as well as vesicular, poikilitic, glomerophyric and some hornblende phenocrysts show resorbed rims. Enclaves with apparently less evolved bulk rock composition have been commonly observed in the collected samples at a macro scale.

5.2.2. Lonquimay volcano

Crystal content from Lonquimay volcano lava flows varies between 23 – 40 vol.%, being the microphenocrysts the most abundant type while the phenocrysts, almost totally absent, represent less than 1% in all the studied samples ((Fig. 14b, Fig. 14e and Fig. 14h). The groundmass is close to be 100% crystalline, with little residual glass in the interstices of crystals. The mineral association in all samples is: plagioclase +

clinopyroxene + orthopyroxene + olivine + oxides in order of abundance. The predominant mineral phase is plagioclase with compositions fluctuating between An_{39-57} in the cores and An_{43-57} in the rims, showing the higher An values for crystal associated to the unit Lonquimay 2 (An_{81}). Concentric oscillatory compositional zoning and patching is very common in this mineral phase, as well as a general tendency to increase the anorthitic component towards the rims. Almost all the microphenocrysts are plagioclase, with small amounts of olivine and pyroxene. The pyroxenes appear as individual subhedral crystals in the case of augites, while anhedral pigeonites grow around olivines in the units Lonquimay 2 and Lonquimay 4. Chemical compositions are in the range of En_{23-46}, Wo_{37-43} Fs_{9-34} (clinopyroxenes) and En_{45-59}, Wo_{4-10}, Fs_{33-41} (orthopyroxenes). Little isolated euhedral pigeonites have been recognized in unit 2. On the other hand, olivines show subhedral habits and compositional zonation in the range of Fo_{31-54} in the rims and Fo_{13-57} at cores. Other textures include sieve texture in some plagioclases, vesicular, glomerophyric and also some of trachytic and poikilitic textures. Reaction rims observed in most olivines are common and are composed of subhedral pigeonite grown around.

5.2.3. Llaima volcano

The more outstanding features observed in these lavas are the high crystallinity, reaching up to 50%, considering phenocrysts (5-13%) and microphenocrysts (35-40%). Large olivines and plagioclases exceeding 3 mm of maximum length are abundant (Fig. 14i). The common mineral association is: Plagioclase + olivine + orthopyroxene +/- clinopyroxene + Fe-Ti oxides (Fig. 14c and Fig. 14f). Plagioclase is the most abundant mineral and its compositions range from An_{68-91} in the cores to An_{52-70} in the rims, showing an evident decrease in anorthite from cores to rims and complex zoning patterns. Olivine is the second most abundant mineral phase occurring as large euhedral crystals. In most cases olivine shows compositional zonation with cores higher in magnesium than the rims, with ranges Fo_{71-78} and Fo_{65-70} respectively. Regarding to pyroxenes, we found augite with compositional range En_{43-49}, $Wo_{31-39,}$ Fs_{14-22} and enstatite varying between En_{67-83}, $Wo_{0.2-4.6}$, Fs_{16-28}. It is common to observe pyroxenes forming cumulus with plagioclases and

olivines, being some of them slightly zoned with a tendency to increase the ferrosilite content and decreasing the enstatite content towards the rims. Other textures observed in these samples are porphyritic, trachytic, vesicular, glomerophyric and poikilitic, as well as zoning in plagioclase, olivine and pyroxene and occasionally sieve and patching in plagioclase.

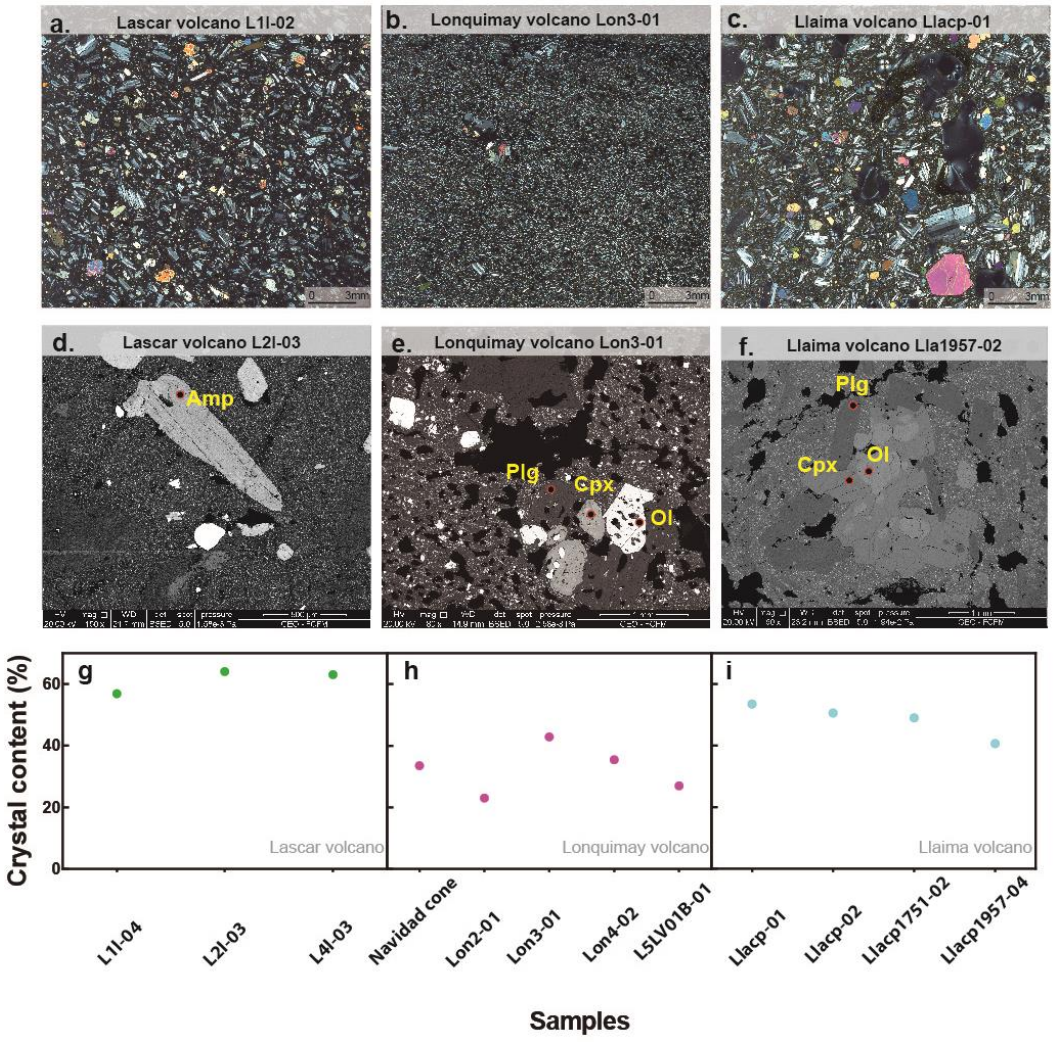

Fig. 14. (a), (b) and (c) Scanned thin sections (in XLP) from Lascar, Lonquimay and Llaima lava flows respectively. (d), (e) and (f) SEM images from Lascar, Lonquimay and Llaima volcanoes, showing the minerals used to apply geothermobarometric methods. (g), (h) and (i) display the results of the modal count of crystal for different samples in every volcano (Detailed crystal fraction by size on Appendix 3). Name of samples are listed in order of age for every volcano.

5.3. Thermobarometry

We selected the crystals based on their sizes (>0.1 mm of maximum length), chemical composition of total oxides (in the range of 98.5 to 101.5) and tested compositions of their cores and rims. Results are reported as the lowest and the highest obtained values for temperature and pressure, and as average value with standard error of estimate (SEE). Results are summarized in Fig. 15.

5.3.1. Lascar volcano

We used the chemical composition of amphiboles according to the model proposed by Ridolfi (2010). This model allowed us to calculate temperature, pressure and H_2O_{melt} –fO_2 conditions from the composition of calcic amphiboles of volcanic calc-alkaline rocks (SEE ±22 °C and around 20% of the pressure value). Results revealed a range of temperatures between 921°C and 987°C and T_{mean}= 967±22 °C, with no special trend between distribution units. Pressure values are uniform in a range of 3.27-4.37 kbar with P_{mean}=3.8±0.7 kbar. Considering a similar crystallization path, based on barometric results, we infer that the magma was likely stored in a single and large reservoir located at a depth of 14 ±2.5 km (Fig. 15a).

5.3.2. Lonquimay volcano

Samples from Lonquimay volcano are scarce in phenocrysts content and show an almost totally crystalline matrix, preventing a direct measurement of the residual glass composition. Mineral-melt pairs were checked to satisfy the equilibrium condition $K_D(Fe\text{-}Mg)_{cpx\text{-}liq}$=0.27 ±0.03 (Rhodes et al., 1979). Calculated values were obtained using bulk rock and matrix compositions , without favorable results. In order to reduce the uncertainty associated to the glass composition, we performed thermobarometric calculations solving 2 equations of Putirka (2008) simultaneously in an iterative procedure: Eq. 32d for pressure and 32a for temperature, both depending only on clinopyroxene composition

(SEE ±3.1 kbar and ±87°C). Results revealed a temperature range for all the units between 1059-1156°C and T_{mean}= 1120 ±87°C, with a moderate increasing trend for the youngest samples. We also estimated temperatures using the olivine-augite Mg-Fe^{2+} cation exchange thermometer proposed by Loucks (1996) (SEE ±6°C). We used augite-olivine pairs from units Lonquimay 3 and Lonquimay 5 obtaining T_{mean}=1120 ±6°C, which overlaps with the results obtained using equations from Putirka (2008). Pressure results indicated several magma storage levels. Crystals from units Lonquimay 2, Lonquimay 3 and Lonquimay 4 constitute the most important cluster and yield the lowest pressure values in a range of 0.3-1.8 kbar with P_{mean}=1.5 ±3.1 kbar. Different pressures were obtained from crystals from unit Lonquimay 5, with values of P_{mean}=3.5 ±3.1 kbar, P_{mean}=4.6 ±3.1 kbar, P_{mean}=6 ±3.1 kbar and P_{mean}=8 ±3.1 kbar. Based on multiple crystallization paths, we thereby believe that our results indicate the possible occurrence of several magma bodies stalled at ~6, ~13, ~17 and ~22 km of depth, being the shallowest the principal (Fig. 15b).

5.3.3. Llaima volcano

The thermometer proposed by Loucks (1996) was applied on augite-olivine pairs yielding temperatures in the range of 1113 – 1169°C with T_{mean}= 1141 ±6 °C. For pressure estimations we used the barometer developed by Nimis and Ulmer (1998) based on the crystal-structure of clinopyroxene in an anhydrous or hydrous basaltic magma (SEE ±1.7 kbar and ±3.1 kbar respectively). The magma H_2O solubility was estimated through an iterative combination of the expressions provided by Moore et al. (1998) and Lange et al. (2009), according the procedure proposed by Morgado et al. (2015). We obtained values ranging from 0.2-0.8%. Here we applied the model for hydrous basaltic magmas as it is more realistic considering solubility estimates. Results reveal different storage conditions with two ranges identified: 0-0.4 kbar and 1.6-2.6 kbar, with the highest values as P_{mean}= 2.1 ±3.1 kbar and the lowest as P_{mean}= 0.2±3.1 kbar. Thereby, our barometric results place the Llaima magma reservoirs at about 6 km and > 1 km of depth (Fig. 15c).

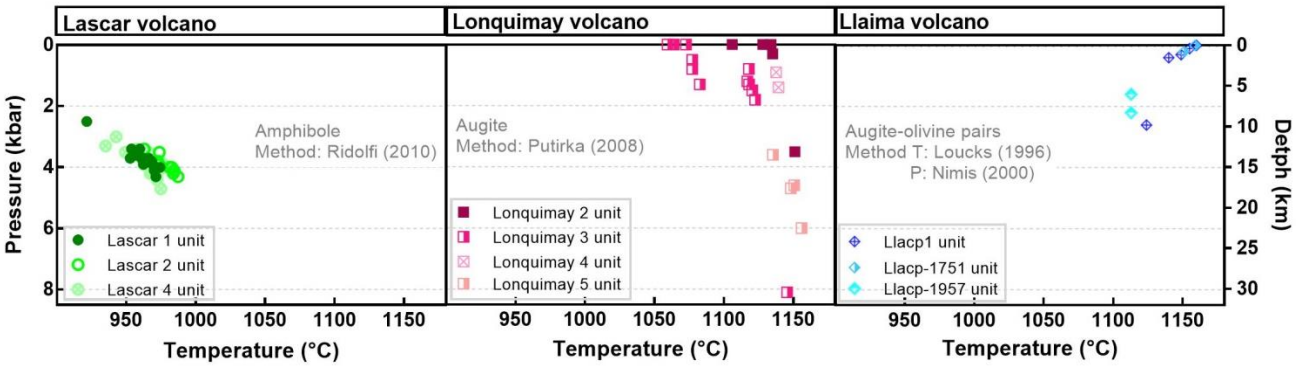

Fig. 15. Magma storage conditions at volcanoes Lascar, Lonquimay and Llaima. Samples were collected from lava flows, from the oldest to the youngest units. Samples analyzed were L1l-04, L2l-03 and L4l-03 (from Lascar volcano), Lon2-01, Lon3-01, Lon4-02 and L5LV01B (from Lonquimay volcano) and Llacp-01, Llacp1751-02 and Llacp1957-04 (from Llaima volcano).

6. DISCUSSIONS

6.1. Model assessment

6.1.1. Magma storage location: comparison with petrological and geophysical technics

In this work, we used internal parameters of the magma plumbing system to explain morphological differences, and hence we evaluate their influence during volcano growth. To support our results, obtained with a morphological approach, we compared them with values obtained using petrological methods. Previous estimates were obtained by thermobarometry at Lascar, Lonquimay and Llaima volcanoes, allowing us to account for a more robust information about the plumbing system at depth and, in some cases, to improve previous models with new ones available in literature.

As consequence of several shifts of vent location, Lascar volcano has an E-W elongated morphology, with marked differences in the shape of their flanks. In these cases, to limit the analysis to a single flank is a valid approximation if the parameters required to run the model are consistent with the selected flank (e.g. basal radius according to the maximum length of lava flows observed in this flank). In the case of the Lascar volcano modelling, a magma chamber stored at 12 km of depth gives the best fitting between the real and theoretical profile. However, a slight mismatch can be observed in the lower flank of Lascar volcano. The lower part of a volcanic edifice is not only formed by lavas, but can be the result of the combined action of deposition from primary pyroclastic flows and falls to syn-and post-eruptive re-working (Davison and De Silva, 2000; Karátson et al., 2010). We believe that the accumulation of pyroclastic deposits most likely modifies the topography, affecting the agreement with our theoretical profile. However, the depth values obtained by applying the model are also supported by our thermobarometric estimations, suggesting that explosive products may not influence the final estimation of H , and that the pilling of lava flows are the main responsible of the volcano construction

and topography. Consequently, despite our topographic model neglects the contribution of explosive products, it could provide favorable results in volcanoes with associated major explosive events.

With respect to the barometric results, we interpret that the similar values obtained for all the units of Lascar volcano are indicative of a plumbing system with a single reservoir through the Lascar volcano evolution. However, we cannot discard the possibility of other reservoirs as contributors of its plumbing system. We must be aware that we have restricted our thermobarometric study to a limited number of lava flows units and we have not considered pumices samples. Matthews et al. (1994) also constrained values for reservoir location at Lascar volcano. They obtained values between 13-24 km (3.45-6.4 kbar) by using aluminum in the hornblende barometer (Johnson and Rutherford, 1989) and 39-58 km (10.36-15.36 kbar) by using models of silica activity calculation (Nicholls et al., 1971; Williams, 1971). These values are deeper and more scattered than our estimations. Nevertheless, it is interesting to note that Matthews et al. (1994) warned about possible inconsistencies in their study due to certain requirements of the applied method, like the presence of alkali feldspar in the hornblende barometer. Other explanation could be associated to the samples used by Matthews et al. (1994): both lavas and pumices. However, to consider explosive eruptive material in our analyses as well as a higher number of samples, could lead to obtain similar results or infer the existence of several reservoirs. Clearly, more work is required to better constrain other depths for magma chamber(s) at Lascar volcano.

Lonquimay volcano lacks recent lava flow emission from the summit and the last flows have limited volume and extension. Considering also the continuous adventitious activity during historical times, we believe this behavior may indicate that Lonquimay volcano is close to its possible maximum altitude and hence, it is an appropriate case to apply the topographic model. Our results suggest that Lonquimay volcano has a reservoir located at 6 km of depth. We noticed some differences between the topographic profile and the model, particularly in the lower flanks. We interpret they are associated to the pyroclastic material accumulation, but mainly associated to the adventitious centers and lava flow,

especially in the northeast flank. Likewise of explosive eruptive material, lava flows not erupted from the summit are neglected by our model. Hence, it is expected a worst fit between real and theoretical profile in the lower flanks where both are accumulated.

Comparison between the depth of Lonquimay volcano's magma chamber (6 km) estimated by applying our topographic model and the P-T estimates using thermobarometry, shows a relative good agreement. The pressure values obtained by using barometers are very scattered, although previous works support these results. Polanco (2010) used the magnetite-ilmenite barometer (Ghiorso and Sack, 1991; Ghiorso and Evans, 2008), and estimated reservoir depth at 16.5–23 km and 26 km. By using the clinopyroxene-liquid barometer (Putirka et al., 1996; 2003; Putirka, 1999; 2008) the storage levels depths are at 0-3.5 km and 6.8-12 km. Gilbert et al. (2012) analyzed tephra layers from Lonquimay volcano and used the amphibole barometer (Ridolfi et al., 2010) and the clinopyroxene-liquid equilibrium barometer (Putirka, 2008) revealing three magma storage levels: 1.5 – 6 km, 8.5-12 km and 14-19 km. It is worth mentioning that both studies include material that does not come only from the main crater which is instead our approach; the first study includes samples also belonging to the adventitious cones, while the tephra provenance source in the second study is undefined. In summary, a complex multi-reservoir plumbing system of Lonquimay volcano has been hypothesized in previous works based on petrological models, and the presence of several reservoirs located at different depths has been suggested, among which one would be around 6km. Although several studies in the volcanology field support the idea of an upper-crustal magma chamber connected with deeper reservoirs (e.g. Di Stefano and Chiarabba, 2002; Koulakov et al., 2013; Schindlbeck et al., 2014), we believe it must be considered the possibility of an ascent path beneath the 6 km depth reservoir as a second option to explain the expanded range of pressure values revealed through thermobarometry. According to Cashman et al. (2013), magma beneath stratovolcanoes is apparently stored in narrow and vertically elongated regions that may segregate into small melt pockets (e.g. Waite and Moran, 2009; Paulatto et al., 2012). Similarly to these studies, the integration of geophysical information could likely provide new views into the Lonquimay volcano

plumbing system. Barrientos and Acevedo-Aránguiz (1992), through the study of the earthquake record previous to the beginning of the Navidad cone eruption in 1988-1990, identified most of the hypocenters at depth shallower than 6 km and deeper than 10 km, suggesting a reservoir between 6 and 10 km, in agreement with the findings of this study. Summarizing, based on previous works and the topographic model combined with the petrological study, the depth of 6 km is probably representing the main reservoir responsible to feed most of the eruptions.

At Llaima volcano, most of the historical effusive activity has occurred through the emission of voluminous lava flows from lateral fissures or adventitious cones. Summit activity has been limited to small volume lava flows such as the one in 1994 and 2008-2009. Our morphological results evidence a good fit in the higher flanks profiles, but a larger mismatch in the lower flanks. Like in Lonquimay volcano, we believe it would be due to the high effusive activity of the volcano through its flank vents which is not included in the model. The best fit is achieved considering a magma chamber stalled at 18 km depth, which disagrees strongly with the <6 km depth obtained with barometry in our study. However, previous works have proposed multiple magma storage levels in Llaima volcano, including similar to the above mentioned depths. Bouvet de Maisonneuve et al. (2012), through the study of olivine hosted melt inclusions from four tephra units from recent historic eruptions, concluded the existence of a dike-like reservoir at ≤4 km beneath the base of the volcano. Ruth et al. (2016) through melt inclusions studies of the 2008 eruption samples, suggested two reservoirs at: 300 m-4 km and 4-14 km depth. Schindlbeck et al. (2014) by using the barometers of Putirka (2008) investigated a post-glacial tephra succession and some lavas, showing how Llaima evolved through 4 distinct phases. These phases involved not only changes in the eruptive behavior of Llaima volcano, but also an upward migration of the magma chamber location from 18 km, to 11-15 km and <4 km during the last 3ka. We believe that our results obtained by thermobarometric analysis, as well as some of the above-mentioned works are biased by the age of the selected samples, all belonging to young lava flow units. Contrasting, P-T studies on oldest products as well as our proposed model, support the existence of a

deeper reservoirs. This statement is reinforced by geophysical studies carried out in Llaima volcano. Bathke et al. (2011) present an InSAR deformation study at Llaima volcano, during 2003-2008, revealing a magma body at depth of 4-12 km. On the other side, magnetoteluric studies identify 20-30 km depth conductors beneath Lonquimay, Llaima and Villarrica volcanoes, which were interpreted as deep magma reservoirs (Kapinos et al., 2016). Nevertheless, in this last study, the shallower chambers revealed by thermobarometry were not recognized.

In conclusion, we believe there is enough evidence to support the existence of several reservoir beneath Llaima volcano. Probably, the deepest reservoir was the first established and during the volcano evolution, other shallow magma bodies formed in the crust. However, we suggest that our model can provide some insights, not only on the magma storage locations, but also on their interplay previous to an eruptive event. In the case of Llaima volcano, the 18 km depth reservoir would receive the input of magma which leads to a critical overpressure triggering an eruption. The low accuracy of thermobarometry (errors ~ 3 kbar, equivalent to ±11 km) and the macroscale of the geophysical methods (in the above-mentioned study the field penetration was around 16-50 km) demand complementary methodologies to obtain more accurate estimations of the plumbing system parameters. Our topographic model could be a complementary to the overmentioned methods, and also, provide information about the dynamic of magma before an eruptive episode. We will discuss further below, in the section about the proposed final model, about the kind of reservoirs connection we need to explain the dynamic of the eruptions in Llaima and the other studied volcanoes.

6.1.2. Volcano dimension prediction and number of eruption required to reach it.

We simulated how Lascar, Lonquimay and Llaima volcanoes grew until they reach their actual height, as a function of their magmatic system properties. Table 5 summarize the values of volcano volume for Lascar, Lonquimay and Llaima available in the literature, as

well as our data obtained by DEMs analyses and modelling. In every case of study, similar volcanic edifice volumes were obtained by using DEMs and by applying our model. This consistency in our results, suggests that despite the restriction of the activity to only effusive seems unrealistic, the piling of lavas could be the main process that builds a stratovolcano. Furthermore, we noticed that both estimations obtained by this study are smaller than values obtained in previous works. It is expected as we are restricting the analysis to the main edifice only, neglecting distal products such as pyroclastic deposits and lava flows from flank vents and/or explosive eruptions, that can add up considerable volume of products. Indeed, volcanoes which present the major differences with previous reports are Lonquimay and Llaima, evidencing an important contribution of flank vents to the edifice dimension. However, we must highlight the concordance of the obtained measures and previous estimations, supporting the fundaments of our proposed model.

Table 5: Comparative table showing estimations of volcano volume for Lascar, Lonquimay and Llaima, carried out in this study through morphometric techniques and running our volcano growth model, as well as previous measures reported.

	This work (DEMs analysis)	This work (modeled volume)	Previous estimations	Reference
Lascar	11	12.70	15	Gardeweg et al. (1998)
			16	González-Ferrán (1995)
			18	Suárez and Emparan (1997)
Lonquimay	12	11.17	59	Polanco (2010)
			22.2	Völker et al. (2011)
			21	Aravena (2016)
			400	Naranjo and Moreno (2005)
Llaima	156	185	377.2	Völker et al. (2011)
			216	Aravena (2016)

The estimated number of eruptive events required to build each volcano is a broad approximation. However, we believe it is a first step towards a better understanding of the processes that build a volcano edifice which until now, has been an unexplored field on volcano morphology studies. With the implementation of our volcano growth model, we could estimate the number of effusive events needed to build Lascar, Lonquimay and Llaima: 50, 224 and 1963 respectively. In composite volcanoes, early lavas tend to be more voluminous and extensive than later lavas (Davison and De Silva, 2000). This behavior is predicted by our model and observed in Lonquimay and Lascar volcanoes.

Hence, it is expected that the main volumetric contribution to the building of a volcanic edifice is by the first lavas. According to our model, 90% of the current volume of Llaima volcano is achieved in 1481 eruptions (out of 1963), 3/4 of the total effusive eruptive events. Since the volume of lava flows decreases as the volcano grows, it is reasonable to state that the last flows contribute poorly to the edifice volume. In terms of time, this is most difficult to constrain due to the unpredictable behavior of the replenishment rate of magma to the chamber (Q_s). Nevertheless, we know that a constant Q_s (assumed in this study) is associated to a gradual increase of eruption frequency as the volcano grows.

Considering a fixed replenishment rate of magma to the chamber (Q_s), the average frequency of lava flow emission is about one eruption every 4000 years for Lascar, 390 for Lonquimay and 99 for Llaima volcano. However, in volcanic systems Q_s is variable in time. Usually its value is inferred from the eruption rate and is often considered equal to it, but it is not entirely true, as it is possible that not all the magma entering a magma chamber will be erupted. Variations on the eruption rate at a scale of thousands of years as well as peak eruption rates during short periods of time are widely recognized. Parinacota volcano is a case where a very fast rebuilt after a larger debris avalanche (6 km^3 from a 18 km^3 volcanic edifice) evidenced a substantial increment on eruptive rate from 0.06 km^3/ky to 2.5km^3/ky, during the last 8 ka (Clavero et al., 2002).

Statistical studies carried out at Lonquimay and Llaima volcanoes regarding historical eruptions and tephra deposits, evidence several changes on the eruptive rate. At Lonquimay volcano two historical eruptions with large volume lava flows (1887 and 1988) and other with minor volumes erupted (1853, 1933 and 1940) appear on the historical record. All this activity occurred in NE flank (Edmundo Polanco, personal communication 2015). Gilbert et al. (2012) identified a change in the eruptive frequency by observing the cumulative number of eruptions in the geological record, concluding the existence of a longer repose time after ~6 ka (Repose intervals increased from 413 to 972 years, with a middle short interval of higher frequency of 53 years). Likewise at Llaima volcano, Dzierma and Wehrmann (2010) proposed a current interval of eruptive activity of ~5.6 years.

Schindlbeck et al. (2014) recognized a long-term average rate of 2.17 eruptions per 1000 years, highlighting a strong increase during the last 3 ka. These studies evidence variable eruptive rates behaviors, in contrast with our model where the frequency increases as the volcano growths. Although the overmentioned studies are limited mainly to explosive events, they are useful to compare our frequency estimations. We notice that in Lonquimay volcano (average eruption recurrence of 390 yr) our results are in the order of magnitude of previous estimations. At Llaima volcano, previous works indicate an increase of the eruptive frequency during the last 3000 ka. This behavior is proposed by our model for volcanic edifices during the late-growth-stage and it is consistent with our suggestion that Llaima volcano is close to reach its maximum height. On the other hand, according to the historical record, despite more than 15 eruptions with lava flow emission associated have occurred, the volumetrically most considerable are the events of 1640, 1751, 1780 and 1957. In this case, the calculated recurrence is ~128 years, much closer to our average estimation. Despite Lascar is by far the most active volcano in the north of Chile in historical times, with more than 30 explosive eruptions since the XIX century, it does not have historical lava flow emissions and it lacks a more detailed statistical study to compare with our estimations. Nevertheless, the last dated lava flow has an age of 7.17±1.25 ka (Gardeweg et al., 2011) which agrees in order of magnitude with our estimated average time of repose between effusive events (~4000 yr).

Finally, it must be said that the values used to test the model (0.053 km^3/ky for Lascar, 0.13 km^3/ky for Lonquimay and 0.95 km^3/ky for Llaima volcanoes) are close to previous estimations of eruptive rate for continental volcanic arcs (1 km^3/ky; White et al., 2006) and exceed 0.01 km^3/ky, the minimum recharge required to keep a reservoir active (Menand et al., 2015), according to thermal analyses. However, we believe a most robust model demand a variable replenishment rate, although possible values are not easy to constrain due to the complexity of the eruptive rate behavior evidenced by the over-mentioned studies.

6.1.3. Summary of the effect of the magma chamber depth and size on volcano growth

The consistency of the above exposed results, indicate that the growth of stratovolcanoes can be simulated by using parameters of the plumbing system, as well as the reservoir location can be constrained analyzing the volcano topography. Clearly, more work is required to produce a precise and accurate model. However, some insights can be inferred based on these results. We considered several factors controlling the volcano construction such as magma chamber depth and size, crustal and magma density, overpressure in the magma chamber, chamber replenishment from a deep source and the effect of vent height exerted by the edifice over the system. Here we analyze mainly the effect exerted by the magma chamber size and depth. To illustrate it, we plot in Fig. 16 the results of the model for 4 volcanic systems whose magma chambers are located at different depths but with all the other parameters fixed. Figure 17 on the contrary, shows the results of the variations only of magma chamber size. In both cases, as it is predicted by Eq. (8), variations on H and V_c involve changes on lava flow volumes, and hence, on the length of the basal radius. To perform the exercise, we used parameters from Lonquimay volcano, relating V_e and $L_{\max}$ with Eq. (11) and using $C = 0.73$, value associated to the Navidad cone lava flow with known length and volume (Moreno and Gardeweg, 1989; Naranjo et al., 1992; Kerr and Lyman, 2007; Castruccio and Contreras, 2016).

Figure 16 shows the influence of reservoir depth on volcano dimensions. As the magma reservoir is located deeper into the crust, the volcano attains larger maximum height and longer period of activity. H not only influences the altitude, but also affects the lava flow volumes and hence the basal radius, which is related to the first lava flows extension. For a deeper chamber, larger volumes of lava flow can be emitted. Consequently, in agreement with previous observations, deeper reservoirs will be associated to more voluminous volcanic edifice, where larger volumes are needed to attain the maximum

altitude. Magma chamber size does not influence the maximum height that a volcano can attain, but influences strongly the lava flow volumes (Fig. 17). Large chambers promote larger lava flow volumes, basal radius and volcanic edifice dimensions. It must be noticed that this simple analysis is restricted only to the effect exerted by H and V_c. However, in a more realistic scenario, changes on this parameter also involve changes in the bulk modulus or the floatability. Indeed, the deeper a chamber is located, the lower is the compressibility, and a larger bulk modulus value can decrease V_e according to Eq. (8).

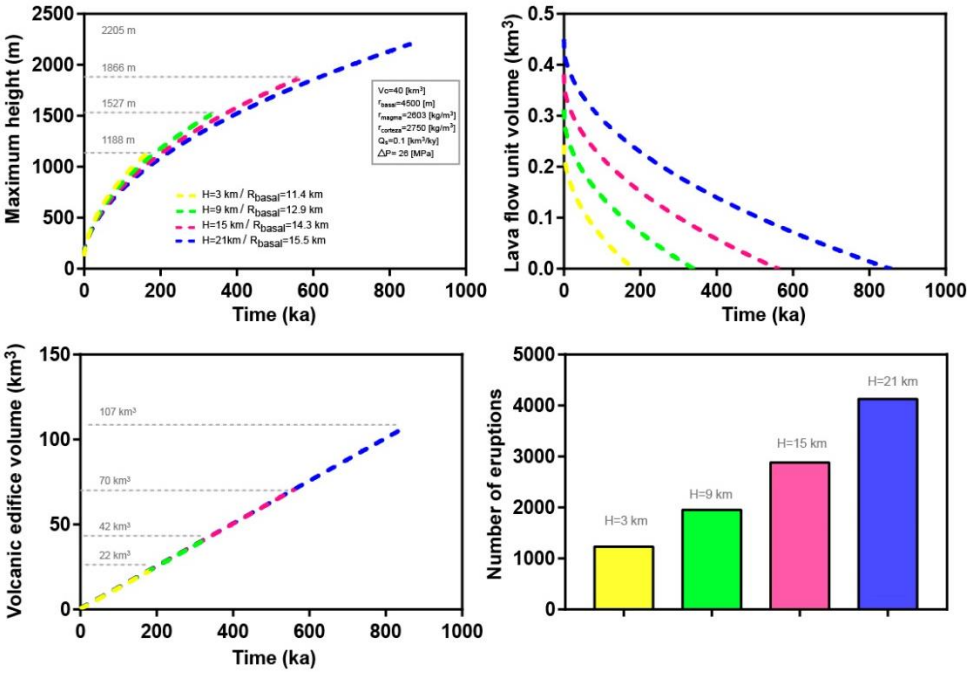

Fig. 16. Influence of magma storage location on volcano growth.

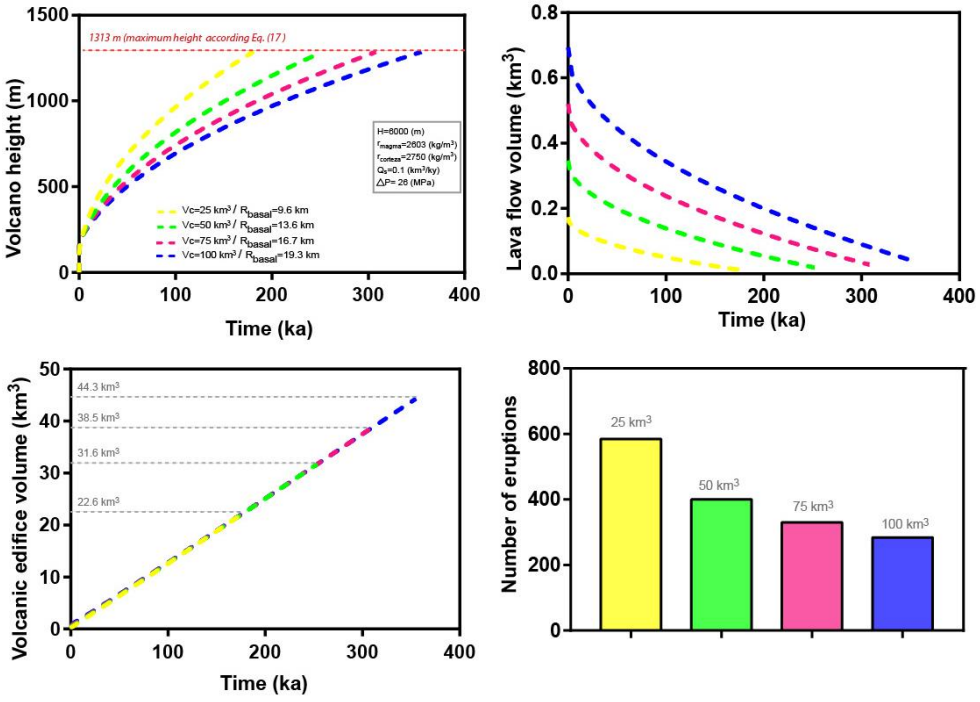

Fig. 17. Influence of magma chamber size on volcano growth.

6.2. Comparing Lascar, Lonquimay and Llaima model results: coupling volcano morphology and plumbing systems properties

6.2.1. Inferring the dynamic of magmas beneath Lascar, Lonquimay and Llaima volcanoes

As we discussed in previous sections, the depth of the reservoirs is a key parameter controlling the altitude that a volcano can attain. Based on Eq. (13), the deeper the reservoir, the higher the volcanic edifice. However, it is not easy to predict the maximum height of a stratovolcano as several factors can be of influence, and the volcano growth is a dynamic process both on surface and at depth (i.e. magma composition evolves, multiple reservoirs originate during the time of activity, etc). Based on our results, we propose some insights about the dynamic of the magma beneath the studied volcanoes, which could be validated in other similar volcanoes (Fig. 18).

We suggest that at Llaima volcano, the magma reservoir at 18 km depth is the source of the overpressure as it is connected with other shallower reservoirs (revealed by thermobarometry) which originated while the volcanic edifice was growing. We support the idea that a growing volcano can inhibit eruptions and induce magma storage at shallow crustal levels, taking advantage of lithological discontinuities (Pinel and Jaupart, 2000; Pinel and Jaupart, 2004). The formation of shallow transient reservoirs just before an eruption volcanoes is also possible. Results of time dependent local earthquake tomography at the Kluchevskoy group of volcanoes show a potential magma storage close to the surface during pre-eruptive periods, disappearing after the eruption (Koulakov et al., 2013). Form literature data, we identified other noticeable voluminous volcanic systems (height >2000 m above the base and volume>100 km^3) with available plumbing system information: Villarrica (H:0-5.3 km/ H:19-35 km; Morgado et al., 2015. h: 2360 m), Fuji (H:15 km; Aizawa et al., 2004. h:3776 km); Klyuchevskoy (H: >30 km/ 10-12 km/<5 km; Koulakov et al., 2013. h:4649 m). In general terms, all of them exhibit compositions and volume similar to Llaima volcano.

Apparently, >2000 m-height volcanoes, built by pilling of less evolved magmas, are associated to magma chambers residing deep in the crust. We suggest that in Llaima-like volcanic systems, the input of fresh magma in the deepest reservoir can be the source of the overpressure needed to trigger the eruptions. The low viscosity associated to less evolved magmas facilitates a fast ascent through the crust, as well as the multiple storage levels of magmas. The shallower reservoirs are hydraulically connected with the deepest reservoir during the eruptions, and consequently, they are also affected by the input of new magma before an eruptive event. Most likely, the mobility of magma is promoted also by the tectonic control exerted in certain zones; in the SVZ for example, by the dextral strike-slip Liquiñe-Ofqui Fault Zone.

In Lonquimay volcano in turns, the source of the overpressure seems to be the 6 km-depth reservoir. The higher P-T conditions would not represent significant reservoirs, but small storage zones, where some crystals are ripped and incorporated to the ascending magma (Fig. 21). We propose that eruptions in Lonquimay-like volcanoes (volume <100 km^3 and height <1500 m) are fed by shallow reservoirs, which would explain their limited height. Some examples of stratovolcanoes showing similar characteristics are: Nevado del Ruiz (H:4.5 km; Sigurdsson et al., 1990. h:1500 m) Calbuco (H:9-11 km; Delgado et al., 2016. h:1612 m).Vesuvius (H:7 km; Agostinetti and Chiarabba, 2008. h:1157 m). All of them share compositions that are more evolved than Llaima volcano.

Based on our model and petrological results, we envision the Lascar volcano plumbing system as an isolated magma chamber, directly connected to the surface and source of the eruptions. However, we believe it is highly probable the existence of several magma chambers below Lascar volcano, despite it has not been fully demonstrated in this work. Geophysical and petrological evidence for development of shallow magma chamber at depths of 5 to 10 km has been found at several andesite and dacite volcanoes (Sparks et al., 2008). Consequently, we suggest that other chambers could be the sources of the overpressure associated to eruptions, however, they would be not connected (Fig. 20). Lascar volcano-like systems most likely lack of the hydraulic connection described for Llaima and Lonquimay volcanoes. The higher viscosity associated to more differentiated

magma would reduce its mobility, and therefore its ascent would be slower. If more than a single reservoir exists, they would be completely separated from each other and only the directly connected to the surface reservoir would be the final responsible of triggering the eruption. Large increase in viscosity can also lead to magma stagnation, thus forming shallow plutons (Annen et al., 2006). In support of this theory, White et al. (2006) and Sparks et al. (2008) indicate that a low regional average rate (around 10^{-3}/yr) would indicate a significant proportion of magma intruded but not erupted. Uturuncu volcano for example, is a moderate-volume stratovolcano (85 km^3; Sparks et al., 2008) located in the CVZ. Its dominant composition is dacite and its reservoir is located at 16-20 km of depth (Comeau et al., 2016). The current unrest revealed by geophysical methods following the 270 ka of dormancy, indicate that the magmatic system is in a prolongated period of intrusion and possible future eruptions are expected (Sparks et al., 2008). Despite the deep Uturuncu volcano magma chamber, its height does not exceed 1612 m. Similarly to Lascar volcano, Uturuncu's vent has migrated several times and probably, due to the low eruptive rate, the growth has continued for a longer period of time until the reach of its maximum height, differently from other volcanic systems associated to less evolved magmas.

Finally, we would like to emphasize that the above proposed plumbing systems models are not a generic rule of course. They work for the volcanoes selected for this study and probably, they could work for some volcanic systems similar to Lascar, Lonquimay and Llaima volcanoes.

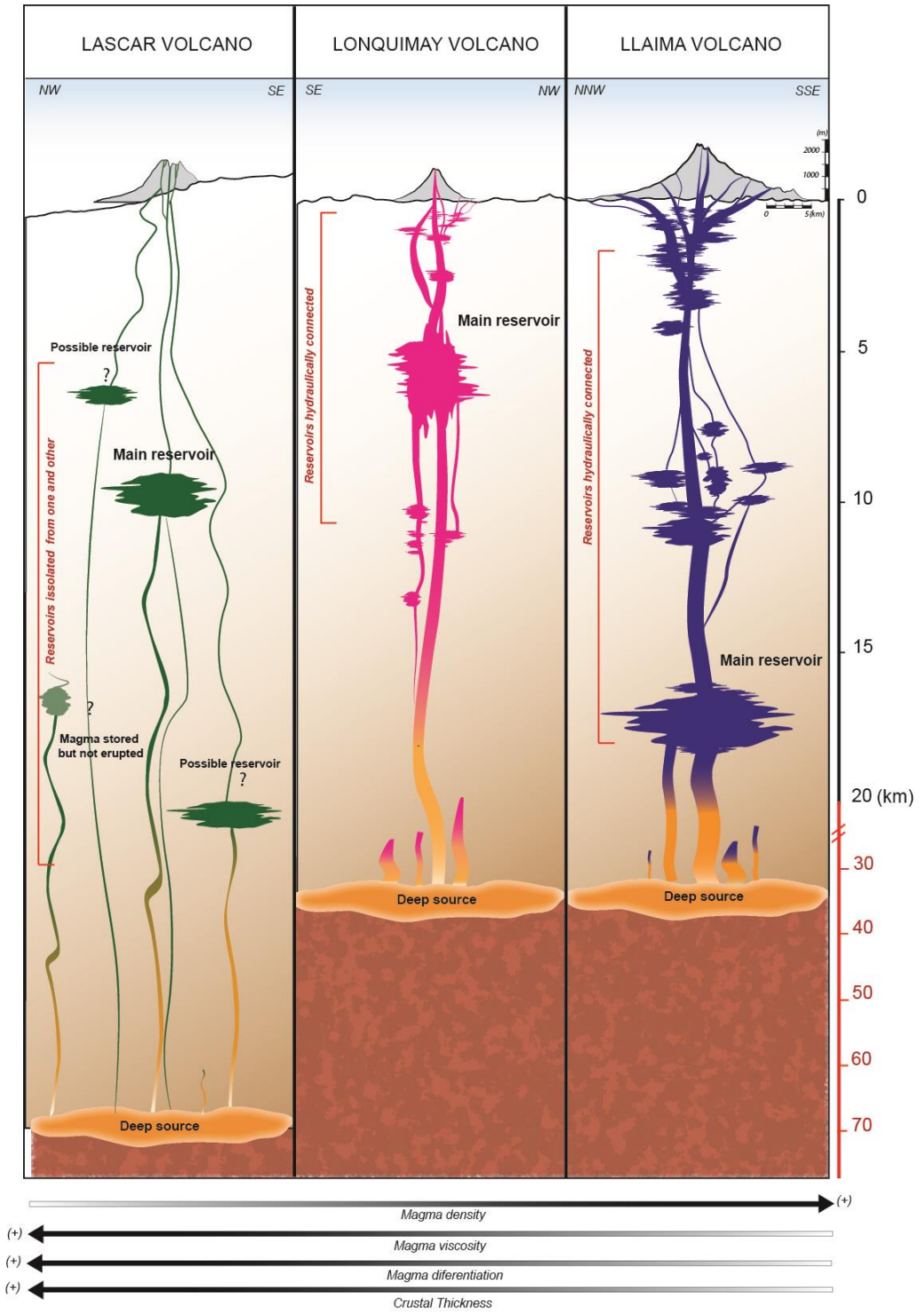

Fig. 18. Final model displaying the main characteristics of the volcanic systems here studied which can also be extended to similar volcanic systems. Hydraulically connected reservoirs are suggested for Lonquimay and Llaima volcanoes, while Lascar volcano-like systems are represented by isolated storage levels. Reservoirs are larger as deeper is their location in the crust. Widths of conduits represent the higher mobility of less viscous magmas into the crust.

6.2.2. Volcano dimension and its geological context: A comparison of the Central (CVZ) and Southern Volcanic Zone (SVZ)

Andesite, dacite and rhyolite are the dominant magmas erupted in the CVZ. Basalt and basaltic andesite are the common compositions in the SVZ, although through the northern and transitional segments of the SVZ andesite predominates (Stern, 2004). The volcanoes considered in this study are representatives of this tendency. In general terms, Lascar's products (CVZ) are in the andesite-dacite range and Lonquimay and Llaima (SVZ) show andesite-basaltic andesite and basalt compositions respectively. Crustal thickness at Lascar volcano latitude is ~70 km (Díaz et al., 2012). From north to south the continental crust thins gradually, showing a thickness of 40 km at the latitude of Lonquimay and Llaima volcanoes (Tassara et al., 2006). The average crustal density is also different: around 2680 kg/m^3 in the Lascar volcano area (Lucassen et al., 2001) and 2750-2820 kg/m^3 in the Lonquimay and Llaima volcanoes area (Tašárová, 2007). In order to elucidate if there are substantial differences in terms of volcano dimension between volcanoes located at different tectonic setting, we carried out a statistical analysis considering 29 and 32 stratovolcanoes from CVZ and SVZ respectively. We selected composite volcanoes with clear boundaries and displaying a morphology similar to a cone. Volcanoes with several vents and irregular morphology (e.g. Lastarria volcano) were excluded. We estimated average height and basal radius (Appendix 6) and plotted the results in Figure 19a and 19b. We do not identify noticeable differences in dimension of volcanoes from the CVZ comparing with the ones in the SVZ. The height of SVZ' volcanoes are similar to the ones of CVZ' volcanoes. Likewise, the comparison of the basal area of CVZ and SVZ' volcanoes does not reveal significant differences. According to Eq. (13), the maximum altitude that a volcano can attain depends on several factors including the magma chamber depth (above analyzed) and magma density. In order to examine the density effect, we considered average values of crustal and magma density. Figure 20a shows the maximum height of 3 hypothetic volcanoes with contrasting magma composition and density, located in the same area (equal density crust). We considered the three next average values for density: 2350 kg/m^3, 2500 kg/m^3 and 2650 kg/m^3,

representing typical density of dacitic, andesitic and basaltic magmas respectively, and an average crustal density of 2750 kg/m^3. The graph shows a strong influence of magma density on volcano's height. The more evolved the magma, the higher the predicted volcano is. A low density of magma favors floatability, and we can expect to observe a higher volcano. On the contrary, the higher density of less evolved magmas decreases the buoyancy and the predicted volcano shows smaller dimensions. It can be inferred that if similar altitudes are observed in volcanoes with contrasting compositions and we assume that they are close to attain their maximum height, differences of reservoir depth could explain their similar dimensions. Volcanoes associated to less evolved magmas most likely are associated to deeper reservoirs feeding eruptions, due to the fact that floatability does not promote a higher volcano. Under this premise, volcanoes associated to differentiated magmas which are favored by the floatability, would most likely be associated to magma storage at shallow levels. The values of crustal and magma density used in this analysis are not representative of the overall volcanic systems, as a more evolved magma not always is associated to a higher floatability, but it depends on the area where the volcano is located. For example, the average magma density for Lascar volcano is ~2542 kg/m^3 and the crustal density in the area where it is emplaced is 2680 kg/m^3 ($\Delta\rho$=138 kg/m^3). In Llaima volcano in turns, the average magma density is greater ~ 2653 kg/m^3, but the crustal density is around 2820 kg/m^3 ($\Delta\rho$=167 kg/m^3), making greater the floatability. These results, along with the associated deep reservoir, explain the Llaima volcano grow height of over 2400 m.

Magma composition is not the only parameter affecting magma density, also volatile contents play a major role. Figure 20b shows the maximum height that a basaltic volcano can attain depending on the magma chamber depth and the dissolved volatile content. A hydrous magma (0.5%wt) is less dense than an anhydrous one. Consequently, in the first case the floatability is promoted and a higher volcano is expected. Considering a 20 km depth magma chamber, a volcano built by hydrous basaltic lava flows, will be 200 m higher than a volcano associated to anhydrous basaltic lava flows. Moreover, if we consider the nucleation of bubbles in the magma (which can be important in hawaiian and strombolian

eruptions), the density decreases dramatically, affecting noticeably the volcano dimension predicted by the model.

As several factors control the maximum height of a volcano, clearly more work is required to produce a precise and accurate assessment of the parameter's influence. It surely must be considered as one of the principal challenges ahead.

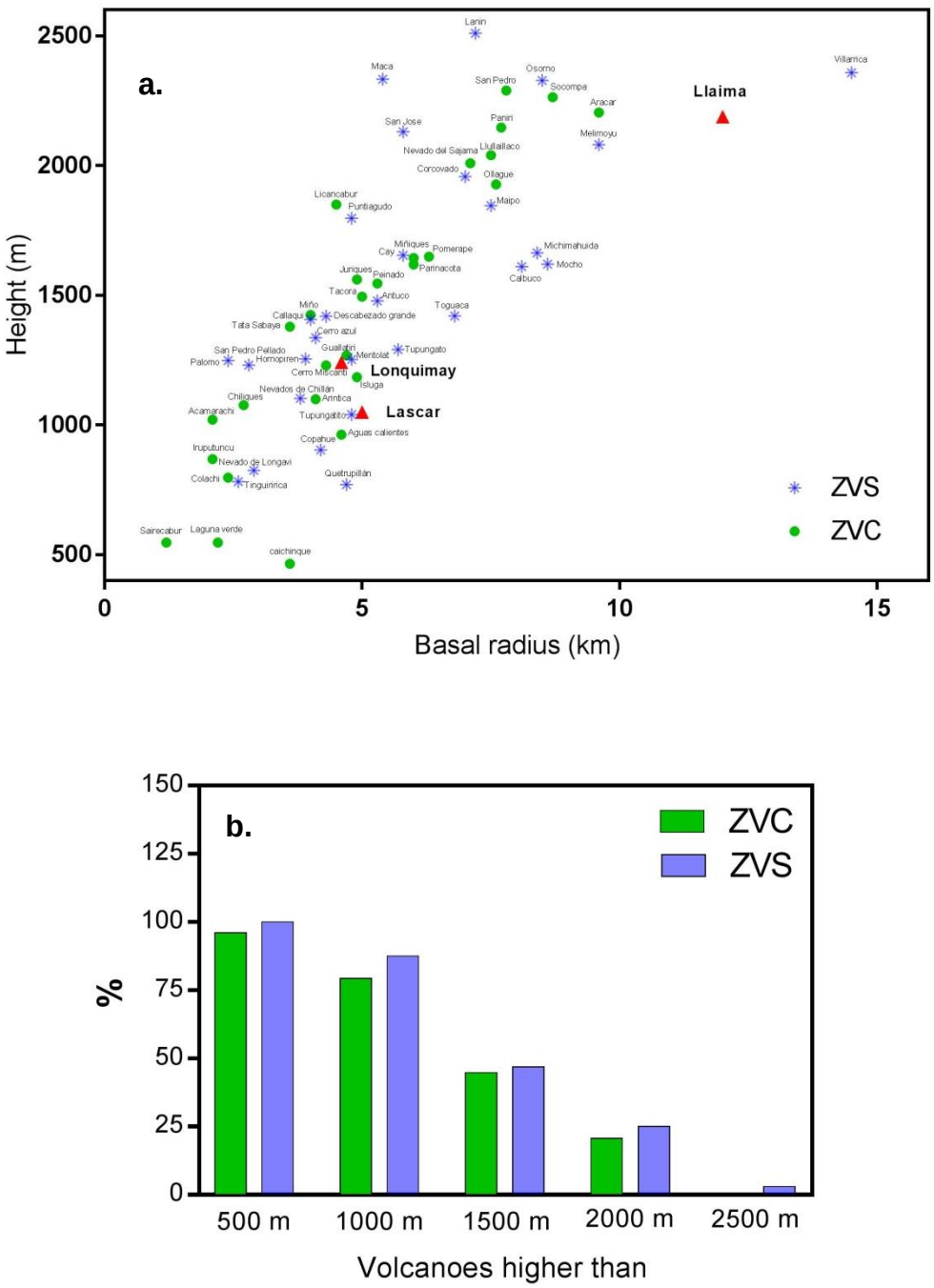

Fig. 19. (a) CVZ and SVZ volcano dimensions. Data were obtained by using DEMs and Google earth images. CVZ volcanoes are represented by green circles, and SVZ volcanoes by purple stars. Volcanoes studied in this work are highlighted as red triangles. (b) Cumulative frequency of volcano heights from SVZ (32 volcanoes) and CVZ (29 volcanoes).

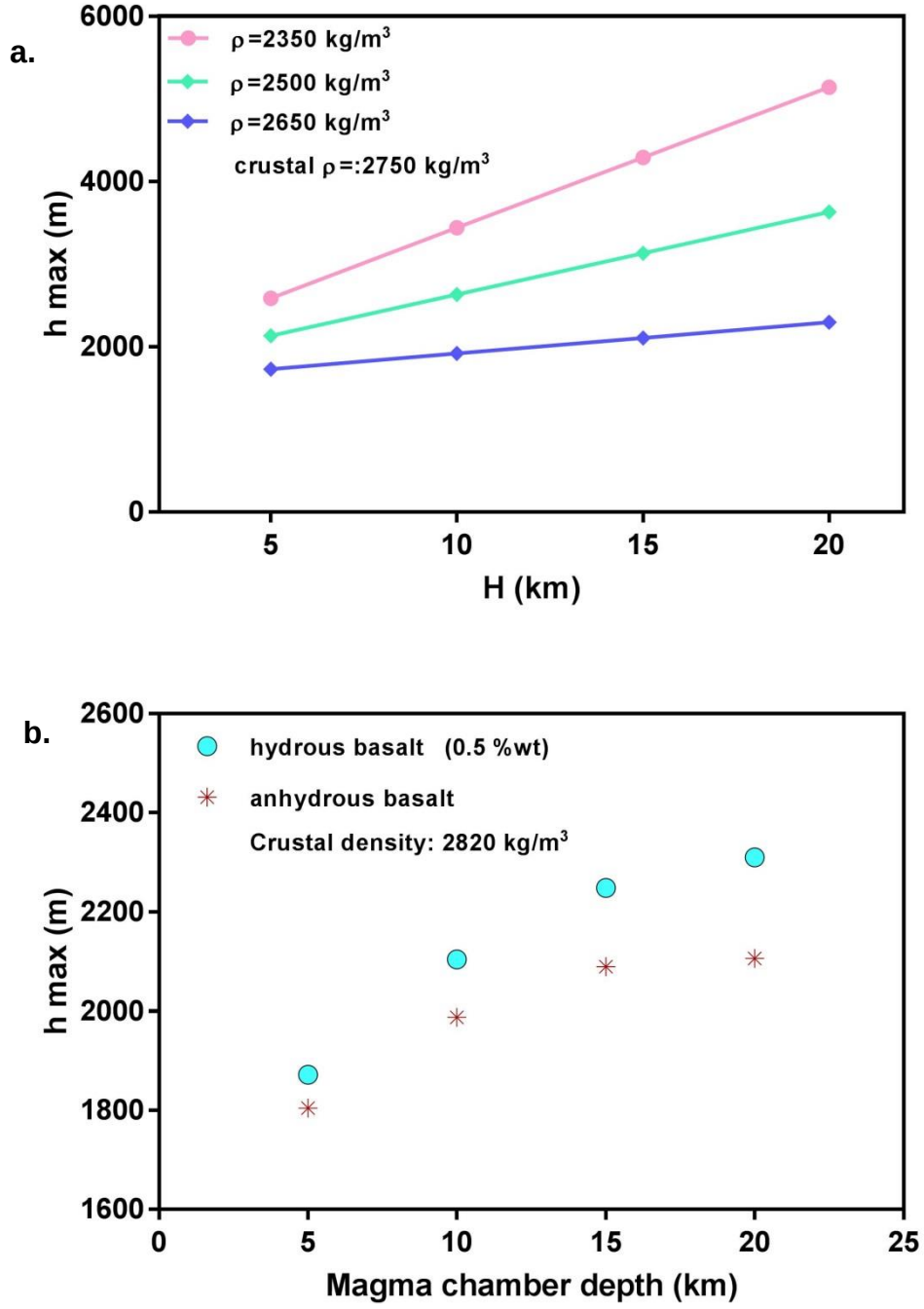

Fig. 20. (a) Magma density control on the maximum volcano height depending on magma composition. (b) Magma density control on the maximum volcano height depending on volatile content.

6.3. Limitations of the model and challenges ahead

Some simplifications have been considered in our study, such as the constant-volume magma chamber, neglecting the effects resulting from cooling and crystallization. In a strict sense, a minimum supply of magma must be guaranteed to sustain melt in a reservoir that loses heat, and future efforts must consider it. We also suppose that the triggering factor leading to a volcanic eruption is the injection of fresh magma into the chamber and the overpressure associated with the remobilizing of the stored and partially crystalline magma. However, other processes can be responsible to lead and trigger an eruptive event, such as buildup of pressure in crystalizing, water-supersaturated magma and/or tectonic triggering (Cashman et al., 2013 and refernces therein). All the triggered eruption mechanisms require processes that enhance small static stress changes, that can convert transient dynamic strains into permanent changes on pressure (Manga and Brodsky, 2006). Every mechanism involves several convoluted processes and the model here proposed is unable to account for all of them. Processes into the reservoir can be extremely complex, including magma mingling/mixing, compositional stratification, disruption of cumulates, and assimilation of wall rock (Cashman et al., 2013). Indeed, Lascar volcano's samples exhibit magma mixing evidence (Matthews et al., 1994). It must be noticed that our model does not faithfully represent most of the processes occurred inside the reservoir. The restrictions introduced in our model are necessary for a first and simplified approach to the understanding of the volcano morphology-magmatic system properties and the relationship among them.

One of the first recognized factors controlling the elevation of volcanoes in subduction zones is the floatability (Ben-Avraham and Nur, 1980). Magma density is a variable parameter along the entire life of a volcano and during magma ascent. Consequently, it is a parameter hard to constrain, and several assumptions must be done. Bubbles in the magma decrease its density and increase the buoyancy, affecting model estimations. It is accepted to consider a bubble-free magma when modeling eruptions of lava (Stasiuk and Jaupart, 1997; Castruccio et al., 2017), as it is assumed that lava flows originate when

magma degassing is sufficiently fast, relative to the rate of ascent, and that magma finally reaches the surface without fragmenting (Cashman et al., 2013). However, we believe future efforts must be focused on the volatiles exsolution effect in magma chambers and during ascent, with particular attention to hawaiian and strombolian eruptions, where bursts of gas and lava are released. Furthermore, these eruptive styles are associated to clastogenic lava flows formed from re-fusion of fragmented material (Parfitt and Wilson, 2007; Cashman et al., 2013), leading to possible mistakes in field measurements, as our model considers lava flows emitted effusively. Previous studies have highlighted about the crucial role that exsolved volatiles play in magma chambers by controlling eruption volume and duration of effusive events, with overpressure controlling eruption rate. As the effective compressibility increases, a decrease in pressure occurs, leading to a greater expansion of the magma and hence, for a given chamber size, a larger mass of magma is erupted (Huppert and Woods, 2002; Woods and Huppert, 2003).

We limited our maximum altitude analyses to the effect caused by the edifice growth and the magma storage depth. Nevertheless, other processes could affect it. For example, if magma supply rate decreases enough, volcanic activity may stop before the replenishment (Pinel et al., 2010).

It would be interesting to add other tools to improve our model considering more realistic scenarios, such as explosive eruptions and pyroclastic deposits, several magma chambers as overpressure source and the lateral (and not only vertical) growth of the volcanic edifice. It would be interesting to account for the influence of shifts of vent location during volcano building at Lascar-like volcanoes. We think that this last process could delate the growth of a volcanic edifice, as longer time will be required to reach its maximum height. By taking into account the over mentioned scenarios, we think that it could be possible to explain why Lascar is the most active volcano in the northern Chilean Andes in historical times, and its remarkable contrast with neighboring volcanoes without historical eruptions.

Magma chamber size estimates using physical models as complement to geophysical approaches is by far one of the most interesting challenges in recent volcanology, as well as a relatively unexplored field. A vast range of chamber sizes has been inferred mainly with geophysical methods, ranging from some tens to several hundred cubic meters (e.g. 11.4 km^3 in Etna; Sharp et al., 1980; 0.01-3000 km^3 in silicic magmas; Bower and Woods, 1997; 30 km^3 in Vesuvius; Agostinetti and Chiarabba, 2008; 650 km^3 in Klyuchevskoy; Fedotov et al., 2010; 13 km^3 in Soufriere Hills; Paulatto et al., 2012). In this work, we estimated reservoir volumes of three stratovolcanoes, resulting in values in the same order of magnitude. It would be interesting to test our model on volcanoes with known magma chamber volume estimates, as we could evaluate the model as an alternative to typical method to constrain this plumbing system parameters.

7. CONCLUSIONS

Magmatic system properties such as magma chamber depth and size have a strong influence on volcano topography and dimension. Estimates on reservoir location using our proposed model are in good agreement with values suggested by thermobarometric and geophysical methods on Lascar, Lonquimay and Llaima volcanoes. Consequently, we suggest that this model can provide an independent and complementary method to estimate magma chamber depth and size as a function of volcano morphology of composite volcanoes.

Llaima-like volcanoes (higher than 2000 m, predominantly basalt-basaltic andesite magma compositions and basal radius over 10 km) would be associated to plumbing systems constituted by several interconnected reservoirs located at different depths in the crust. These less evolved and low viscous magmas, facilitate the transport through the crust, the rapid ascent and the multiple reservoir formation. These magma chambers would be hydraulically connected during every eruption: due to the reservoirs being physically connected, the input of fresh magma in the deepest reservoirs triggers the movement of magma in the other shallower ones. Hence, the overpressure caused by the input of fresh magma into the deepest reservoir would be the responsible of the eruptions.

Viscous and more evolved magmas move slowly into the crust and the reservoirs associated would not be hydraulically connected. Probably several batches of magma will not be able to reach the surface and will cool in the crust. Consequently, in Lascar volcano-like systems, the input of magma responsible of a given eruptive event is received by the reservoir directly connected to the surface.

Magmas stored deeper than 10 km in the crust are associated to voluminous volcanoes with more than 2000 m high, with large basal radius (usually >10 km) (e.g. Llaima volcano). On the other hand, volcanoes associated to shallower reservoirs (<6 km) only reach less than 1500 m high and the basal radius does not over 10 km (e.g. Lonquimay

volcano). Large magma chambers favor larger erupted volumes and hence, the construction of voluminous volcanoes.

Our analyses suggest that Lonquimay and Llaima volcanoes reached or are close to reach their maximum height and volumetrically large eruptions will occur at their flanks, with only minor activity through their summit. Lascar volcano has not reached its maximum height and consequently large eruptions are still expected to occur from the summit crater.

Although our model is simplified, we believe it is a contribution to a better understanding of the link between surface properties and deep plumbing volcanic systems. We think the challenge now is to generate more accurate estimates especially of the more sensitive parameters. Also, it is important to consider a more complete scenario with variable replenishment rate from the deep source, several levels of storage reservoirs, shifts of vent location during the volcano growth and the inclusion of explosive events.

BIBLIOGRAPHY

Agostinetti N. P. and Chiarabba C. (2008) Seismic structure beneath Mt Vesuvius from receiver function analysis and local earthquakes tomography: Evidences for location and geometry of the magma chamber. *Geophys. J. Int.* **175**, 1298–1308. https://doi.org/10.1111/j.1365-246X.2008.03868.x.

Aizawa K., Yoshimura R. and Oshiman N. (2004) Splitting of the Philippine Sea Plate and a magma chamber beneath Mt. Fuji. *Geophys. Res. Lett.* **31**, 2–5. https://doi.org/10.1029/2004gl019477

Annen C., Blundy J. D. and Sparks R. S. J. (2006) The genesis of intermediate and silicic magmas in deep crustal hot zones. *J. Petrol.* **47**, 505–539. https://doi.org/10.1093/petrology/egi084.

Aravena D. (2016) Balance volumétrico comparativo de edificios volcánicos en la Zona Volcánica Sur. Tesis doctoral. Universidad de Chile (in spanish).

Barrientos S. and Acevedo-Aránguiz P. S. (1992) Seismological aspects of the 1988-1989 Lonquimay (Chile) volcanic eruption. *J. Volcanol. Geotherm. Res.* **53**, 73–87. https://doi.org/10.1016/0377-0273(92)90075-o

Bathke H., Shirzaei M. and Walter T. R. (2011) Inflation and deflation at the steep-sided Llaima stratovolcano (Chile) detected by using InSAR. *Geophys. Res. Lett.* **38**, L10304. https://doi.org/10.1029/2011gl047168.

Ben-Avraham Z. and Nur A. (1980) The elevation of volcanoes and their edifice heights at subduction zones. *J. Geophys. Res.* **85**, 4325–4335. https://doi.org/10.1029/jb085ib08p04325.

Blake S. (1981) Volcanism and the dynamics of open magma chambers. *Nature* **289**, 783–785. https://doi.org/10.1038/289783a0.

Bouvet de Maisonneuve C., Dungan M. A., Bachmann O. and Burgisser A. (2012) Insights into shallow magma storage and crystallization at Volcán Llaima (Andean Southern Volcanic Zone, Chile). *J. Volcanol. Geotherm. Res.* **211**–**212**, 76–91. http://dx.doi.org/10.1016/j.jvolgeores.2011.09.010.

Bower S. M. and Woods A. W. (1997) Control of magma volatile content and chamber depth on the mass erupted during explosive volcanic eruptions. *J. Geophys. Res.* **102**, 10273. https://doi.org/10.1029/96jb03176.

Cashman K. V., Stephen R. and Sparks J. (2013) How volcanoes work: A 25 year perspective. *Bull. Geol.*

Soc. Am. **125**, 664–690. https://doi.org/10.1130/B30720.1.

Castruccio A., Rust A. C. and Sparks R. S. J. (2010) Rheology and flow of crystal-bearing lavas: Insights from analogue gravity currents. *Earth Planet. Sci. Lett.* **297**, 471–480. http://dx.doi.org/10.1016/j.epsl.2010.06.051.

Castruccio A. and Contreras M. A. (2016) The influence of effusion rate and rheology on lava flow dynamics and morphology: A case study from the 1971 and 1988–1990 eruptions at Villarrica and Lonquimay volcanoes, Southern Andes of Chile. *J. Volcanol. Geotherm. Res.* https://doi.org/10.1016/j.jvolgeores.2016.09.015.

Castruccio A., Diez M. and Gho R. (2017) The influence of plumbing system properties on volcano dimensions and topography. *J. Geophys. Res.* **122**. https://doi.org/10.1002/2017JB014855.

Cembrano J., Hervé F. and Lavenu A. (1996) The Liquiñe Ofqui fault zone: a long-lived intra-arc fault system in southern Chile. *Tectonophysics* **259**, 55–66. https://doi.org/10.1016/0040-1951(95)00066-6

Cembrano J., Schermer E., Lavenu A. and Sanhueza A. (2000) Contrasting nature of deformation along an intra-arc shear zone, the Liquiñe–Ofqui fault zone, southern Chilean Andes. *Tectonophysics* **319**, 129–149. https://doi.org/10.1016/S0040-1951(99)00321-2.

Cembrano J. and Lara L. (2009) The link between volcanism and tectonics in the southern volcanic zone of the Chilean Andes: A review. *Tectonophysics* **471**, 96–113. http://dx.doi.org/10.1016/j.tecto.2009.02.038.

Charles Stern (2004) Active Andean volcanism: its geologic and tectonic setting. *Andean Geol.* **31**, 161–206. https://doi.org/10.4067/s0716-02082004000200001.

Clavero J., Sparks R., Huppert H. and Dade W. (2002) Geological constraints on the emplacement mechanism of the Parinacota debris avalanche, Northern Chile. *Bull. Volcanol.* **64**, 40–54. https://doi.org/10.1007/s00445-001-0183-0.

Davison J. and De Silva S. (2000). Composite volcanoes. In Sigurdsson, H. (ed) *Encyclopedia of volcanoes*. Academic Press. 1417 pp.

Delgado F., Pritchard M. E., Ebmeier S., González P. and Lara L. (2016) Recent unrest (2002-2015) imaged by space geodesy at the highest risk Chilean volcanoes: Villarrica, Llaima, and Calbuco (Southern Andes). *J. Volcanol. Geotherm. Res.* http://dx.doi.org/10.1016/j.jvolgeores.2017.05.020.

Denton G. H., Heusser C. J., Lowell T. V., Moreno P. I., Andersen B. G., Heusser L. E., Schluchter C. and Marchant D. R. (1999) Interhemispheric Linkage of Paleoclimate druing the last Glaciation. *Geogr. Ann. Ser. A Phys. Geogr.* **81**, 107. https://doi.org/10.1111/j.0435-3676.1999.00055.x

Di Stefano R. and Chiarabba C. (2002) Active source tomography at Mt. Vesuvius: Constraints for the magmatic system. *J. Geophys. Res.* **107**, 2278. http://doi.wiley.com/10.1029/2001JB000792.

Díaz D., Brasse H. and Ticona F. (2012) Conductivity distribution beneath Lascar volcano (Northern Chile) and the Puna, inferred from magnetotelluric data. *J. Volcanol. Geotherm. Res.* **217**–**218**, 21–29. http://dx.doi.org/10.1016/j.jvolgeores.2011.12.007.

Fedotov S. A., Zharinov N. A. and Gontovaya L. I. (2010) The magmatic system of the Klyuchevskaya group of volcanoes inferred from data on its eruptions, earthquakes, deformation, and deep structure. *J. Volcanol. Seismol.* **4**, 1–33. https://doi.org/10.1134/s074204631001001x.

Gardeweg M. C., Sparks R. S. J. and Matthews S. J. (1998) Evolution of Lascar Volcano, Northern Chile. *J. Geol. Soc. London.* **155**, 89–104. https://doi.org/10.1144/gsjgs.155.1.0089.

Gardeweg M., Matthews S. J., Sparks R. S. J., Clavero, J. (2011) *Geología del volcán Láscar*, Región de Antofagasta. Servicio Nacional de Geología y Minería, Carta Geológica de Chile, Serie Geología Básica 131:40 p., 1 mapa escala 1:50.000. Santiago (in spanish).

Ghiorso M. S. and Sack O. (1991) Fe-Ti oxide geothermometry: thermodynamic formulation and the estimation of intensive variables in silicic magmas. *Contrib. to Mineral. Petrol.* **108**, 485–510. https://doi.org/10.1007/bf00303452.

Ghiorso M. S. and Evans B. W. (2008) Thermodynamics of rhombohedral oxide solid solutions and a revision of the Fe-Ti two-oxide geothermometer and oxygen-barometer. *Am. J. Sci.* **308**, 957–1039. https://doi.org/10.2475/09.2008.01.

Gho R. (2013) Determinación de parámetros eruptivos de flujos de Lava del Complejo Volcánico Lonquimay (38°S), Andes del sur. Memoria de título. Universidad de Chile. (in spanish).

Gilbert D., Freundt A. and Kutterolf S. (2012) Post-glacial time series of explosive eruptions and associated changes in the magma plumbing system of Lonquimay volcano , south central Chile. *Int J Earth Sci (Geol Rundsch)*. https://doi.org/10.1007/s00531-012-0796-x.

Giordano D., Russell J. K. and Dingwell D. B. (2008) Viscosity of magmatic liquids: A model. *Earth Planet. Sci. Lett.* **271**, 123–134. https://doi.org/10.1016/j.epsl.2008.03.038.

Grosse P., van Wyk de Vries B., Petrinovic I. A., Euillades P. A. and Alvarado G. E. (2009) Morphometry and evolution of arc volcanoes. *Geology* **37**, 651–654. https://doi.org/10.1130/g25734a.1.

Grosse P., van Wyk de Vries B., Euillades P. A., Kervyn M. and Petrinovic I. A. (2012) Systematic morphometric characterization of volcanic edifices using digital elevation models. *Geomorphology* **136**, 114–131. http://dx.doi.org/10.1016/j.geomorph.2011.06.001.

Huppert H. E. and Woods A. W. (2002) The role of volatiles in magma chamber dynamics. *Nature* **420**, 493–495. https://doi.org/10.1038/nature01211.

Johnson M. C. and Rutherford M. J. (1989) Experimental calibration of the aluminum-in-hornblende geobarometer with application to Long-Valley Caldera (California) volcanic-rocks. *Geology* **17**, 837–841. https://doi.org/10.1130/0091-7613(1989)017<0837:ecotai>2.3.co;2.

Kapinos G., Montahaei M., Meqbel N. and Brasse H. (2016) Three-dimensional electrical resistivity image of the South-Central Chilean subduction zone. *Tectonophysics* **666**, 76–89. http://dx.doi.org/10.1016/j.tecto.2015.10.016.

Karátson D., Favalli M., Tarquini S., Fornaciai A. and Wörner G. (2010) The regular shape of stratovolcanoes: A DEM-based morphometrical approach. *J. Volcanol. Geotherm. Res.* **193**, 171–181. http://dx.doi.org/10.1016/j.jvolgeores.2010.03.012.

Kerr R. C. and Lyman A. W. (2007) Importance of surface crust strength during the flow of the 1988-1990 andesite lava of Lonquimay Volcano, Chile. *J. Geophys. Res. Solid Earth* **112**, 1–8. https://doi.org/10.1029/2006jb004522.

Kervyn M., Ernst G. G. J., Van Wyk De Vries B., Mathieu L. and Jacobs P. (2009) Volcano load control on dyke propagation and vent distribution: Insights from analogue modeling. *J. Geophys. Res.* **114**, 26. https://doi.org/10.1029/2008jb005653.

Kilburn C. R. J. and Lopes R. M. C. (1991) General patterns of flow field growth: Aa and blocky lavas. *J. Geophys. Res.* **96**, 19721–19732. https://doi.org/10.1029/91jb01924.

Koulakov I., Gordeev E. I., Dobretsov N. L., Vernikovsky V. A., Senyukov S., Jakovlev A. and Jaxybulatov K. (2013) Rapid changes in magma storage beneath the Klyuchevskoy group of volcanoes inferred from time-dependent seismic tomography. *J. Volcanol. Geotherm. Res.* **263**, 75–91. http://dx.doi.org/10.1016/j.jvolgeores.2012.10.014.

Lange R. A., Frey H. M. and Hector J. (2009) A thermodynamic model for the plagioclase-liquid

hygrometer/thermometer. *Am. Mineral.* **94**, 494–506. https://doi.org/10.2138/am.2009.3011.

Loucks R. R. (1996) A precise olivine-augite Mg-Fe-exehange geothermometer. *Contrib. to Mineral. Petrol.* **125**, 140–150. https://doi.org/10.1007/s004100050211.

Lucassen F., Becchio R., Harmon R., Kasemann S., Franz G., Trumbull R., Wilke H. G., Romer R. L. and Dulski P. (2001) Composition and density model of the continental crust at an active continental margin - The Central Andes between 21° and 27°S. *Tectonophysics* **341**, 195–223. https://doi.org/10.1016/s0040-1951(01)00188-3.

Manga M. and Brodsky E. (2006) SEISMIC TRIGGERING OF ERUPTIONS IN THE FAR FIELD: Volcanoes and Geysers. *Annu. Rev. Earth Planet. Sci.* **34**, 263–291. https://doi.org/10.1146/annurev.earth.34.031405.125125.

Matthews S. J., Gardeweg M. C. and Sparks R. S. J. (1997) The 1984 to 1996 cyclic activity of Lascar Volcano, northern Chile: cycles of dome growth, dome subsidence, degassing and explosive eruptions. *Bull. Volcanol.* **59**, 72–82. Available at: http://link.springer.com/10.1007/s004450050176.

Matthews S. J., Jones A. P. and Gardeweg M. C. (1994) Lascar volcano, northern Chile; evidence for steady-state disequilibrium. *J. Petrol.* **35**, 401–432. https://doi.org/10.1093/petrology/35.2.401.

Menand T., Annen C. and Blanquat M. de Saint (2015) Rates of magma transfer in the crust: Insights into magma reservoir recharge and pluton growth. *Geology* **43**, 199–202. https://doi.org/10.1130/g36224.1.

Moore G., Vennemann T. and Carmichael I. S. E. (1998) An empirical model for the solubility of H_2O in magmas to 3 kilobars. *Am. Mineral.* **83**, 36–42. https://doi.org/10.2138/am-1998-1-203.

Moreno H. and Gardeweg M. C. (1989) La erupcion reciente en el complejo volcanico Lonquimay (Diciembre 1988-), Andes del Sur. *Rev. Geològica Chile* **16**, 93–117.

Morgado E., Parada M. A., Contreras C., Castruccio A., Gutiérrez F. and McGee L. E. (2015) Contrasting records from mantle to surface of Holocene lavas of two nearby arc volcanic complexes: Caburgua-Huelemolle Small Eruptive Centers and Villarrica Volcano, Southern Chile. *J. Volcanol. Geotherm. Res.* **306**, 1–16. https://doi.org/10.1016/j.jvolgeores.2015.09.023.

Naranjo J. A. and Moreno H. (2005) *Geología del volcán Llaima*, Región de la Araucanía. Servicio Nacional de Geología y Minería, Carta Geológica de Chile, Serie Geología Básica 88:33 p., 1 mapa escala 1:50.000. Santiago. (in spanish).

Naranjo J. A., Sparks R. S. J., Stasiuk M. V., Moreno H. and Ablay G. J. (1992) Morphological, structural and textural variations in the 1988-1990 andesite lava of Lonquimay volcano, Chile. *Geol. Mag.* **129**, 657–678. https://doi.org/10.1017/s0016756800008426.

Nicholls J., Carmichael I. S. E. and Stormer J. C. (1971) Silica activity and P total in igneous rocks. *Contrib. to Mineral. Petrol.* **33**, 1–20. https://doi.org/10.1007/bf00373791.

Nimis P. and Ulmer P. (1998) Clinopyroxene geobarometry of magmatic rocks Part 1: An expanded structural geobarometer for anhydrous and hydrous, basic and ultrabasic systems. *Contrib. to Mineral. Petrol.* **133**, 122–135. https://doi.org/10.1007/s004100050442.

Parfitt E. A. and Wilson L. (2007) *Fundamentals od physical volcanology*, Academic Press. 219 pp.

Paulatto M., Annen C., Henstock T. J., Kiddle E., Minshull T. A., Sparks R. S. J. and Voight B. (2012) Magma chamber properties from integrated seismic tomography and thermal modeling at Montserrat. *Geochemistry, Geophys. Geosystems* **13**, 1–18. https://doi.org/10.1029/2011gc003892.

Pinel V. and Jaupart C. (2000) The effect of edifice load on magma ascent beneath a volcano. *Philos. Trans. R. Soc. A Math. Phys. Eng. Sci.* **358**, 1515–1532. https://doi.org/10.1098/rsta.2000.0601.

Pinel V., Jaupart C. and Albino F. (2010) On the relationship between cycles of eruptive activity and growth of a volcanic edifice. *J. Volcanol. Geotherm. Res.* **194**, 150–164. Available at: http://dx.doi.org/10.1016/j.jvolgeores.2010.05.006.

Polanco E. (2010) Volcanoestratigrafía, geoquímica y peligro volcánico del volcán Lonquimay (38°30'S), Andes del Sur (Chile). Universidad de Barcelona. (in spanish).

Putirka K., Johnson M., Kinzler R., Longhi J. and Walker D. (1996) Thermobarometry of mafic igneous rocks based on clinopyroxene-liquid equilibria, 0-30 kbar. *Contrib. to Mineral. Petrol.* **123**, 92–108. https://doi.org/10.1007/s004100050145.

Putirka K. (1999) Clinopyroxene + liquid equilibria to 100 kbar and 2450 K. *Contrib. to Mineral. Petrol.* **135**, 151–163. https://doi.org/10.1007/s004100050503.

Putirka K. D., Mikaelian H., Ryerson F. and Shaw H. (2003) New clinopyroxene-liquid thermobarometers for mafic, evolved, and volatile-bearing lava compositions, with applications to lavas from Tibet and the Snake River Plain, Idaho. **88**, 1542–1554. https://doi.org/10.2138/am-2003-1017.

Putirka K. D. (2008) Thermometers and Barometers for Volcanic Systems. *Rev. Mineral. Geochemistry* **69**,

61–120. https://doi.org/10.2138/rmg.2008.69.3.

Rhodes J. M., Dungan M. A., Blanchard D. P. and Long P. E. (1979) Magma mixing at mid-ocean ridges: Evidence from basalts drilled near 22° N on the Mid-Atlantic Ridge. *Tectonophysics* **55**, 35–61. https://doi.org/10.1016/0040-1951(79)90334-2.

Ridolfi F., Renzulli A. and Puerini M. (2010) Stability and chemical equilibrium of amphibole in calc-alkaline magmas: An overview, new thermobarometric formulations and application to subduction-related volcanoes. *Contrib. to Mineral. Petrol.* **160**, 45–66. https://doi.org/10.1007/s00410-009-0465-7.

Ruth D. C. S., Cottrell E., Cortés J. A., Kelley K. A. and Calder E. S. (2016) From passive degassing to violent strombolian eruption: The case of the 2008 eruption of Llaima volcano, Chile. *J. Petrol.* **57**, 1833–1864.

Schindlbeck J. C., Freundt A. and Kutterolf S. (2014) Major changes in the post-glacial evolution of magmatic compositions and pre-eruptive conditions of Llaima Volcano , Andean Southern Volcanic Zone , Chile. https://doi.org/10.1007/s00445-014-0830-x.

Sharp A. D. L., Davis P. M. and Gray F. (1980) A low velocity zone beneath Mount Etna and magma storage. *Nature* **287**, 587–591. https://doi.org/10.1038/287587a0.

Sigurdsson H., Carey S., Palais J. M. and Devine J. (1990) Pre-eruption compositional gradients and mixing of andesite and dacite magma erupted from Nevado del Ruiz Volcano, Colombia in 1985. *J. Volcanol. Geotherm. Res.* **41**, 127–151. https://doi.org/10.1016/0377-0273(90)90086-u.

Sparks R. S. J., Folkes C. B., Humphreys M. C. S., Barfod D. N., Clavero J., Sunagua M. C., McNutt S. R. and Pritchard M. E. (2008) Uturuncu volcano, Bolivia: Volcanic unrest due to mid-crustal magma intrusion. *Am. J. Sci.* **308**, 727–769. https://doi.org/10.2475/06.2008.01.

Stasiuk M. V. and Jaupart C. (1997) Lava flow shapes and dimensions as reflections of magma system conditions. *J. Volcanol. Geotherm. Res.* **78**, 31–50. https://doi.org/10.1016/s0377-0273(97)00002-4.

Stern C. R. (2004) *Active Andean volcanism: its geologic and tectonic setting*. Andean Geology. 21, 161-206.

Tašárová Z. A. (2007) Towards understanding the lithospheric structure of the southern Chilean subduction zone (36°S-42°S) and its role in the gravity field. *Geophys. J. Int.* **170**, 995–1014. https://doi.org/10.1111/j.1365-246x.2007.03466.x.

Tassara A., Götze H. J., Schmidt S. and Hackney R. (2006) Three-dimensional density model of the Nazca plate and the Andean continental margin. *J. Geophys. Res. Solid Earth* **111**, 1–26. https://doi.org/10.1029/2005jb003976.

Vergniolle S. and Mangan M. (2000). Composite volcanoes. In Sigurdsson, H. (ed) *Encyclopedia of volcanoes*. Academic Press. 1417 pp.

Völker D., Kutterolf S. and Wehrmann H. (2011) Comparative mass balance of volcanic edifices at the southern volcanic zone of the Andes between 36°S and 46°S. *J. Volcanol. Geotherm. Res.* **205**, 114–129. https://doi.org/10.1016/j.jvolgeores.2011.03.011.

Wadge G. (1981) The variation of magma discharge during basaltic eruptions. *J. Volcanol. Geotherm. Res.* **11**, 139–168. https://doi.org/10.1016/0377-0273(81)90020-2.

Waite G. P. and Moran S. C. (2009) VP Structure of Mount St. Helens, Washington, USA, imaged with local earthquake tomography. *J. Volcanol. Geotherm. Res.* **182**, 113–122. http://dx.doi.org/10.1016/j.jvolgeores.2009.02.009.

White S. M., Crisp J. A. and Spera F. J. (2006) Long-term volumetric eruption rates and magma budgets. *Geochemistry, Geophys. Geosystems* **7**. https://doi.org/10.1029/2005gc001002.

Williams R. J. (1971) Reaction constants in the system Fe-MgO-SiO2-O2 at 1 atm between 900 and 1300C: experimental results. *Am. J. Sci.* **270**, 334–360. https://doi.org/10.2475/ajs.270.5.334.

Wilson L., Head J. W. and Parfitt E. A. (1992) The relationship between the height of a volcano and the depth to its magma source zone: A critical reexamination. *Geophys. Res. Lett.* **19**, 1395–1398. https://doi.org/10.1029/92gl01073.

Wood C. a (1982) On the geometric form of volcanoes - Comment. *Earth Planet. Sci. Lett.* **57**, 451. Available at: http://adsabs.harvard.edu/abs/1982E&PSL..57..451W. https://doi.org/10.1016/0012-821x(82)90164-9.

Wood C. A. (1980) Morphometric evolution of cinder cones. *J. Volcanol. Geotherm. Res.* **7**, 387–413. https://doi.org/10.1016/0377-0273(80)90040-2.

Woods A. W. and Huppert He. E. (2003) On magma chamber evolution during slow effusive eruptions. *J. Geophys. Res.* **108**, 2403. http://doi.wiley.com/10.1029/2002JB002019.

Appendix 1

Erupted volume as function of the magmatic system properties. Analytic solution of Equation (4).

Combining Eq. (1) and Eq. (3) we obtain an expression to relate the erupted volume and some magmatic system properties:

$$Q(t) = \frac{\partial V_e(t)}{\partial t} = \frac{w^3 l}{12\mu}\left(\Delta\rho g + \frac{k}{V_c H}\left(\Delta V_i - V_e(t)\right)\right) \qquad \text{(A1)}$$

$$\frac{\partial V_e(t)}{\partial t} = \frac{w^3 l}{12\mu}\Delta\rho g + \frac{w^3 l k \Delta V_i}{12\mu H V_c} - \frac{w^3 l k V_e(t)}{12\mu V_c H} \qquad \text{(A2)}$$

Which we can rewrite as:

$$\frac{\partial V_e(t)}{\partial t} = A - BV_e(t) \quad \text{(A3)}$$

With A and B equals to:

$$A = \frac{w^3 l}{12\mu}\left(\Delta\rho g + \frac{k\Delta V_i}{HV_c}\right) \qquad B = \frac{w^3 l}{12\mu}\frac{k}{V_c H}$$

(A3) can be solved analytically being the solution an exponential function (Wadge, 1981):

$$Q(t) = Ae^{-Bt} \quad \text{(A4)}$$

$$V_e(t) = \int Ae^{-Bt} \qquad \text{(A5)}$$

$$V_e(t) = -\frac{A}{B}e^{-Bt} + c \quad \text{(A6)}$$

With $V_e(t=0)=0$, $c=\frac{A}{B}$ (A7)

$$V_e(t)=-\frac{A}{B}(1-e^{-Bt}) \quad \text{(A8)}$$

Substituting A and B, the total erupted volume of magma erupted during an eruption is given by:

$$V_e(t)=-\frac{A}{B}(1-e^{-Bt}) \quad \text{(A9)}$$

$$V_e(t\to\infty)=\frac{A}{B}=\frac{V_c}{k}(\Delta P_i+\Delta\rho gH) \quad \text{(A10)}$$

Appendix 2

Building the topographic profile of a volcanic edifice

All sets of equations here presented were obtained from Castruccio et al. (2017). We considered a volcano built by a pile of lava flow units, distributed radially from a central vent. First, we assume that all the flows have the same length L, width W and thickness T. Using geometrical considerations, after a high number of eruptions, the volcano grows in such a way that the height decreases with the distance from the vent, as the planimetric area to cover with lavas at certain distance r is proportional to the perimeter of a circle of radius r. At a certain distance r, the ratio between the sum of the widths of all lavas nw (with n number of lavas) and the perimeter $2 \cdot \pi \cdot r$ is $\frac{nW}{2\pi r}$ and the mean height of the volcano at r will be this ratio multiplied by the thickness of lavas T:

$$h(r) = \frac{nTW}{2\pi r} \quad \text{valid for } r_{basal} > r > \frac{W}{2\pi} \qquad \text{(B1)}$$

Considering that the sum of individual lava flows corresponds to the volcano volume, we obtain:

$$h(r) = \frac{V_v}{2\pi r L} = \frac{D}{r} \quad \text{with} \quad D = \frac{V_v}{2\pi L} \quad \text{(B2)}$$

If we consider a volcanic edifice formed by lava flows, that reduce their volume through time due to the height of the volcano, a more appropriate expression would be:

$$h(r) = \sum_{i=1}^{n} \frac{V_i}{2\pi L_i r} \qquad \text{(B3)}$$

Where V_i is the nth emitted lava flow and n is the number of lava flows that reached a distance $> r$. Must be noticed that according to this equation, when $r = r_{basal}$ (n=1), $h(r)$

is close to cero and for distances close enough to the vent, $h(r)$ is very similar to the value given by (A2). Considering these observations, a representative relationship to describe them is:

$$h(r) = \alpha\left(\frac{1}{r} - \frac{1}{r_{basal}}\right) \qquad \text{(B4)}$$

With α constant. From simple trigonometry, we have that the topography slope ϕ is: $\phi = \tan^{-1}\left(\frac{\alpha}{r^2}\right)$. The smaller is the value for r, the larger is the slope of the volcano. For most volcanoes on earth, the repose angle rarely exceeds slopes >30°. Here we define the repose angle ϕ_{crit}, and for distance from the vent closer than r_{crit}, the slope is constant and equal to ϕ_{crit}.

$$r_{crit} = \sqrt{\frac{\alpha}{\tan(\phi_{crit})}} \qquad \text{(B5)}$$

In this segment the height of the volcano will be given by:

$$h(r) = (r_{crit} - r)\tan\phi_{crit} + \alpha\left(\frac{1}{r} - \frac{1}{r_{basal}}\right) \qquad \text{(B6)}$$

Combining (A4) and (A5) and using $h(0) = h_{\max}$:

$$r_{crit} = r_{basal}\left(1 - \sqrt{1 - \frac{h_{\max}}{r_{basal}\tan(\phi_{crit})}}\right) \qquad \text{(B7)}$$

$$\alpha = r_{basal}{}^2 \left(1 - \sqrt{1 - \frac{h_{\max}}{r_{basal} \tan(\phi_{crit})}} \right)^2 \tan(\phi_{crit}) = r_{crit}{}^2 \tan(\phi_{crit}) \quad \text{(B8)}$$

Finally, the volume of the volcanic edifice associated to these parameters is given by the solid of revolution with the profile given by (A4) and (A6).

$$V_v = \pi\alpha(r_{basal} - r_{crit}) + \frac{\pi r_{crit}{}^3 \tan(\phi_{crit})}{3} \quad \text{(B9)}$$

Appendix 3

Crystal fraction

Crystal content was obtained by point count on scanned thin sections using the *JMicroVision* software.

Sample	Phenocrysts	Microphenocrysts	Total	Ground mass
L1l-04	23.14	33.71	56.86	43.14
L2l-03	1.14	62.86	64.00	36.00
L4l-03	8.11	54.95	63.06	36.94
Nav	4.00	15.00	19.00	81.00
Lon2-01	0.85	22.16	23.01	76.99
Lon3-01	0.89	41.96	42.86	57.14
Lon4-02	0.00	35.41	35.41	64.59
L5LV01B	5.00	25.00	27.00	63.00
Llacp-02	13.90	36.68	50.58	49.42
Llacp-01	13.46	40.00	53.46	46.54
Llacp1751-02	11.74	37.25	48.99	51.01
Llacp1957-04	5.24	35.37	40.61	59.39

Size ranges:

*Phenocrysts: >1 mm

*Microphenocrysts: 0.1 mm- 1 mm

Appendix 4

Mineral chemical composition

In the following tables, the second column contains the name of the analyzed sample. For example, lon2-px1 refers to an analysis performed on pyroxene #1 contained in a sample from Unit 2. The sample is LFlon2 and the mineral studied is a pyroxene. The first column shows the location in the crystal where the measurement was performed. Numbers represent positions according the figure below:

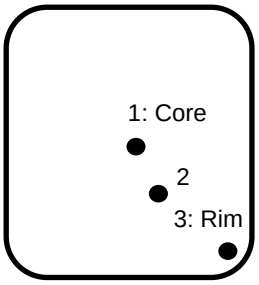

Sample name	Volcano unit defined on the geological map
LFLa1	Lascar/ Unit 1
LFLa2a	Lascar/ Unit 2
LFLa2b	Lascar/ Unit 2
LFLa4	Lascar/ Unit 4
LFLon1	Navidad cone
LFLon2	Lonquimay/ Unit 2
LFLon3	Lonquimay/ Unit 3
LFLon4	Lonquimay/ Unit 4
LFLon5	Lonquimay/ Unit 5
LFLla_a	Llaima/ Unit Llaima Ancestral
LFLla1	Llaima/ Unit Llcp
LFLla2	Llaima/ Unit Llcp
LFLla3	Llaima/ Unit Llcp
LFLla4	Llaima/ Unit Llcp

PYROXENE (LONQUIMAY VOLCANO)

Point location	Point name	SiO_2	TiO_2	Al_2O_3	FeO	MnO	MgO	CaO	Cr_2O_3	total
3	lon2-px1	52,45	0,34	0,55	20,94	0,87	21,10	4,07	0	100,40
3	lon2-px2	53,23	0,39	0,70	21,44	0,89	19,88	4,51	0,01	101,20
3	lon2-px3	51,82	0,54	1,51	11,37	0,46	15,49	18,98	0	100,40
1	lon2-px4	52,03	0,61	1,68	11,56	0,44	15,39	18,75	0,03	100,82
1	lon2-px5	53,28	0,38	0,64	22,14	0,85	19,63	4,46	0	101,52
3	lon2-px6	51,59	0,70	1,98	12,38	0,51	15,30	18,13	0	100,91
2	lon2-px7	51,03	0,81	2,22	11,64	0,42	14,90	19,09	0	100,46
1	lon2-px8	51,58	0,72	1,84	12,64	0,46	15,38	18,08	0	101,05
1	lon2-px9	51,08	0,86	2,49	12,31	0,51	14,07	18,68	0,03	100,40
1	lon3-px1	51,31	0,54	1,78	13,94	0,59	12,20	19,87	0	100,54
3	lon4-px2	51,15	0,55	1,87	13,79	0,56	12,16	20,02	0,01	100,44
2	lon3-px3	51,18	0,57	1,89	13,51	0,55	12,21	19,95	0,01	100,21
1	lon3-px4	51,06	0,59	1,99	13,98	0,55	12,44	20,00	0	101,00
1	lon3-px5?	52,12	0,52	1,67	14,31	0,60	12,33	20,11	0	101,97
3	lon3-px6	50,49	0,31	1,09	19,82	0,97	8,92	18,85	0,01	100,78
2	lon3-px7	50,18	0,33	1,07	19,25	0,97	9,18	18,80	0,01	100,13
1	lon3-px8	49,20	0,33	1,06	18,58	0,89	9,41	19,47	0,02	99,26
3	lon3-px9	50,46	0,29	1,03	18,93	0,92	9,27	19,36	0	100,59
1	lon3-px10	55,02	0,27	1,05	19,15	0,93	7,04	18,08	0,00	101,77
3	lon3-px11	50,62	0,30	1,08	19,27	0,94	8,75	19,20	0	100,52
2	lon3-px12	50,79	0,29	1,00	20,47	1,03	9,01	18,32	0	101,17
1	lon3-px13	50,66	0,30	0,96	18,80	0,89	9,34	19,48	0,03	100,77
1	Lon4-px2	51,83	0,53	1,72	12,39	0,50	14,30	18,91	0	100,45
3	Lon4-px3	51,54	0,58	1,96	11,94	0,47	14,28	19,49	0	100,58
1	Lon4-px6	51,19	0,55	0,75	25,98	1,00	17,19	4,29	0,02	101,06
1	Lon4-px7	51,40	0,47	0,63	25,49	1,00	17,07	5,14	0,02	101,38
1	Lon4-px8	46,47	1,00	2,28	15,93	0,74	12,02	19,31	0,00	98,05
1	Lon4-px9	49,77	0,52	1,53	28,47	1,05	15,48	4,32	0,01	101,46
1	Lon4-px11	51,51	0,61	0,91	25,67	1,02	16,90	4,65	0,03	101,37
	Un 16 Lon5_ol-px1	57,56	0,03	27,28	0,37	0,01	0,02	9,50	0,01	99,47

Point location	Point name	SiO_2	TiO_2	Al_2O_3	FeO	MnO	MgO	CaO	Cr_2O_3	total
3	Un 16 Lon5_ol-px1	52,21	0,54	1,68	13,92	0,56	13,40	17,88	0	100,49
3	Un 17 Lon5_ol-px2	52,21	0,42	1,31	14,67	0,64	12,23	18,59	0	100,36
3	Un 18 Lon5_ol-px3	51,94	0,60	1,86	13,94	0,57	13,02	18,16	0	100,43
3	Un 19 Lon5_ol-px5	50,39	1,19	3,53	13,04	0,47	13,15	18,19	0	100,37

PYROXENE (LLAIMA VOLCANO)

Point location	Point name	SiO_2	TiO_2	Al_2O_3	FeO	MnO	MgO	CaO	Cr_2O_3	total
3	Un 34 Llacp-01-ol-px4	52,68	0,47	2,03	8,76	0,26	16,39	18,52	0,48	99,89
3	Un 20 Llacp-01-ol-px2	51,84	0,48	1,95	9,58	0,30	16,97	16,99	0,26	98,67
1	Un 21 Llacp-01-ol-px6	53,81	0,22	0,91	14,98	0,36	25,94	2,16	0,10	98,50
3	Un 22 Llacp-01-ol-px6	52,90	0,40	1,05	18,00	0,45	23,81	2,27	0,01	98,96
3	Un 25 Llacp-01-ol-px9	51,56	0,46	2,12	9,08	0,27	16,52	18,04	0,47	98,87
3	Un 27 Llacp-01-ol-px11	53,69	0,29	1,33	14,59	0,36	25,80	2,37	0,16	98,68
3	Un 29 Llacp-01-ol-px12	52,51	0,47	1,93	8,65	0,25	16,62	18,19	0,36	99,32
3	Un 31 Llacp-01-ol-px19	53,65	0,23	1,03	14,61	0,35	26,21	2,16	0,10	98,40
3	Un 31 Llacp-01-ol-px19	51,08	0,54	2,32	9,17	0,29	16,39	17,71	0,49	98,32
3	Un 32 Llacp-01-ol-px18	51,62	0,48	1,88	9,67	0,27	16,78	17,62	0,23	98,85
3	Un 33 Llacp-01-ol-px17	51,80	0,47	1,97	8,97	0,25	16,50	18,17	0,34	98,75
1	Un 34 Llacp-01-px16	53,76	0,29	1,19	15,55	0,37	25,51	2,25	0,08	99,05
3	Un 34 Llacp-01-px16	53,06	0,36	0,95	17,82	0,44	24,08	2,11	0	98,88
1	Un 36 Llacp-1751-px1	53,74	0,29	1,30	14,65	0,37	26,01	2,29	0,26	98,98
3	Un 38 Llacp-1751-ol-px2	51,60	0,52	2,32	8,28	0,24	16,16	18,58	0,59	98,63
3	Un 39 Llacp-1751-ol-px3	52,05	0,50	2,21	8,26	0,22	16,26	18,66	0,53	99,04
1	Un 40 Llacp-1751-px4	53,59	0,32	1,19	15,49	0,35	25,22	2,25	0,09	98,48
3	Un 40 Llacp-1751-px4	52,21	0,42	1,56	9,02	0,29	16,58	17,41	0,29	98,09
1	Un 41 Llacp-1751-ol-px5	50,03	0,66	2,77	8,42	0,23	15,66	18,18	0,69	96,98
1	Un 49 Llacp-1751-px7	53,36	0,49	1,97	8,79	0,27	16,49	17,58	0,38	99,66
3	Un 49 Llacp-1751-px7	52,43	0,79	1,76	13,50	0,39	14,30	16,39	0,01	99,89

Point location	Point name	SiO_2	TiO_2	Al_2O_3	FeO	MnO	MgO	CaO	Cr_2O_3	total
3	Un 51 Llacp-1751-ol-px8	54,07	0,47	1,99	9,28	0,29	16,55	17,34	0,27	100,61
1	Un 53 Llacp-1751-px_clots10	53,47	0,45	2,05	9,28	0,26	16,16	17,83	0,19	100,03
2	Un 53 Llacp-1751-px_clots10	53,04	0,64	1,92	11,38	0,31	14,83	17,69	0,05	100,20
3	Un 54 Llacp-1751-px_clots10	53,74	0,52	2,01	9,93	0,28	17,03	16,28	0,47	100,54
1	Un 54 Llacp-1751-px_clots10	53,23	0,57	1,64	11,84	0,35	15,46	16,61	0,01	100,04
2	Un 54 Llacp-1751-px_clots10	53,53	0,52	1,72	10,13	0,29	15,91	17,38	0,12	99,92
3	Un 54 Llacp-1751-px_clots10	54,33	0,51	1,56	10,21	0,33	17,88	15,16	0,29	100,50
3	Un 55 Llacp-1751-ol-px12	53,66	0,47	2,02	8,42	0,24	16,26	18,07	0,36	99,86
3	Un 55 Llacp-1751-ol-px12	53,91	0,47	1,92	8,52	0,27	16,30	18,36	0,40	100,44
1	Un 57 Llacp-1751-ol15	41,13	0,00	0,01	15,25	0,21	44,03	0,17	0,01	100,93
1	Un 59 Llacp-1751-ol-px22	53,02	0,62	2,27	9,00	0,28	16,27	17,73	0,55	100,08
1	Un 59 Llacp-1751-ol-px22	52,72	0,64	1,90	11,06	0,31	15,48	17,22	0,07	99,72
3	Un 59 Llacp-1751-ol-px22	53,91	0,47	1,58	9,43	0,27	17,09	16,78	0,40	100,20
1	Un 62 Llacp-1751-px20	53,05	0,48	1,90	8,88	0,27	16,54	17,58	0,28	99,28
1	Un 62 Llacp-1751-px20	53,33	0,48	1,91	8,92	0,25	16,46	17,66	0,24	99,56
1	Un 63 Llacp-1751-ol-px19	55,27	0,28	1,26	14,77	0,35	25,76	2,29	0,17	100,20
1	Un 63 Llacp-1751-ol-px19	53,13	0,47	1,94	9,43	0,29	16,68	16,80	0,39	99,44
3	Un 10 Llacp-02-ol6	55,07	0,27	1,15	16,04	0,35	24,10	2,03	0.03	99,09
3	Un 10 Llacp-02-ol6	55,18	0,32	1,25	15,85	0,34	24,27	2,13	0.06	99,45
1	Un 18 Llalh-1957-ol-px7	55,32	0,29	1,12	15,02	0,35	25,54	2,16	0,12	99,96
1	Un 18 Llalh-1957-ol-px7	55,58	0,25	1,07	14,99	0,34	25,59	2,23	0,06	100,17
3	Un 30 Llalh-1957-ol-px2	51,94	0,54	2,08	8,76	0,26	16,28	18,08	0,40	98,62
3	Un 30 Llalh-1957-ol-px2	51,77	0,49	2,18	8,41	0,25	16,07	18,49	0,51	98,46
3	Un 30 Llalh-1957-ol-px2	52,44	0,49	1,97	8,57	0,25	16,55	18,00	0,43	98,97
3	Un 31 Llalh-1957-ol-px2	52,20	0,51	1,83	9,09	0,27	16,44	17,91	0,16	98,71

OLIVINE (LONQUIMAY VOLCANO)

Point location	Point name	SiO_2	Al_2O_3	FeO	MnO	MgO	CaO	total
3	lon2-ol3	30,78	2,84	32,99	0,77	32,96	0,29	100,80
1	lon2-ol9	36,74	0,02	34,50	0,83	29,69	0,26	102,08
1	lon3-ol3?	33,88	0,82	40,22	1,03	21,89	0,33	98,27
3	lon3-ol6	32,73	0,01	53,39	1,93	13,52	0,33	101,95
1	lon3-ol7	32,13	0	57,82	2,18	9,44	0,25	101,85
3	lon3-ol8	31,79	0	58,09	2,14	9,33	0,51	101,89
1	lon3-ol9	32,03	0	57,69	2,14	9,53	0,36	101,82
1	lon3-ol3	33,02	0,00	51,41	1,60	15,54	0,24	101,87
3	lon3-ol4	34,77	0,04	42,03	0,98	23,84	0,30	102,05
1	lon3-ol6	34,50	0,02	43,87	1,07	21,63	0,50	101,68
3	lon3-ol7	34,08	0,02	43,86	1,10	21,34	0,31	100,83
1	lon3-ol8	8,55	2,40	65,95	0,73	5,59	0,10	98,08
1	lon3-ol10	35,25	0,02	39,58	0,90	25,84	0,21	101,84
3	lon3-ol11	34,85	0,02	42,40	1,08	22,55	0,30	101,38
1	lon3-ol12	35,59	0,01	37,01	0,83	27,74	0,22	101,46
1	lon3-ol13	33,66	0,04	49,17	1,24	16,09	0,56	101,09
3	lon3-ol14	33,87	0,01	48,01	1,18	18,37	0,36	102,00
1	lon3-ol15	33,88	0,01	47,56	1,15	18,62	0,30	101,87
3	lon3-ol16	35,15	0,08	39,03	0,91	25,42	0,24	100,95
2	lon3-ol17	36,03	0	36,39	0,83	28,18	0,22	101,74
1	lon3-ol18	36,38	0	35,94	0,80	28,60	0,21	101,98
3	Un 16 Lon5_ol-px1	35,77	0	38,13	0,85	25,90	0,19	100,87
3	Un 16 Lon5_ol-px1	36,06	0	38,17	0,85	25,88	0,25	101,22
3	Un 17 Lon5_ol-px2	35,69	0	39,51	0,89	24,80	0,26	101,17
3	Un 18 Lon5_ol-px3	35,60	0	39,97	0,92	24,75	0,22	101,46
3	Un 19 Lon5_ol-px5	35,92	0	38,20	0,84	25,73	0,19	100,88

OLIVINE (LLAIMA VOLCANO)

Point location	Point name	SiO_2	FeO	MnO	MgO	CaO	total
3	Un 34 Llacp-01-ol-px4	37,60	24,47	0,39	36,19	0,29	99,00
3	Un 15 Llacp-01-ol-px2	37,26	26,82	0,43	34,41	0,29	99,31
3	Un 21 Llacp-01-ol-px6	37,19	24,71	0,41	35,94	0,27	98,60
1	Un 23 Llacp-01-ol7	37,51	25,28	0,38	35,88	0,26	99,43

Point location	Point name	SiO_2	FeO	MnO	MgO	CaO	total
1	Un 23 Llacp-01-ol7	37,27	25,18	0,40	35,96	0,24	99,15
1	Un 24 Llacp-01-ol8a	37,88	24,03	0,39	37,11	0,25	99,75
1	Un 24 Llacp-01-ol8a	37,73	24,07	0,36	36,95	0,25	99,45
1	Un 24 Llacp-01-ol8a	37,90	24,10	0,40	37,06	0,25	99,82
1	Un 25 Llacp-01-ol-px9	37,77	24,55	0,39	36,26	0,25	99,33
3	Un 26 Llacp-01-ol-px11	38,19	25,65	0,40	36,19	0,27	100,82
1	Un 28 Llacp-01-ol10	37,85	23,93	0,41	37,16	0,26	99,67
3	Un 28 Llacp-01-ol10	37,52	27,60	0,45	33,75	0,30	99,76
1	Un 28 Llacp-01-ol10	37,54	24,03	0,38	36,39	0,25	98,65
3	Un 28 Llacp-01-ol10	38,37	20,46	0,33	39,59	0,24	99,07
3	Un 29 Llacp-01-ol-px12	37,80	24,61	0,39	36,18	0,31	99,37
1	Un 30 Llacp-01-ol13-14	37,51	25,42	0,40	35,52	0,25	99,21
3	Un 30 Llacp-01-ol13-14	37,55	24,37	0,40	36,62	0,25	99,30
3	Un 31 Llacp-01-ol-px19	37,26	24,28	0,39	36,87	0,27	99,16
3	Un 32 Llacp-01-ol-px18	36,97	26,03	0,41	35,41	0,27	99,19
3	Un 33 Llacp-01-ol-px17	37,36	24,68	0,40	36,26	0,28	99,12
1	Un 35 Llacp-01-px15	37,48	23,56	0,36	36,99	0,24	98,75
3	Un 35 Llacp-01-px15	36,43	27,74	0,42	33,16	0,24	98,10
3	Un 36 Llacp-1751-px1	37,61	24,08	0,40	36,43	0,25	98,84
1	Un 38 Llacp-1751-ol-px2	37,69	23,56	0,37	36,86	0,26	98,83
3	Un 38 Llacp-1751-ol-px2	36,52	28,36	0,46	32,59	0,34	98,37
1	Un 39 Llacp-1751-ol-px3	38,03	23,29	0,40	36,91	0,25	98,97
3	Un 39 Llacp-1751-ol-px3	36,15	33,08	0,61	28,71	0,38	99,10
1	Un 41 Llacp-1751-ol-px5	37,44	23,78	0,37	36,57	0,25	98,49
3	Un 41 Llacp-1751-ol-px5	36,00	30,36	0,52	30,78	0,25	98,03
1	Un 43 Llacp-1751-ol-px6	37,68	23,94	0,39	36,56	0,26	98,92
3	Un 43 Llacp-1751-ol-px6	36,98	25,68	0,39	34,75	0,28	98,15
3	Un 50 Llacp-1751-ol-px9	39,13	23,27	0,38	36,82	0,24	99,94
3	Un 50 Llacp-1751-ol-px9	38,53	25,72	0,42	34,74	0,24	99,72
1	Un 51 Llacp-1751-ol-px8	39,76	24,54	0,41	35,76	0,35	100,94
3	Un 52 Llacp-1751-ol-px8	41,63	28,18	0,56	27,20	1,49	99,54
1	Un 55 Llacp-1751-ol-px12	39,00	23,39	0,37	36,60	0,27	99,71
3	Un 55 Llacp-1751-ol-px12	37,90	29,46	0,50	31,49	0,28	99,73
1	Un 56 Llacp-1751-ol13	39,14	23,42	0,40	36,97	0,25	100,24
3	Un 56 Llacp-1751-ol13	38,16	29,32	0,49	31,70	0,26	100,06
1	Un 57 Llacp-1751-ol15	38,91	22,91	0,37	37,31	0,22	99,81
1	Un 57 Llacp-1751-ol15	38,87	24,40	0,41	35,92	0,27	99,96
1	Un 58 Llacp-1751-ol16	39,06	23,29	0,38	36,87	0,23	99,90

Point location	Point name	SiO_2	FeO	MnO	MgO	CaO	total
1	Un 58 Llacp-1751-ol16	38,90	24,21	0,39	35,96	0,25	99,83
1	Un 59 Llacp-1751-ol-px22	38,62	24,26	0,39	35,69	0,27	99,30
1	Un 60 Llacp-1751-ol25	39,03	23,08	0,37	36,89	0,24	99,71
3	Un 60 Llacp-1751-ol25	37,99	26,96	0,39	33,62	0,22	99,26
1	Un 60 Llacp-1751-ol25	38,69	23,04	0,38	36,78	0,24	99,23
3	Un 60 Llacp-1751-ol25	37,96	27,96	0,46	32,97	0,29	99,74
1	Un 61 Llacp-1751-ol23	38,16	23,75	0,41	36,37	0,25	99,03
3	Un 61 Llacp-1751-ol23	37,32	29,29	0,54	31,39	0,30	98,97
1	Un 61 Llacp-1751-ol23	40,39	14,10	0,21	44,18	0,17	99,22
3	Un 61 Llacp-1751-ol23	37,93	27,17	0,47	33,28	0,25	99,23
1	Un 63 Llacp-1751-ol-px19	38,77	23,96	0,40	36,12	0,26	99,61
1	Un 63 Llacp-1751-ol-px19	38,62	24,07	0,39	36,12	0,26	99,53
1	Un 64 Llacp-1751-ol18	39,67	19,08	0,31	40,35	0,17	99,71
1	Un 64 Llacp-1751-ol18	38,95	23,60	0,37	36,54	0,24	99,84
1	Un 4 Llacp-02-ol2	39,07	21,31	0,33	37,84	0,23	98,77
3	Un 4 Llacp-02-ol2	38,21	25,29	0,37	34,13	0,20	98,18
1	Un 5 Llacp-02-ol3	37,98	26,74	0,40	32,93	0,24	98,29
2	Un 5 Llacp-02-ol3	39,53	21,14	0,31	37,75	0,20	98,93
3	Un 5 Llacp-02-ol3	38,87	24,91	0,39	34,94	0,18	99,28
1	Un 6 Llacp-02-ol4	38,07	23,70	0,37	35,16	0,26	97,54
3	Un 6 Llacp-02-ol4	37,72	26,11	0,39	33,50	0,22	97,96
1	Un 8 Llacp-02-ol5	39,07	19,67	0,28	38,63	0,17	97,84
3	Un 8 Llacp-02-ol5	37,71	25,42	0,39	33,47	0,15	97,14
1	Un 9 Llacp-02-ol5	39,73	19,91	0,29	38,50	0,19	98,60
3	Un 9 Llacp-02-ol5	38,50	26,85	0,43	32,86	0,13	98,79
3	Un 10 Llacp-02-ol6	38,42	25,88	0,35	33,61	0,24	98,52
3	Un 10 Llacp-02-ol6	38,70	24,51	0,36	34,71	0,25	98,54
1	Un 11 Llacp-02-ol8	38,30	20,77	0,30	38,50	0,23	98,12
3	Un 14 Llacp-02-ol8	37,92	25,34	0,38	34,27	0,23	98,15
1	Un 15 Llacp-02-ol7	39,46	20,05	0,29	38,78	0,21	98,83
3	Un 15 Llacp-02-ol7	37,95	29,33	0,47	31,11	0,19	99,10
1	Un 12 Llalh-1957-ol10	38,58	24,25	0,39	35,77	0,26	99,34
3	Un 13 Llalh-1957-ol10	38,33	24,78	0,39	35,03	0,26	98,86
1	Un 13 Llalh-1957-ol10	38,69	24,34	0,37	35,78	0,26	99,50
1	Un 14 Llalh-1957-ol11	39,75	18,84	0,29	40,35	0,17	99,53
3	Un 14 Llalh-1957-ol11	38,55	24,68	0,39	35,36	0,23	99,31
1	Un 15 Llalh-1957-ol-px9	39,42	20,18	0,32	39,31	0,22	99,57
1	Un 16 Llalh-1957-ol-px9	39,22	20,53	0,34	39,35	0,21	99,75

Point location	Point name	SiO_2	FeO	MnO	MgO	CaO	total
1	Un 17 Llalh-1957-olclots8	39,34	20,57	0,33	39,36	0,23	99,92
2	Un 17 Llalh-1957-olclots8	39,45	20,33	0,32	39,55	0,22	100
3	Un 17 Llalh-1957-olclots8	39,54	20,06	0,35	39,73	0,24	100,03
3	Un 17 Llalh-1957-olclots8	38,37	25,54	0,40	34,99	0,24	99,59
1	Un 17 Llalh-1957-olclots8	39,65	20,00	0,34	38,93	0,23	99,23
3	Un 17 Llalh-1957-olclots8	38,09	27,84	0,45	32,61	0,24	99,29
1	Un 17 Llalh-1957-olclots8	39,27	20,33	0,34	39,28	0,22	99,53
1	Un 17 Llalh-1957-olclots8	39,57	20,47	0,34	39,09	0,23	99,81
3	Un 17 Llalh-1957-olclots8	38,19	25,43	0,41	34,55	0,22	98,88
1	Un 18 Llalh-1957-ol-px7	38,84	24,67	0,38	35,67	0,26	99,89
1	Un 18 Llalh-1957-ol-px7	38,60	24,60	0,38	35,37	0,22	99,25
1	Un 19 Llalh-1957-ol-px6	39,16	21,55	0,33	38,88	0,20	100,15
1	Un 19 Llalh-1957-ol-px6	39,22	21,95	0,35	37,93	0,23	99,74
1	Un 20 Llalh-1957-ol4	39,24	21,51	0,36	38,44	0,25	99,91
3	Un 21 Llalh-1957-ol4	38,68	25,08	0,38	35,29	0,23	99,72
1	Un 22 Llalh-1957-ol3	39,01	22,79	0,33	37,31	0,22	99,79
3	Un 23 Llalh-1957-ol3	38,61	26,53	0,44	33,94	0,23	99,85
1	Un 24 Llalh-1957-ol-px5	38,85	23,47	0,39	36,24	0,30	99,33
3	Un 28 Llalh-1957-ol-px5	37,50	23,66	0,37	36,56	0,26	98,45
3	Un 29 Llalh-1957-ol-px2	37,70	25,83	0,41	34,65	0,27	98,90
3	Un 30 Llalh-1957-ol-px2	37,38	25,25	0,37	35,11	0,26	98,41
3	Un 30 Llalh-1957-ol-px2	37,62	25,48	0,40	34,99	0,26	98,83
3	Un 30 Llalh-1957-ol-px2	37,98	24,26	0,39	36,08	0,25	99,02
3	Un 30 Llalh-1957-ol-px2	37,38	23,93	0,38	36,58	0,24	98,57

ANPHIBOLE (LASCAR VOLCANO)

Point location	Point name	Na_2O	MgO	SiO_2	Al_2O_3	K_2O	CaO	FeO	MnO	TiO_2	total
3	l1-hbl1	2,30	15,38	43,19	12,66	0,47	11,41	9,81	0,10	2,41	100
2	l1-hbl2	2,64	15,30	43,22	12,56	0,49	11,52	10,05	0,13	2,45	100
1	l1-hbl3	2,58	15,90	43,74	12,33	0,44	11,43	9,72	0,11	2,40	100
3	l1-hbl4	2,38	14,20	41,94	11,92	0,45	11,00	11,15	0,12	2,67	100
1	l1-hbl5	2,47	14,60	42,61	12,26	0,43	11,41	11,51	0,09	2,72	100
3	l1-hbl6	2,34	14,21	42,42	12,87	0,46	11,20	12,13	0,12	2,70	99,95
2	l1-hbl7	2,43	13,35	42,16	11,74	0,56	11,14	12,65	0,16	3,28	100
1	l1-hbl8	2,47	14,15	43,43	11,95	0,51	11,41	12,44	0,18	3,12	100

Point location	Point name	Na_2O	MgO	SiO_2	Al_2O_3	K_2O	CaO	FeO	MnO	TiO_2	total
3	l1-hbl9	2,49	14,71	42,70	12,46	0,46	11,25	11,47	0,14	2,69	100
1	l1-hbl10	2,44	14,36	42,19	11,68	0,47	11,22	11,55	0,13	2,67	100
3	l1-hbl11	2,32	13,34	42,67	12,12	0,55	11,24	13,30	0,18	2,90	99,99
1	l1-hbl12	2,48	14,05	42,90	12,11	0,52	11,23	12,37	0,13	2,88	99,92
3	l1-hbl13	2,32	14,47	42,60	12,21	0,41	11,28	11,83	0,15	2,72	100
2	l1-hbl14	2,43	14,58	42,75	12,31	0,48	11,28	11,65	0,12	2,75	100
1	l1-hbl15	2,40	14,48	42,77	12,39	0,48	11,12	11,58	0,15	2,69	100
1	l1-hbl16	2,22	14,35	43,95	10,60	0,48	11,28	12,18	0,19	2,80	100
3	l2l-hbl1	2,31	15,17	42,04	12,72	0,38	11,46	11,15	0,14	2,59	100
1	l2l-hbl2	2,45	15,20	42,19	12,89	0,38	11,50	10,96	0,11	2,57	100
3	l2l-hbl3	2,44	15,49	42,80	12,85	0,38	11,70	10,97	0,11	2,60	100
1	l2l-hbl4	2,40	15,28	42,22	12,57	0,37	11,54	11,02	0,13	2,56	100
3	l2l-hbl5	2,37	14,49	42,49	11,87	0,41	11,33	12,09	0,15	2,30	99,97
1	l2l-hbl6	2,40	15,46	42,43	12,51	0,33	11,14	11,27	0,11	2,58	100
3	l2l-hbl7	2,36	14,83	42,58	12,31	0,45	11,37	12,03	0,20	2,40	99,99
3	l2l-hbl9	2,31	15,31	42,97	11,90	0,41	11,53	11,01	0,14	2,55	100
2	l2l-hbl10	2,30	14,77	41,96	12,43	0,42	11,65	11,37	0,12	2,63	100
1	l2l-hbl11	2,28	14,54	41,86	12,32	0,40	11,35	11,97	0,13	2,52	100
3	l2l-hbl12	2,37	15,37	42,87	12,43	0,41	11,58	11,22	0,13	2,43	100
1	l2l-hbl13	2,25	15,50	42,12	12,04	0,40	11,41	11,34	0,13	2,60	100
3	l4l-hbl1	2,82	14,63	43,56	13,23	0,57	11,58	10,21	0,11	1,93	100
3	l4l-hbl2	2,43	15,79	44,76	12,14	0,47	11,77	9,95	0,10	1,73	100
2	l4l-hbl3	2,58	15,96	44,01	12,56	0,43	11,77	10,32	0,12	1,79	100
1	l4l-hbl4	2,43	15,77	43,52	12,61	0,49	11,92	9,68	0,11	1,86	99,89
1	l4l-hbl6	2,29	14,56	42,89	12,42	0,47	11,58	11,64	0,13	2,31	100
1	l4l-hbl7	2,41	15,05	43,52	12,22	0,45	11,47	11,71	0,10	2,06	100
3	l4l-hbl8	1,85	11,91	36,21	10,60	0,41	10,18	10,14	0,14	2,11	99,92
1	l4l-hbl9	2,29	16,01	43,71	12,84	0,45	11,78	10,52	0,13	1,99	99,95
3	l4l-hbl10	2,91	15,98	44,31	12,64	0,42	11,82	9,73	0,06	1,83	100,12
2	l4l-hbl11	2,42	15,52	44,00	12,38	0,45	11,87	9,72	0,12	1,87	100,00
2	l4l-hbl12	3,57	10,93	44,77	15,01	0,68	11,65	10,81	0,09	2,40	100,02
1	l4l-hbl13	2,47	14,64	43,05	12,96	0,50	11,50	11,21	0,11	2,23	100
3	l4l-hbl15	2,59	15,85	44,34	12,54	0,45	12,02	9,83	0,10	1,92	100,22
2	l4l-hbl16	2,48	16,07	44,05	12,21	0,48	11,81	9,71	0,11	1,87	100,00
1	l4l-hbl17	1,81	16,09	42,99	13,54	0,42	10,99	13,17	0,14	1,34	100,50
1	l4l-hbl18	2,53	15,71	43,92	12,44	0,43	11,64	11,11	0,12	2,16	100,22

Point location	Point name	Na_2O	MgO	SiO_2	Al_2O_3	K_2O	CaO	FeO	MnO	TiO_2	total
3	l4l-hbl19	2,36	14,75	42,98	12,65	0,46	11,81	11,24	0,10	2,35	100
2	l4l-hbl20	2,38	14,89	42,90	12,64	0,44	11,58	11,34	0,11	2,34	100
2	l4l-hbl21	2,44	15,48	42,61	12,26	0,44	11,62	10,42	0,10	2,12	100
1	l4l-hbl22	2,40	14,40	42,66	12,69	0,48	11,32	11,87	0,10	2,39	99,99
1	l4l-hbl23	2,68	15,26	42,52	12,42	0,42	11,52	11,27	0,15	2,12	100
1	l4l-hbl24	1,90	11,61	36,89	9,62	0,36	9,82	9,63	0,13	2,00	99,97
3	l4l-hbl25	2,70	15,06	45,08	11,91	0,53	11,21	10,91	0,16	2,20	100,60
1	l4l-hbl26	2,35	15,47	43,67	11,30	0,54	11,23	10,84	0,14	2,41	100
1	l4l-hbl27	2,76	15,63	43,35	11,99	0,41	11,60	10,46	0,12	2,07	100
3	l4l-hbl28	2,52	15,10	43,28	12,63	0,49	11,71	11,28	0,13	2,35	100
1	l4l-hbl29	2,17	16,13	38,46	14,27	0,35	10,98	14,56	0,16	2,35	100
3	l4l-hbl30	2,35	15,37	43,60	12,59	0,43	11,79	10,43	0,12	2,17	99,99
2	l4l-hbl31	2,40	14,14	42,74	12,66	0,52	11,48	11,94	0,11	2,34	100
2	l4l-hbl32	2,44	15,15	43,57	13,02	0,46	11,66	10,96	0,12	2,17	100
1	l4l-hbl33	2,40	14,67	43,53	12,46	0,48	11,76	11,27	0,11	2,21	100
1	l4l-hbl34	2,46	15,97	43,73	12,03	0,48	11,41	10,47	0,13	1,94	99,99
3	l4l-hbl35	2,55	15,24	43,23	12,70	0,42	11,76	11,22	0,09	2,46	100,01
1	l4l-hbl36	1,72	17,67	41,90	12,35	0,27	10,88	13,48	0,14	1,79	100,38

PLAGIOCLASE (LASCAR VOLCANO)

Point location	Point name	SiO_2	Al_2O_3	FeO	MgO	CaO	Na_2O	K_2O	total
3	l1-plg1	55,69	27,60	0,51	0,03	10,63	5,27	0,25	100,01
2	l1-plg2	54,48	28,16	0,42	0,03	11,26	4,75	0,21	99,37
1	l1-plg5	51,04	31,29	0,51	0,04	14,49	3,18	0,13	100,79
3	l1-plg8	47,96	31,68	0,56	0,03	16,08	2,24	0,06	98,65
2	l1-plg9	48,18	31,66	0,52	0,05	15,93	2,29	0,08	98,76
1	l1-plg10	49,40	32,49	0,51	0,05	16,05	2,12	0,12	100,82
3	l1-plg11	53,90	29,22	0,56	0,04	12,55	4,38	0,19	100,90
1	l1-plg12	49,38	31,86	0,55	0,04	15,65	2,38	0,10	100,00
1	l1-plg13	48,59	32,59	0,57	0,02	16,19	2,29	0,07	100,35
1	l2l-plg1	53,24	29,78	0,88	0,10	13,01	4,25	0,20	101,57
3	l2l-plg2	55,81	24,05	2,47	0,60	10,91	3,68	1,74	99,62
2	l2l-plg4	53,94	28,55	0,38	0,05	11,94	4,79	0,30	100,01
1	l2l-plg5	54,79	27,48	0,35	0,04	10,70	5,02	0,38	98,80
1	l4l-plg1	54,87	28,10	0,97	0,06	11,03	5,17	0,27	100,57
1	l4l-plg2	52,93	29,15	0,72	0,06	12,50	4,31	0,20	99,99
1	l4l-plg3	54,70	29,01	0,70	0,06	12,02	4,73	0,20	101,51

Point location	Point name	SiO_2	Al_2O_3	FeO	MgO	CaO	Na_2O	K_2O	total
3	l4l-plg5	52,83	29,60	0,71	0,06	13,23	3,84	0,18	100,51
2	l4l-plg6	48,31	33,11	0,53	0,04	16,73	2,10	0,08	100,98
2	l4l-plg7	65,47	14,23	5,06	0,87	5,27	3,43	2,65	100,76
1	l4l-plg9	54,93	28,25	0,33	0,01	11,48	4,89	0,27	100,21

PLAGIOCLASE (LONQUIMAY VOLCANO)

Point location	Point name	SiO_2	Al_2O_3	FeO	MgO	CaO	Na_2O	K_2O	total
3	lon2-plg1	51,89	29,66	1,01	0,06	13,07	4,13	0,12	100,01
2	lon2-plg3	47,32	32,37	0,74	0,06	16,55	2,22	0,04	99,36
1	lon2-plg4	47,22	32,90	0,71	0,05	16,58	2,11	0,05	99,65
1	lon2-plg5	58,75	25,34	0,99	0,08	8,13	6,98	0,29	100,68
1	lon3-plg1	54,72	27,40	0,40	0,03	10,71	5,49	0,10	98,93
1	lon3-plg2	55,21	27,80	0,36	0,05	10,82	5,39	0,08	99,76
1	lon3-plg3	58,48	25,44	0,34	0,03	8,12	6,50	0,16	99,13
3	lon3-plg4	57,06	27,33	0,77	0,11	9,82	6,10	0,18	101,50
3	lon3-plg5	59,74	25,17	0,35	0,02	7,27	7,36	0,20	100,19
2	lon3-plg6	58,53	25,81	0,24	0,00	8,23	6,88	0,18	99,92
1	lon3-plg7	57,84	25,92	0,26	0,04	8,51	6,52	0,16	99,32
1	lon3-plg8	58,38	26,78	0,32	0,03	8,83	6,52	0,16	101,07
3	lon3-plg9	55,63	26,63	0,57	0,08	10,11	5,94	0,16	99,15
2	lon3-plg10	58,86	24,94	0,25	0,00	7,62	7,24	0,22	99,14
1	lon3-plg11	59,17	24,97	0,27	0,02	7,67	7,11	0,21	99,50
1	lon3-plg12	54,34	27,99	0,50	0,05	11,25	5,04	0,10	99,36
1	lon3-plg13	55,40	27,42	0,55	0,05	10,31	5,67	0,12	99,58
3	Lon4-plg1	54,25	28,09	0,39	0,05	11,28	5,04	0,09	99,24
2	Lon4-plg2	54,83	27,87	0,36	0,04	10,71	5,46	0,11	99,41
1	Lon4-plg3	55,33	27,52	0,31	0,04	10,35	5,54	0,12	99,22
1	Un 3 Lon5-plg1	58,05	25,57	0,39	0,06	8,06	6,79	0,14	99,05
3	Un 3 Lon5-plg1	54,86	27,60	0,41	0,06	10,08	6,03	0,12	99,16
1	Un 3 Lon5-plg1	59,01	25,07	0,22	0,03	7,54	6,77	0,20	98,82
3	Un 3 Lon5-plg1	56,53	26,75	0,31	0,03	8,78	6,34	0,15	98,88
1	Un 4 Lon5-plg2	55,91	27,18	0,28	0,03	9,56	5,96	0,11	99,06
3	Un 4 Lon5-plg2	54,48	28,21	0,46	0,05	11,03	5,21	0,08	99,53
1	Un 5 Lon5-plg3	56,69	26,70	0,29	0,04	9,04	6,05	0,14	98,99
3	Un 5 Lon5-plg3	55,62	27,78	0,44	0,05	10,62	5,29	0,10	99,95
1	Un 6 Lon5-plg4	55,09	27,80	0,39	0,04	10,48	5,33	0,11	99,22
3	Un 6 Lon5-plg4	56,75	26,91	0,39	0,05	9,48	5,97	0,14	99,66

Point location	Point name	SiO_2	Al_2O_3	FeO	MgO	CaO	Na_2O	K_2O	total
1	Un 7 Lon5-plg5	54,86	27,70	0,34	0,05	10,24	5,46	0,11	98,75
3	Un 7 Lon5-plg5	54,57	28,12	0,42	0,06	10,45	5,22	0,10	98,94
2	Un 8 Lon5-plg5	60,35	24,48	0,26	0,01	7,13	7,15	0,21	99,53
1	Un 10 Lon5-plg7	57,14	26,80	0,28	0,02	9,14	5,90	0,14	99,37
2	Un 10 Lon5-plg7	54,54	28,75	0,41	0,07	11,72	4,74	0,07	100,30
1	Un 11 Lon5-plg8	54,32	28,55	0,37	0,06	11,32	4,99	0,06	99,66
2	Un 11 Lon5-plg8	52,13	30,03	0,41	0,08	12,98	4,13	0,05	99,84
3	Un 11 Lon5-plg8	54,63	28,13	0,42	0,06	10,49	5,27	0,10	99,14
1	Un 12 Lon5-plg9	56,98	26,69	0,28	0,03	8,79	6,13	0,12	99,03
2	Un 12 Lon5-plg9	53,99	28,86	0,39	0,03	11,33	4,69	0,09	99,38
3	Un 12 Lon5-plg9	55,76	27,51	0,48	0,06	9,77	5,43	0,12	99,16
1	nvsupplg1core	54,89	28,15	0,52	0,08	11,12	4,92	0,17	99,96
2	nvsupplg1int	54,61	28,51	0,58	0,09	11,24	4,64	0,14	99,88
3	nvsupplg1rim	55,82	27,53	0,81	0,10	10,55	5,09	0,07	100,10
1	nvsupplag2	54,40	28,86	0,65	0,08	11,71	4,68	0,09	100,51
3	nvsupplag2rim	55,02	28,38	0,61	0,08	10,97	5,09	0,14	100,31
1	nvsupplg3	56,03	27,60	0,46	0,07	10,35	5,41	0,12	100,07
3	nvsupplg3rim	56,26	27,45	0,58	0,07	10,26	5,60	0,16	100,49
1	nvsupplg4	57,45	26,46	0,94	0,12	9,36	5,76	0,22	100,45
3	nvsupplg4rim	58,17	26,08	0,84	0,08	8,68	6,25	0,22	100,51
1	nvsupplg5	54,96	28,11	0,63	0,08	11,01	5,06	0,12	99,95
3	nvsupplg5rim	56,62	27,22	0,74	0,08	10,06	5,47	0,16	100,41

PLAGIOCLASE (LLAIMA VOLCANO)

Point location	Point name	SiO_2	Al_2O_3	FeO	MgO	CaO	Na_2O	K_2O	total
1	Un 38 Llacp-01-plg1	49,62	31,15	0,53	0,15	14,76	2,99	0,09	99,27
2	Un 38 Llacp-01-plg1	53,69	28,56	0,61	0,16	11,88	4,74	0,18	99,84
1	Un 39 Llacp-01-plg2	48,32	31,90	0,52	0,14	15,87	2,09	0,08	98,93
2	Un 39 Llacp-01-plg2	52,30	29,10	0,62	0,16	12,57	3,99	0,15	98,90
1	Un 39 Llacp-01-plg2	48,20	32,06	0,63	0,12	16,08	2,08	0,05	99,25
2	Un 39 Llacp-01-plg2	52,72	28,91	0,63	0,16	12,24	4,00	0,13	98,84
1	Un 30 Llacp-02-plg4	46,92	32,77	0,59	0,09	16,48	1,75	0,04	98,67
2	Un 30 Llacp-02-plg4	52,48	29,07	0,79	0,17	12,25	3,89	0,13	98,81
1	Un 33 Llacp-02-plg6	46,14	33,70	0,46	0,08	17,09	1,28	0,04	98,80
1	Un 35 Llacp-02-plg7	52,35	29,15	0,71	0,17	12,94	4,16	0,10	99,62
1	Un 36 Llacp-02-plg8	46,69	33,57	0,56	0,09	16,88	1,62	0,03	99,53
2	Un 36 Llacp-02-plg8	48,06	31,71	0,58	0,14	16,36	2,04	0,05	98,96
3	Un 36 Llacp-02-plg8	51,39	29,51	0,66	0,19	12,93	3,93	0,11	98,75

Point location	Point name	SiO_2	Al_2O_3	FeO	MgO	CaO	Na_2O	K_2O	total
1	Un 36 Llacp-02-plg8	49,89	30,47	0,61	0,13	14,10	3,28	0,08	98,58
3	Un 36 Llacp-02-plg8	54,34	27,52	0,87	0,14	10,86	5,30	0,24	99,32
1	Un 36 Llacp-02-plg8	49,11	31,66	0,59	0,15	15,42	2,68	0,06	99,70
3	Un 37 Llacp-02-plg8	52,20	29,52	0,72	0,16	12,96	3,68	0,11	99,35
1	Un 41 Llacp-1751-plg1	45,83	33,74	0,46	0,08	17,36	1,45	0,00	98,89
3	Un 41 Llacp-1751-plg1	54,07	28,81	0,59	0,17	11,91	4,44	0,18	100,20
1	Un 42 Llacp-1751-plg2	46,33	34,15	0,42	0,09	17,77	0,94	0,03	99,74
3	Un 42 Llacp-1751-plg2	53,96	28,50	0,68	0,15	11,97	4,00	0,15	99,43
1	Un 42 Llacp-1751-plg2	49,27	32,23	0,63	0,12	15,51	2,21	0,07	100,06
3	Un 42 Llacp-1751-plg2	53,53	29,27	0,67	0,17	13,02	4,12	0,14	100,90
1	Un 43 Llacp-1751-plg3	50,52	30,95	0,78	0,11	14,57	3,02	0,12	100,03
2	Un 43 Llacp-1751-plg3	52,68	28,67	0,81	0,17	12,29	4,12	0,14	98,89
1	Un 43 Llacp-1751-plg3	46,99	33,39	0,51	0,13	17,45	1,42	0,03	99,93
3	Un 43 Llacp-1751-plg3	53,98	28,50	0,75	0,17	12,42	4,54	0,14	100,52
1	Un 43 Llacp-1751-plg3	48,95	32,32	0,57	0,12	16,42	2,40	0,06	100,85
3	Un 43 Llacp-1751-plg3	54,94	28,46	0,62	0,16	11,47	4,58	0,20	100,43
	Un 44 Llach-1957-plg1	48,81	31,88	0,62	0,13	14,97	2,45	0,05	98,93
3	Un 44 Llach-1957-plg1	50,98	30,23	0,67	0,15	13,88	3,10	0,11	99,13
1	Un 44 Llach-1957-plg1	46,54	33,25	0,59	0,09	17,59	1,51	0,02	99,63
2	Un 44 Llach-1957-plg1	47,90	32,08	0,66	0,14	16,46	1,92	0,04	99,20
3	Un 44 Llach-1957-plg1	54,54	27,08	1,41	0,62	10,71	4,68	0,19	99,35
1	Un 44 Llach-1957-plg1	49,64	30,86	0,74	0,16	14,73	2,77	0,07	98,94
3	Un 44 Llach-1957-plg1	52,77	28,27	0,84	0,20	12,40	4,12	0,16	98,75
1	Un 45 Llach-1957-plg2	50,92	30,42	0,72	0,20	14,26	3,07	0,09	99,68
3	Un 45 Llach-1957-plg2	52,42	28,63	0,92	0,21	12,40	4,61	0,13	99,39
3	Un 45 Llach-1957-plg2	53,77	27,36	1,54	0,18	11,53	4,41	0,27	99,17
1	Un 45 Llach-1957-plg2	51,03	29,55	0,59	0,17	13,58	3,56	0,10	98,59
1	Un 46 Llach-1957-plg3	49,11	31,33	0,63	0,17	15,45	2,42	0,05	99,20
3	Un 46 Llach-1957-plg3	53,14	28,87	0,63	0,17	12,26	3,92	0,12	99,21
1	Un 46 Llach-1957-plg3	48,39	31,86	0,62	0,13	15,47	2,42	0,04	98,98
3	Un 46 Llach-1957-plg3	53,16	28,18	0,74	0,20	12,46	4,32	0,12	99,22

Appendix 5

Magma viscosity

In order to evaluate if the magma viscosity of Lascar, Lonquimay and Llaima volcanoes is invariant through time, we estimated its value using the Einstein-Roscoe equation (Eq. (21)). This has been previously used to calculate viscosity of crystal-bearing magmas (Castruccio et al., 2010).

$$\mu(\phi) = \mu_0\left(1 - \frac{\phi}{\phi_m}\right)^{-2.5} \quad \text{(C1)}$$

with μ viscosity, μ_0 liquid viscosity, ϕ crystal content and ϕ_m maximum packing fraction. We studied samples from different stages during the volcano growth (Table 3). The crystal content was obtained by point count on scanned thin sections using the *JMicroVision* software. We considered phenocrysts (>1 mm) as we assume they crystalize prior to the eruption. We used ϕ_m =70 for Lascar and Llaima samples and ϕ_m =40 for Lonquimay samples (Castruccio and Contreras, 2016). Glass viscosity was estimated from Giordano et al. (2008). Temperature values were obtained by thermometry (see section 5.3.4) and H_2O solubility was estimated following Moore et al. (1998) and Lange et al. (2009). Obtained values obtained are in the range of 5.9-6%wt, 1-2%wt and 0.2-0.5%wt for Lascar, Lonquimay and Llaima lavas respectively.

Results are shown in the below figure showing a stable range of viscosity for magmas from Lascar, Lonquimay and Llaima volcanoes, and supporting the hypothesis that each volcano had a stable rheology during its evolution.

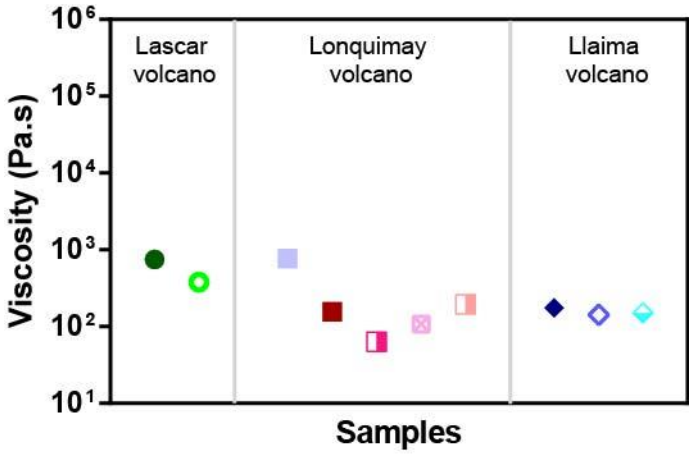

Estimated viscosity values using Eq. (C1) for samples from Lascar, Lonquimay and Llaima volcanoes.

Appendix 6

Average height and basal radius of volcanoes from the SVZ and CVZ.

VOLCANO NAME	LOCATION	AVERAGE BASAL RADIUS (km)	AVERAGE HEIGHT (m)
Parinacota	Central Volcanic Zone	6,0	1619
Pomerape	Central Volcanic Zone	6,3	1649
Nevado del Sajama	Central Volcanic Zone	7,1	2009
Tacora	Central Volcanic Zone	5,0	1495
Guallatiri	Central Volcanic Zone	4,7	1268
Arintica	Central Volcanic Zone	4,1	1099
Isluga	Central Volcanic Zone	4,9	1184
Tata Sabaya	Central Volcanic Zone	3,6	1379
Iruputuncu	Central Volcanic Zone	2,1	868
Miño	Central Volcanic Zone	4,0	1424
Ollague	Central Volcanic Zone	7,6	1928
San Pedro	Central Volcanic Zone	7,8	2290
Paniri	Central Volcanic Zone	7,7	2147
Sairecabur	Central Volcanic Zone	1,2	546
Licancabur	Central Volcanic Zone	4,5	1850
Juriques	Central Volcanic Zone	4,9	1561
Colachi	Central Volcanic Zone	2,4	797
Laguna verde	Central Volcanic Zone	2,2	546
Acamarachi	Central Volcanic Zone	2,1	1021
Lascar	Central Volcanic Zone	5,0	1050
Aguas calientes	Central Volcanic Zone	4,6	963
Chiliques	Central Volcanic Zone	2,7	1077
Cerro Miscanti	Central Volcanic Zone	4,3	1230
Miñiques	Central Volcanic Zone	6,0	1644
caichinque	Central Volcanic Zone	3,6	465
Aracar	Central Volcanic Zone	9,6	2205
Socompa	Central Volcanic Zone	8,7	2264
Llullaillaco	Central Volcanic Zone	7,5	2040
Peinado	Central Volcanic Zone	5,3	1546
Tupungato	Southern Volcanic Zone	5,7	1291
Maipo	Southern Volcanic Zone	7,5	1846
Tupungatito	Southern Volcanic Zone	4,8	1040
San Jose	Southern Volcanic Zone	5,8	2130

Palomo	Southern Volcanic Zone	2,4	1248
Tinguiririca	Southern Volcanic Zone	2,6	781
Descabezado grande	Southern Volcanic Zone	4,3	1419
Cerro azul	Southern Volcanic Zone	4,1	1336
San Pedro Pellado	Southern Volcanic Zone	2,8	1231
Nevado de Longavi	Southern Volcanic Zone	2,9	825
Nevados de Chillán	Southern Volcanic Zone	3,8	1102
Antuco	Southern Volcanic Zone	5,3	1478
Callaqui	Southern Volcanic Zone	4,0	1407
Copahue	Southern Volcanic Zone	4,2	904
Toguaca	Southern Volcanic Zone	6,8	1424
Lonquimay	Southern Volcanic Zone	4,6	1286
Llaima	Southern Volcanic Zone	12,0	2188
Quetrupillán	Southern Volcanic Zone	4,7	770
Lanin	Southern Volcanic Zone	7,2	2510
Villarrica	Southern Volcanic Zone	14,5	2358
Mocho	Southern Volcanic Zone	8,6	1620
Puntiagudo	Southern Volcanic Zone	4,8	1797
Osorno	Southern Volcanic Zone	8,5	2328
Calbuco	Southern Volcanic Zone	8,1	1611
Hornopiren	Southern Volcanic Zone	3,9	1255
Michimahuida	Southern Volcanic Zone	8,4	1664
Corcovado	Southern Volcanic Zone	7,0	1958
Melimoyu	Southern Volcanic Zone	9,6	2081
Mentolat	Southern Volcanic Zone	4,8	1253
Cay	Southern Volcanic Zone	5,8	1654
Maca	Southern Volcanic Zone	5,4	2333